MEMBRANE BINDING AND LIPID EXTRACTION STUDIES OF THE GM2 ACTIVATOR PROTEIN

By

STACEY-ANN BENJAMIN

A DISSERTATION PRESENTED TO THE GRADUATE SCHOOL
OF THE UNIVERSITY OF FLORIDA IN PARTIAL FULFILLMENT
OF THE REQUIREMENTS FOR THE DEGREE OF
DOCTOR OF PHILOSOPHY

UNIVERSITY OF FLORIDA

2012

To Toto and my sister Camille Benjamin

ACKNOWLEDGMENTS

I thank my advisor Dr. Gail E. Fanucci for all her assistance and guidance throughout my entire graduate career. She has expertly taught me more than I could ever imagine learning during my time in her research group. She has facilitated my growth as a scientist through motivation, challenge and support. I am most grateful that she allowed me to pursue my own goals and offered unselfish advice regarding my career interests whenever I needed it. I am particularly appreciative for her playing a huge role in me overcoming my fear of, and becoming a lover of dogs.

I am grateful to Dr. Daniel R. Talham for ‘adopting’ me in his lab for the latter part of my graduate career. He always made me feel like a part of his group, and never hesitated to offer suggestions when I asked. The Talham lab became a second home for me and I will always be grateful to him, and his students for the accommodation and making me feel welcomed.

I would like to thank past and current Fanucci and Talham group members for numerous scientific conversations and for providing a desirable work environment in which to work. I would especially like to thank Dr. Yong Ran, Dr. Jamie Kear, Dr. Mandy Blackburn, Dr. Jordan Mathias, Dr. Jeff Carter, Dr. Roxane Fabre, Hao Liu, and Captain Emily Pollard for their unwavering support both in and outside the lab.

The Chemistry department on the whole has provided support during my time here. I am grateful for the close friendships I developed while in Gainesville – Dr. Marilyn Prieto, Whitney Stutts, Robert Menger, Pascale Attallah, Dr. Danniebelle Haase, Matt Baker, Dr. Richard Farley, Dr. Jared Lynch, Joey Lott, and Ms. Glennis Brown have all enriched my graduate experience and they hold a special place in my heart. I

thank Stacy-Ann Stephenson, Michelle Jurcak, and Dr. Latanya Fisher for being amicable roommates who have grown to be my good friends.

I am most thankful for my teaching mentor Dr. Jeff Keaffaber for inspiring me to become the best instructor I can be, and for encouraging me to constantly seek ways in which to perfect my craft. I am grateful to Dr. Phil Brucat for allowing me to teach my own undergraduate class on more than one occasion – an invaluable experience that I will always treasure. I thank Dr. Ben Smith for always being available and for engaging me in thought provoking conversations. I am most grateful to Ms. Lori Clark for sharing my joys, and constantly going above and beyond the duties of her responsibilities to assist me with any problems I may face. I have developed a great sense of respect and love for her, and will treasure our friendship well beyond my years at the University of Florida.

Last and by no means least, without the love and support of my family and close friends, graduate school would have been difficult. I am appreciative of my parents, Sonia and Georgie Benjamin, my aunt Sharon, and my sister Camille, for always being there for me when I need them the most. It is because of them that I am able to complete my degree. I thank my vacation buddies Tamar, Lamonde, and Tracey-Ann for always keeping me entertained and indulging with me in my second love – fine dining. I would also like to acknowledge Wendy Batchelor and Dominic Watson for being very special persons in my life, and for encouraging me to be the best version of me. Finally, I will always remember Toto Benjamin for being my best friend and for teaching me what it means to love unconditionally.

TABLE OF CONTENTS

page

LIST OF TABLES

LIST OF FIGURES

LIST OF ABBREVIATIONS

A	Alanine
Asp	Aspartic acid
BMP	Bis(monoacylglycero)Phosphate
Cer	Ceramide
D	Aspartic acid
Dansyl-DHPE	*N*-(5-dimethylaminonaphthalene-1-sulfonyl)-1, 2-dihexadecanoyl-sn-glycero-3-phosphoethanolamine
DMSO	dimethylsulfoxide
dNTP	deoxynucleotide triphosphate
E	Glutamic acid
EPR	Electron paramagnetic resonance
Fuc	Fucose
Gal	gGalactose
GalNAc	*N*-acetylgalactosamine
Glc	Glucose
GlcNAc	*N*-acetylglucosamine
Glu	Glutamic acid
GM2AP	GM2 Activator Protein
GSLs	Glycosphingolipids
L	Left-handed
LB	Langmuir-Blodgett
IPTG	Isopropyl-β-D-thiogalacatopyranoside
NeuNAc	*N*-acetylneuraminic acid
Hex A	beta-Hexosaminidase A
n	Refractive index

ODM	Octadecyl mercaptan
ODPA	Octadecylphosphonic acid
PA	Phosphatidic acid
PAF	Platelet activating factor
PC	Phosphatidylcholine
PCR	Polymerase chain reaction
PE	Phosphatidylethanolamine
PG	Phosphatidylglycerol
PI	Phosphatidylinositol
PMT	Photomultiplier tube
PS	Phosphatidylserine
R	Right-handed
SAM	Self assembled monolayer
SEC	Size exclusion chromatography
sn	stereospecific numbering
SPR	Surface plasmon resonance
SPREE	Surface plasmon enhanced ellipsometry
TIRE	Total internal reflection ellipsometry
W	Tryptophan

Abstract of Dissertation Presented to the Graduate School
of the University of Florida in Partial Fulfillment of the
Requirements for the Degree of Doctor of Philosophy

MEMBRANE BINDING AND LIPID EXTRACTION STUDIES OF THE GM2 ACTIVATOR PROTEIN

By

Stacey-Ann Benjamin

August 2012

Chair: Gail E. Fanucci
Major: Chemistry

GM2AP is an accessory protein that solubilizes the GM2 ganglioside from intralysomal vesicles in neuronal cells for hydrolytic cleavage by HexA to form GM3. This non-enzymatic protein functions also a lipid transfer protein. The precise molecular interactions and method of extraction of GM2 and other lipids from vesicles are unknown. GM2AP contains three native tryptophan residues (W5, W63 and W131), with two of these (W63 and W131) located in the putative membrane binding loops of the protein. In this report, we use fluorescence spectroscopy and surface plasmon resonance enhanced ellipsometry (SPREE) to investigate the interaction of GM2AP with lipids as a function of protein electrostatics and hydrophobicity. Utilizing fluorescence spectroscopy, dansyl-labeled phospholipids were used to monitor the changes in the rates of lipid extraction and transfer by GM2AP from liposomes as a function of both pH and a series of tryptophan to alanine substituted constructs of the protein. The ability of GM2AP to bind and/or extract dansyl-labeled lipids from liposomes was affected with increased pH of the lipid environment with optimal lipid extraction efficiency occurring at pH 4.8. Amino acid substitutions from tryptophan to alanine in the putative membrane binding loops of the protein resulted in slower lipid extraction rates, suggesting the

relevance of these residues for membrane binding by GM2AP. Additionally, a resorcinol based GM2 extraction assay provided results suggesting that though extraction rates slowed, total ganglioside extraction efficiency was not affected by the W to A substitutions.

SPREE analysis allowed us to study the interaction of GM2AP with lipids on surface supported lipid bilayers. When PG, a negatively charged lipid was added to the lipid bilayer, GM2AP was able to adsorb onto the surface possibly due to electrostatic interactions between the protein and the immobile lipid bilayer on the functionalized surface. Protein adsorption was not affected by increased concentrations of PG to the lipid bilayer but adsorption increased with increasing protein concentration. This provided us with a system with which we could study GM2AP membrane binding in an attempt to gain a better understanding of the molecular protein interactions involved in the GM2AP lipid membrane binding process.

CHAPTER 1
INTRODUCTION AND BIOLOGICAL RELEVANCE

Gangliosides

Gangliosides are a group of glycosphingolipids(GSLs) found primarily in the outer leaflet of eukaryotic neuronal cell plasma membranes.[1] Gangliosides are comprised of a sialic acid-containing oligosaccharide chain and a ceramide (sphingosine linked to a fatty acid) moiety.[2] Synthesis occurs in the endoplasmic reticulum and golgi apparatus where ceramide is first made, followed by the stepwise addition of sugar and sialyl groups to an oligosaccharide chain by specific glycosyltransferases.[2,3] The glycosyltranferases involved in synthesis determine the particular sequence, linkage positions, and configurations of gangliosides.

Six monosaccharides, namely, fucose (Fuc), glucose (Glc), galactose (Gal), *N*-acetyl-glucosamine (GlcNAc), *N*-acetylgalactosamine (GalNAc), and sialic acid *N*-acetylneuraminic acid (NeuNAc), are the only carbohydrates that appear in the oligosaccharide component of gangliosides characterized from vertebrate cells and tissue to date.[2] All ganglioside names begin with the letter G for ganglioside, followed by one of the letters M (mono), D (di), T (tri) or Q (quarto) indicating the number of sialic acids that are in its structure. The name ends with a number x, where 5 – x depicts how many non-sialic acid monosaccharides are parts of the structure. The letter ‘a’ or ‘b’ is placed after the number in higher gangliosides to indicate that there are one or two sialic acid residues linked to the galactose residue nearest to the ceramide moiety of the lipid respectively. For example, Figure 1-1 shows a structure of GD1a, a ganglioside that consists of two sialic acid residues linked to four other monosaccharides where one

of the sialic acid residues in connected to the galactose residue closest to the ceramide moiety.

Function and Catabolism of Gangliosides

Gangliosides are ubiquitous constituents of tissues and cells, and their oligosaccharide groups undergo alterations with cell differentiation, cellular development, and ontogenesis.[2] Often times, the sialic acid residue(s) in gangliosides serve as recognition sites and allow these GSLs to act as receptors for bacteria, viruses, bacterial toxins, and adhesive proteins.[2] They also function as antigens, mediators of cell adhesion and modulators of signal transduction,[4] as well as support the functions of membrane bound receptors and enzymes.[5] Additionally, gangliosides are essential in homeostasis of biological functions, they participate in transmembrane cell signaling events, cell-cell interactions, and preventing inappropriate degradation by forming a protective layer on biological membranes.[3,6]

Gangliosides and other components of membranes are degraded by endosomal/lysosomal membrane digestion. This process is essential for cellular membrane stability.[7] Once degraded, the products are either recycled and re-used in salvage processes, or are further degraded.[8,9] First, components of plasma membranes are endocytosed by coated pits, and are trafficked in the form of vesicles through the endosomes where lipids are sorted and sent to the Golgi apparatus, lysosome, or back to the plasma membrane.[10] During endocytosis the lipid composition of internal membranes and the cell's luminal pH decreases from the early endosome, to the late endosome and then to the lysosome. The lysosome exhibits a decrease in membrane-stabilizing cholesterol and other sterols, and an increase in the anionic lipid, bis(monoacylglycero)phosphate (BMP), and an acidic pH of 4.5.[7,10]

Once in the acidic lysosomal cell compartment, gangliosides and other glycosphingolipids are catabolized by a stepwise cleavage of sialic acid and monosaccharide groups from the nonreducing end of the oligosaccharide chain by water-soluble exohydrolases. For multisialogangliosides, degradation begins with the sequential removal of sialic acid residues by neuraminidase until GM1 is formed (Figure 1-2).[11] In vivo, membrane bound monosialogangliosides with four or fewer sugar head groups are not sufficiently accessible to the exohydrolases so sphingolipid activator proteins (SAPs) are required for cleavage.[3,7,9,10] GM1 is degraded to GM2 by β-galactosidase in the presence of SAP-B of GM2 Activator Protein (GM2AP).[12] GM2 is further degraded by β-hexosaminidase A (Hex A) in the presence of GM2AP to form GM3.[13] Sialidase in the presence of Sap-B degrades GM3 to form lactosylceramide,[14] which is further degraded to glucosylceramide by GalCer- β-galactosidase or GM1- β-galactosidase in the presence of Sap-B and Sap-C.[15] Glucosylceramide catabolises to form ceramide by glucosylceramid- β-glucosidase in the presence of Sap-C and then finally sphingosine is formed by acid ceramidase in the presence of Sap-D.[16] Figure 1-3 shows a flow chart of the catabolism of the above mentioned gangliosides as well as other GSLs.

In the absence of SAPs or detergents, exohydrolases are not able to degrade membrane bound gangliosides with four or fewer sugar head groups because they are not far enough into the aqueous space and away from the lipid core.[17] Defects in ganglioside degradation due to genetic mutations of exohydrolases or SAPs can lead to a buildup of gangliosides in the lysosome resulting in apoptosis and a wide range of

lysosomal storage diseases called gangliosidoses. This dissertation will further discuss the GM2-gangliosidoses.

GM2 Gangliosidoses

The degradation of GM2 to GM3 relies on the exohydrolase, Hex A. This enzyme is a heterodimer with α and β subunits. Together with GM2AP, these three gene products are required for the degradation of GM2.[3] Since gangliosides are found primarily in neuronal cells, gangliosidoses are diseases of the nervous system. GM2 gangliosidoses are inherited, genetic disorders with incidences of about 1 in every 310,000 births.[18] When there is a genetic mutation in the Hex A α subunit, the catabolism of GM2 ganglioside is inhibited, resulting in Tay-Sachs disease. Similarly, defects in the β subunit of Hex A and GM2AP causes Sandhoff disease and AB Variant respectively, due to a buildup of GM2 in the cell.[3]

Tay-Sachs disease

Tay-Sachs disease is the most prevalent of the GM2 gangliosidoses and is inherited as a Mendelian autosomal recessive trait.[19] Infantile Tay-Sachs disease is caused by the absence or catalytic defect of Hex A due to mutations of the gene encoding the α subunit of the enzyme. If the mutations allow Hex A some degree of residual activity, milder forms of the disease, namely Juvenile Tay-Sachs and Adut Tay-Sachs disease, arise with a later onset. The gene coding for this subunit is on chromosome 15 and more than 75 mutations have been reported.[20] The disease is more prevalent among persons of Ashkenazi Jewish and French Canadian descents.[21]

Tay-Sachs disease was first reported in 1881 by the British ophthalmologist Warren Tay,[22] and fifteen years later by Bernard Sachs, an American neurologist.[23] The classical infantile form of the disease appears usually six months after birth with

progressive psychomotor retardation, regression and loss of mental skills.[19] By age one, patients experience seizures, blindness and the inability to crawl or stand. After age two, persons with Tay-Sachs disease develop spastic quadriplegia and reach a decerebrate stage, which leads to death by age four.[19,21]

Sandhoff disease

Genetic defects in the β subunit of Hex A give rise to Sandhoff disease, a similar and almost indistinguishable neurological condition from Tay-Sachs. Konrad Sandhoff and his colleagues first differentiated this disease from Tay-Sachs when they discovered a massive accumulation of glycosphingolipids and other glycoprotein fragments with a terminal hexosamine residue both in the central nervous system and systematic organs.[24] The increase in glycosphingolipid accumulation is due to defects also in β-hexosaminidase B, a homodimer with β subunits of hexosaminidase.[25] The gene coding for the β subunit is coded on chromosome 5 and only a few mutations have been reported.[3] Unlike Tay-Sachs disease mutations in the subunit is more prevalent in the Creole/Spanish community of Cordoba, Argentina, the Maronite community of Cyprus, and the Metis Indians of Saskatchewan.[21]

Though clinically and neurologically similar to Tay-Sachs, Sandhoff disease also causes nonneurologic events including the simultaneous enlargement of the liver and spleen, occasional foamy histocytes in the bone marrow, and the occurrence of N-acetylglucosamine-containing oligosaccharides in urine.[3] The most common neuropathological findings are related to delayed myelination or demyelination and the degree of GM2 accumulation is more severe than in Tay-Sachs disease.[21] Persons with infantile Sandhoff disease usually die by age three though late onsets variants of the

disease have been reported where the symptoms are delayed for two to ten years (juvenile) or even into late adult life.[3]

AB Variant

Persons who exhibit an accumulation of GM2 in neuronal cells, despite showing normal activities of Hex A are said to have AB variant.[26] This rarely diagnosed variant is due to a deficiency of the GM2 Activator protein, the accessory protein necessary for the hydrolysis of GM2 by Hex A.[3] The gene coding for GM2AP is located on chromosome 5 and only five mutations in the gene have been reported.[26] AB variant presents in similar fashion to classical infantile Tay-Sachs, where infants lose motor skills, develop seizures and, vision and hearing loss, paralysis and ultimately death during early childhood.[26] The disease isn't prevalent among any ethnic group and no cases of late onset variants have been described.

β-Hexosaminidase A

β-hexosaminidase A (Hex A) is one of three isoenzymes of lysosomal hexosaminidases that exist; the other two being β-hexosaminidase B (Hex B), and β-hexosaminidase S (Hex S). Collectively the β-hexosaminidases hydrolyze the β-glycosidic bond of N-acetylglucosamine (GlcNAc) and N-acetylgalactosamine (GalNAc) residues from glycoproteins, oligosaccharides, and glycosphingolipids.[3] Each isoenzyme is composed of two noncovalently linked subunits, α and β, which differ in their substrate specificity.[27,28] Hex A is a αβ heterodimer, while Hex B and Hex S are ββ and αα homodimers respectively. Both the α and β subunits of the hexosamindases contain active sites but dimerization is required for catalytic cleavage.[3]

The active site on the β subunit of hexosaminidases cleaves neutral, water-soluble oligosaccharide chains with terminal GlcNAc and GalNAc terminal residues, but the less

active site on the α subunit can also cleave the sugar groups from negatively charged substrates.[29] Because of this, only Hex A is able to catabolize GM2 in the lysosome. GM2 consists of four sugar head groups, hence steric hindrance prevents Hex A from directly hydrolyzing the membrane bound GM2 ganglioside. Therefore, GM2AP, a sphingolipid activator protein, is required to solubilize GM2 from the membrane and present the ganglioside in the proper orientation for cleavage. The accepted mechanism is that GM2AP binds to the ceramide moiety of GM2 forming a 1:1 complex. The protein:lipid complex then interacts with the α subunit of Hex A and forms a ternary complex where the terminal GalNAc group is cleaved, forming GM3.[3,30]

Sphingolipid Activator Proteins

Sphingolipid Activator Proteins (SAPs) are a group of small, heat stable glycoproteins that are essential for the degradation of gangliosides and other glycosphingolipids with short (four or fewer) oligosaccharide headgroups.[13,31] When glycosphingolipids with a short carbohydrate chain reach the lysosome for catabolism after endocytosis, the terminal sugar residue is not situated far enough from the vesicular membrane for cleavage by exohydrolases at the water-lipid interface. SAPs facilitate this process by binding to the lysosomal membrane vesicles, solubilizing the glycosphingolipids and making the substrate accessible to its specific enzyme for degradation.[10,13]

There are five known SAPs to date and they are encoded by two genes. One gene codes for a precursor protein, prosaposin, which is proteolytically processed to form four highly homologous proteins called Saposin A, B, C and D.[32-34] The second gene codes for the fifth SAP, GM2 Activator Protein, which doesn't share structural homology with the other SAPs.[25,35-37]

Saposins A-D

Saposins A, B, C and D are water soluble, lipid membrane binding, and transfer proteins. They are derived from the proteolytic processing of the 70 kDa precursor glycoprotein, prosaposin in the late endosomes and lysosomes of cells.[7,32] First, the N-terminal peptide preceding the saposin A domain is cleaved, followed by the release of saposin A, which results in the formation of a saposin B-D trimer. The trimer is then cleaved via sap B/C and C/D dimers, forming mature proteins of about 80 amino acids each, weighing 8-11 kDa.[10,13]

The x-ray crystallographic structures of the human recombinant forms for all four saposins have been determined.[38-40] Saposins A-D are structurally homologous showing a conserved *N*-glycosylation site and six highly conserved cysteine residues that have the same pairings to form three disulfide bonds.[41] They contain an α-helical bundle of five α-helices where several hydrophobic residues serve as the internal structure. The structure is stabilized by the disulfide bridges which are thought to be necessary for protein function, and also responsible for the high level of stability against heat, acid, and proteolytic enzymes.[13,42,43]

The saposins differ in specificity despite their high degree of homology. *In vivo,* saposin A is required for the degradation of galactoceramide by galactoceramide-β-galactosidase,[9] and a genetic defect in the protein results in juvenile and sometimes a late onset of Krabbe disease.[10] *In vitro*, saposin A is shown to bind to GM1 and GM2, and to stimulate the hydrolysis of glucosyl- and galactocylceramide.[44] Saposin B was the first saposin to be discovered and it seems to be the least specific of the enymes.[25,31] *In vivo,* it is required for the catabolism of a number of GSLs including sulfatide, globotriaosylceramide, digalactosylceramide, sphingomyelin and GM1 (Figure

1-3). Due to this, saposin B is said to behave like a general, physiological detergent.[9,25] Saposin C is specific for the degradation of glucosylceramide by glucosylceramide-β-gucosidase and a deficiency of this protein leads to a juvenile form of Gaucher disease.[45,46] Saposin D participates in the degradation of ceramide by acid ceramidase both in cultured cells,[47] and *in vitro.*[44] It has also been reported that saposin D binds to, and solubilized vesicles that contain negatively charged lipids.[48]

GM2 Activator Protein

GM2AP, the fifth SAP, is essential for the degradation of the ganglioside GM2 by β-hexosaminidase A (Hex A). The protein's role involves binding to, and solubilizing GM2 from intralysomal vesicle membranes. It is believed that GM2AP recognizes the hydrophobic ceramide moiety,[49] the sialic acid moiety, and the N-acetyl-galactosamine moiety of GM2.[50] The protein-lipid complex leaves vesicles and is recognized by HexA where GM2 is hydrolyzed in solution, and GM3 is released.[1,51,52] Specifically, the terminal GalNAc sugar residue is cleaved from the GM2 tetrasaccharide (GalnAcβ1→3(NeuAcα2→3)Galβ1→4Glc1→1'Cer) head group to form GM3(Figure 1-4).[1,53] It has been determined from in vitro sedimentation experiments that less than 15% of the activator protein is membrane associated and BMP, which is found in the lysosome in increased concentrations, enhances the extraction efficiency of GM2AP.[54]

GM2AP is structurally different from saposins A-D. It is larger, carries one n-glycosylation, contains eight cysteine residues and adopts a β-cup topology instead of the predominantly α-helical secondary structure seen in the saposins.[13] A detailed description of GM2AP will be given below.

Biosynthesis and posttranslational modifications

GM2AP is synthesized on the endoplasmic reticulum as a 193 amino acid prepro-polypeptide. The pre-sequence is a 23 amino acid signal peptide that directs both the protein synthesis and its extrusion into the lumen; it is believed that the pre-sequence is cleaved from the newly formed protein cotranslationally.[25] As was previously mentioned, GM2AP contains eight cysteines. The oxidizing environment of the ER helps the formation of four disulfide bridges. The GM2AP sequence contains a N-glycosylation site at Asn63-Val-Thr with the initiating Met being considered residue 1 (another style starts numbering the final protein at residue 32 due to the preprosequence). The preassembled oligosaccharide is made of many mannose groups where one or more is phosphorylated in the endoplasmic reticulum and golgi after glycosylation, so that the protein can be delivered to the lysosome via the mannose-6-phosphate receptor.[3,55] Once in the lysosome, the 8 amino acid prosequence is removed during processing of the N-terminus, leaving a mature, 162 amino acid protein weighing between 20 and 27kDa depending on its oligosaccharide composition.[25] The deglycosylated form of GM2AP weighs approximately 18 kDa.[7]

GM2AP structure

The crystal structure of the nonglycosylated form of GM2AP purified in *Escherichia coli* has been solved and shows that there are three distinct monomers of the protein in the 11 monomer unit cell (Figure 1-5).[53] The properly folded protein forms a single globular domain with dimensions 45 Å x 28 Å x 25 Å.[53] The secondary structure of the protein comprises of an eight-stranded β-cup fold forming a hollow hydrophobic pocket which includes approximately half of the total amino acid residues in the protein.[53] The dimensions of the cavity are 12 Å x 14 Å x 22 Å and together with the hydrophobic

residues that line the cavity, it is suitable for binding the acyl chains of lipids like the protein's specific ligand, GM2.[53] The hydrophobic pocket is accessible from one end of the protein only,[56] and is lined by surface loops and a 2.5-turn alpha helix at its rim, which is thought to be the interaction site with HexA to allow GM2 degradation.[53] The four independent disulfide bonds are located at surface regions of the protein, where they connect flexible loops at the rim of the hydrophobic cavity and are thought to be the reason for GM2AP's high stability.[53]

Loop regions in GM2AP were identified after structural refinement analysis of the crystals at sites spanning residues 58-78, 87-97, and 120-133.[53] The residues in these regions exhibited high B-factors and were found in different conformations for different monomers within a unit cell, with the loop region of residues 120-133 being the most flexible.[53] Figure 1-5 shows crystal structures of the three monomers found in the 11 monomer cell. Monomers A and B shows the position of the loop region of residues 120-133 in a somewhat 'closed' conformation, but monomer C shows the region in an 'open' conformation with the side chains rotated outward and away from the protein's hydrophobic cavity. The entrance to the hydrophobic cavity of GM2AP differs by 3Å with the two loop conformations, suggesting the region may facilitate lipid extraction.[57,58]

GM2AP function

In vivo, GM2AP participates in the lysosomal catabolism of GM2 to GM3 by HexA. Without GM2AP, HexA is not able to hydrolyze the terminal GalNAc group of GM2 in liposomes.[49] Like the other SAPs, one known function of GM2AP is to act as a biological detergent and act as a 'liftase', forming water soluble complexes with glycolipids.[59] Because of this, GM2AP is known to function as a general glycosphingolipid transfer protein, where it is known to extract other GSLs like GM1 and

GA1 from liposomes or micelles and transfer them as soluble 1:1 complexes between membranes.[25,56-58,60,61] Utilizing a fluorescence dequenching assay, the binding affinity and specificity of GM2AP were determined.[50] The results indicated that the binding affinity to selected gangliosides is GM2 >> GT1b >> GM1 ≈ GM3 > GA2.

Crystal structure analyses of ligands bound in the hydrophobic pocket of GM2AP shows that the protein accommodates ligands in different binding modes – one for gangliosides, and another for glycerophospholipids.[57] It has been shown that GM2AP binds GM2 in such a way that the 18-carbon acyl chains are within the hydrophobic pocket while the tetrasaccharide head group of the ligand sticks out of the protein, into the aqueous environment.[57] While the fatty acid tails of phosphatidylglycerol (PG) binds in a similar position to the acyl chains of GM2, the head group of the head group on the other hand is buried in the hydrophobic pocket.[57]

Other physiological roles have been credited to GM2AP for example, it has been thought to act as a factor that stimulates and enhances the association between phospholipase D and enzyme activators.[62,63] GM2AP is also thought to participate in the regulation of proton pumps in intercalated kidney cells.[64,65] Additionally, GM2AP was shown to bind platelet activating factor (PAF), inhibiting its action.[66] A GM2AP:lysoPAF complex was observed via X-ray crystallography, and introduced the possibility that GM2AP may display some hydrolase activity towards PAF.[60]

Glycerophospholipids

Glycerophospholipids, also known as phosphoglycerides, are the most common group of structural lipids that constitute eukaryotic cell membranes. They are a group of glycerol containing lipids with a phosphate headgroup, that are derived from sn-3-glycero-phosphate(Figure 1-6A).[11] Glycerophospohlipid anatomy and nomenclature

utilizes the stereospecific numbering (sn) system where two fatty acid chains, R1 and R2, are attached via an ester linkage to the first (sn-1 position) and second (sn-2 position) carbons of the glycerol backbone.[67,68] The R groups consist of saturated or cis-unsaturated acyl tails of varying length (Table 1-1), and make up the hydrophobic portion of the lipid.[11,69] The polar portion of the lipid consists of the glycerol backbone and a highly polar or charged functional group, Y (Table 1-2), attached via a phosphodiester linkage to the third (sn-3 position) carbon of glycerol.[67,68] Figure 1-6B depicts the general anatomy of glycerophospholipids. The specific functional group along with the nature and chain length of fatty acids determine physiochemical properties and structural and functional roles of glycerophospholipids in cell membranes.[11,70]

Selected lipid systems as biological membrane models: Lipid systems have been used in a number of scientific research fields to mimic biological membranes. One of the first and still the most common lipid system used as biological membrane models is the lipid vesicle, also called the liposome (Figure 1-7A). Liposomes are spherical in shape and are typically composed of amphiphilic molecules such as phospholipids. They provide a closed, stable and regular bilayer membrane and have been utilized to study protein and DNA interactions with lipids,[71] the permeability of ions and drugs[72,73] and other molecular biological processes. Liposomes may exist as small unilamellar vesicles with diameters less than 50 nm, as large unilamellar vesicles with diameters between 100 and 1000 nm, or as multilamellar vesicles consisting concentric, multiple vesicular bilayers.

Under physiological conditions, membrane lipids can exist as two lipid monolayers forming a two dimensional sheet, called a bilayer (Figure 1-7B).[70] Bilayer formation occurs more readily with glycerophospholipids and sphingolipids, where the cross-sectional areas of the head groups and acyl tails are similar.[67] Because the hydrophobic regions at the edges of bilayers are transiently in contact with water, the sheets are unstable and tend to spontaneously fold back on itself to form liposomes.[70] Lipid bilayers on solid supports solve this problem. Tamm and McConnell developed the first solid supported lipid bilayer system when they deposited lipid membranes separated by a thin aqueous layer on quartz, glass, and oxidized silicon.[74] These bilayers on solid supports resemble cell membranes because they retain and represent fluidity and lateral mobility;[75] and provide a system with which to investigate molecular biological processes like protein-lipid interactions.

Substrates used to support phospholipid bilayers with high lipid mobility and little or no defects, need to be hydrophilic, smooth and clean.[75] Fused silica, borosilicate glass, mica, oxidized silicon, as well as thin films like titanium IV oxide, indium-tin-oxide, silver, gold, and platinum have been utilized as supports for lipid bilayers.[74,75] Lipid layers tethered to metal surface offer a means to study biological membrane processes via electrochemical or optical means.[76] It has also been reported that inorganic supports like zirconium phosphonate may also be used to support phospholipid bilayers.[77] Langmuir-Blodgett (LB) technique and Langmuir-Schaefer procedures,[74] along with lipid adsorption and fusion,[78] are the usual methods used for the formation of supported phospholipid bilayers on substrate supports. The Langmuir deposition methods involve controlled dipping or pulling of a support through an organic amphipatic monolayer,

while lipid adsorption and vesicle fusion involve exposing the hydrophilic support to liposomes.

Hybrid bilayers are another approach to mimicking cell membranes.[76,79,80] This process involves the use of metal supported alkanethiol self assembled monolayer (SAM), and monolayer of a phospholipid (Figure 1-7C). The term hybrid is used because the bilayer consists of natural and synthetic parts. The SAM layer is formed by incubating a clean gold substrate with an alkanethiol solution in ethanol and allowing the alkanethiol to self assemble on the gold surface, rendering the surface hydrophobic. The resulting covalent interaction with the gold surface is not chemically affected by changes in pH, ionic strength, lipid composition, or type of buffer.[80] The phospholipid monolayer is then added to the SAM either by vesicle fusion,[79] or lipid transfer from an air-water interface.[81]

Research Overview

This project aims to investigate membrane binding and extraction of lipids by GM2AP in order to determine the precise molecular interactions involved in these processes. Studies on the interaction of GM2AP with its specific ligand GM2 have been performed using several techniques such as sucrose density ultracentrifugation, sucrose density isoelectric focusing, polyacrylamide gel electrophoresis, circular dichroism, and steady-state fluorescence spectroscopy.[51,52] Additionally, GM2AP's role as a lipid transfer protein has also been investigated using gel filtration chromatography, thin-layer chromatography (TLC), fluorescence resonance energy transfer (FRET), fluorescence dequenching assays, surface plasmon resonance and a dansyl- based fluorescence assay.[27,51,52,82-84]

Despite the fact that the crystal structure and function of GM2AP are known, the orientation of the protein when interacting with lipid bilayers and the specific mechanism of interaction with vesicular membranes, followed by extraction and transfer of lipids/ligands, are still being determined. Due to the intrinsic tryptophan fluorescence of GM2AP, and the fact that two of the three tryptophan residues are located in regions thought to be involved in binding to the vesicular membrane, fluorescence spectroscopy is deemed a useful technique to resolve these questions. Additionally, gel filtration chromatography has also been proven to be convenient for studying the interactions of GM2AP with GSLs.[51]

First, a series of tryptophan to alanine mutations were constructed via site-directed mutagenesis to determine the fraction of accessible intrinsic fluorophore to charged and neutral quencher in solution. Gel filtration and dansyl-based fluorescence assays were employed to determine the changes in lipid binding and/or extraction as a function of pH and hydrophobicity as a result of substituting A for W in the putative membrane binding loops of the protein.

The membrane perturbing properties and function of SAPs including GM2AP have been shown to be dependent on, or greatly increased in the presence of acidic lipids like BMP, PI, PS and PG in lipid membranes.[27,42,43,85] Surface plasmon resonance enhanced ellipsometry (SPREE) was used to further study interactions between GM2AP and select phospholipids (PC and PG) on a solid supported membrane model system. Additionally, a newly developed zirconium octadecylphosphonate surface based system,[77] was investigated to determine its suitability for studying glycerophospholipid membrane binding by GM2AP.

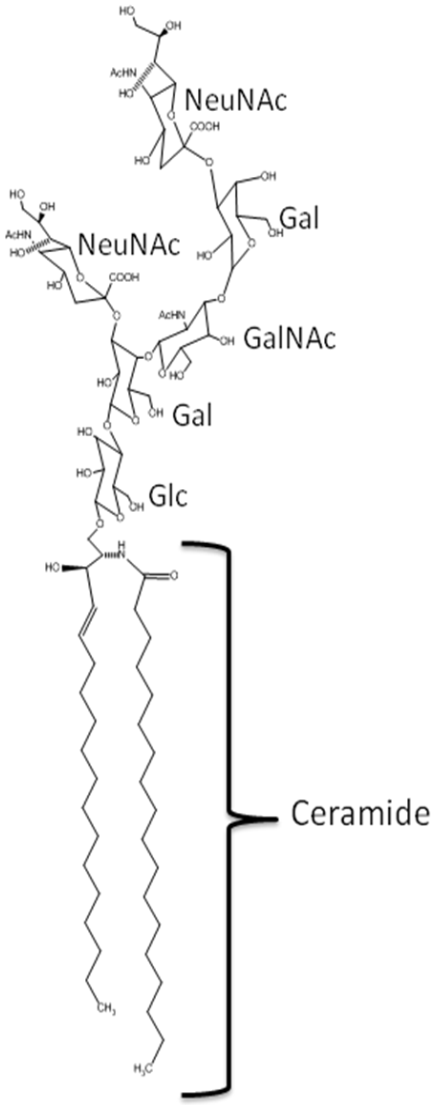

Figure 1-1. Structure of GD1a ganglioside. Gangliosides consists of a ceramide tail and oligosaccharide head group, of which two of the sugar residues are sialic acids

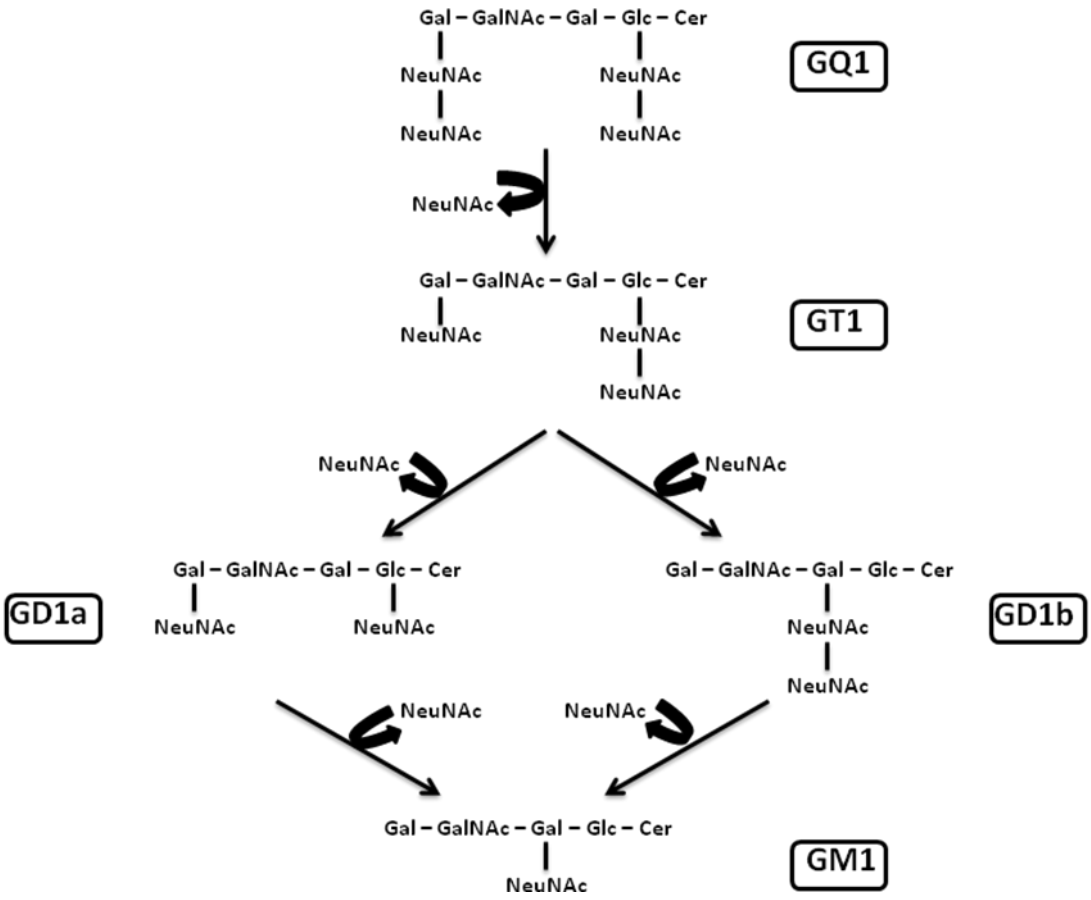

Figure 1-2. Degradation pathway of multisialogangliosides to form GM1

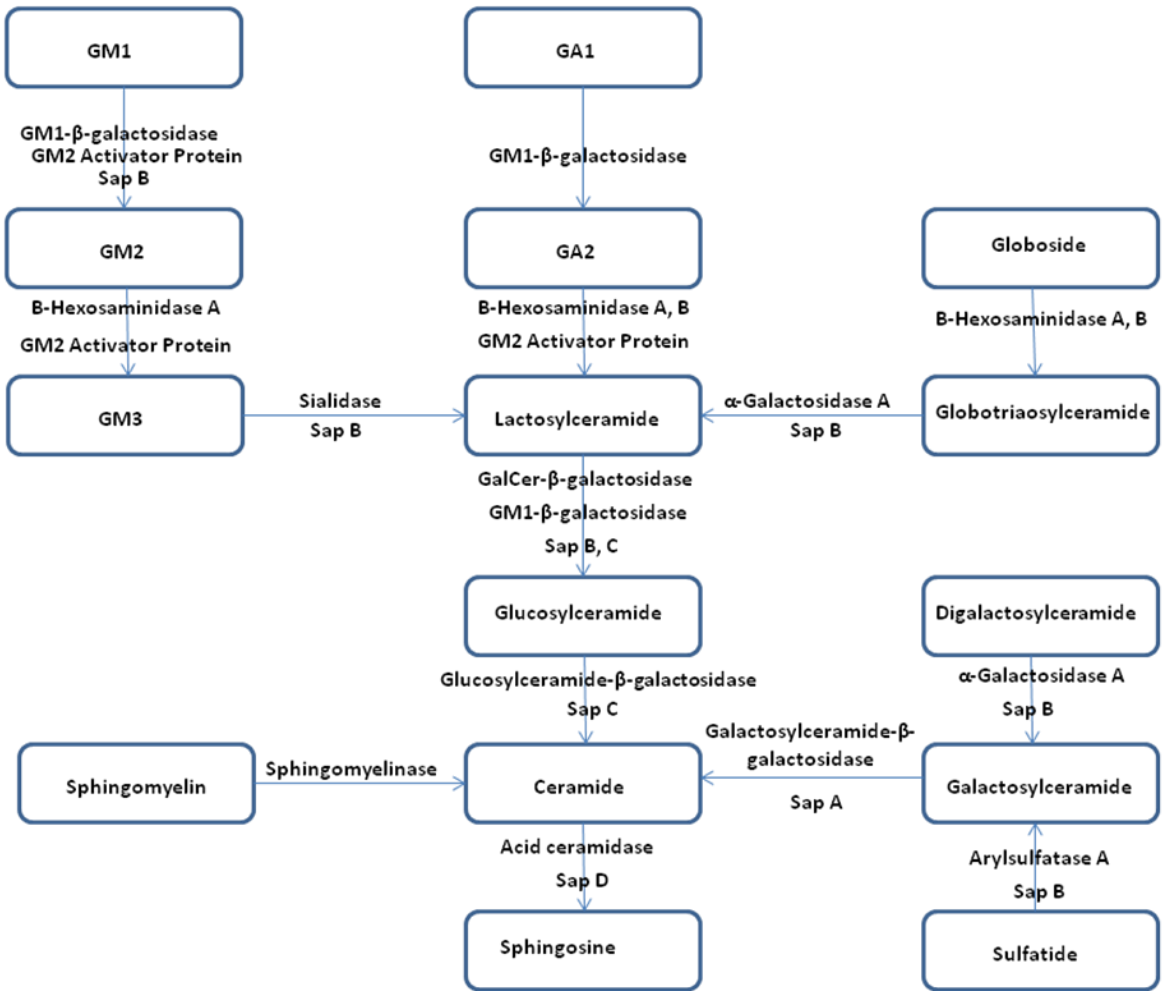

Figure 1-3. Lysosomal catabolism of gangliosides and other glycosphingolipids showing the necessary exohydrolases and sphingolipid activator proteins required for degradation

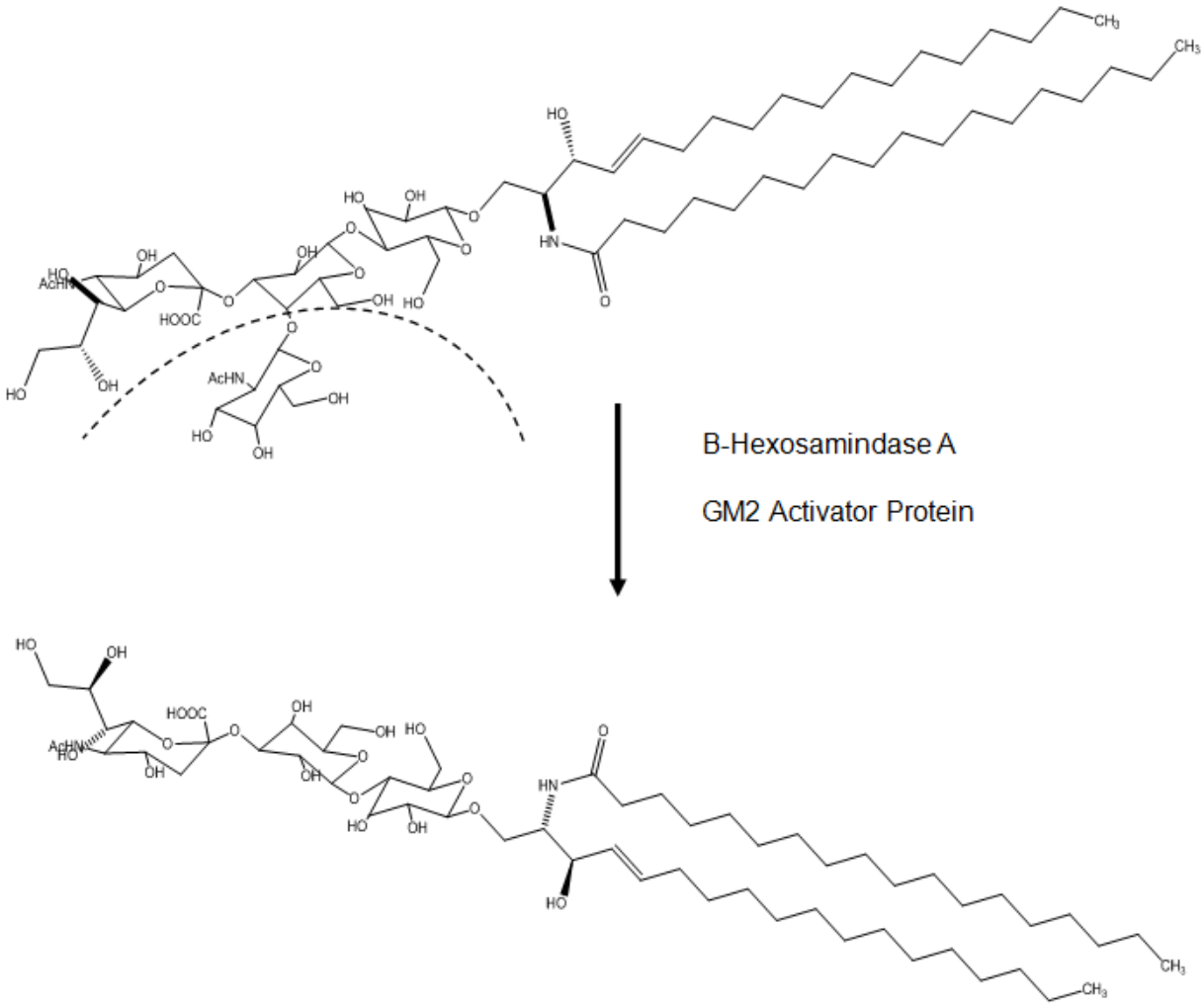

Figure 1-4. GM2 Activator protein assisted hydrolysis reaction that converts GM2 to GM3. The terminal N-acetylgalactose (GalNAc) monosaccharide is cleaved by β-hexosaminidase A (Hex A)

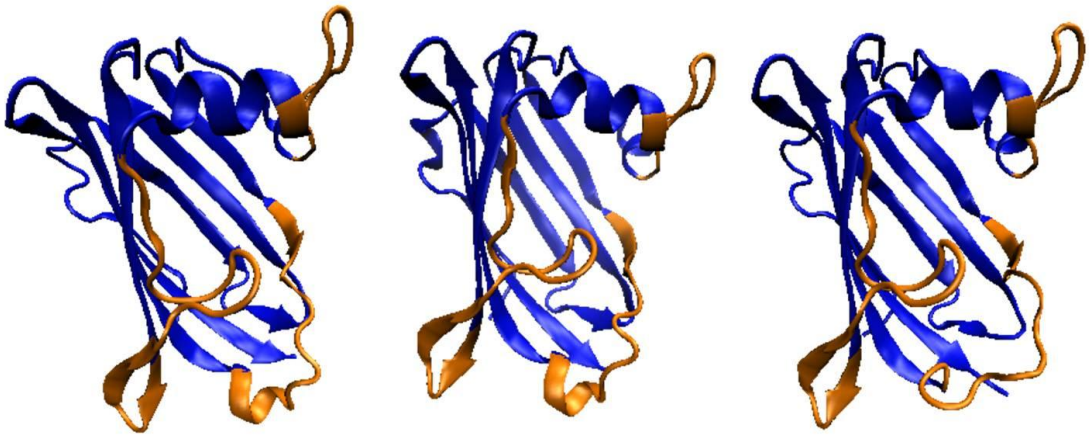

Chain A Chain B Chain C

Figure 1-5. Ribbon diagrams showing three different structural conformations of GM2AP (PDB ID 1G13) within one unit cell. The mobile loops of the protein are highlighted in gold

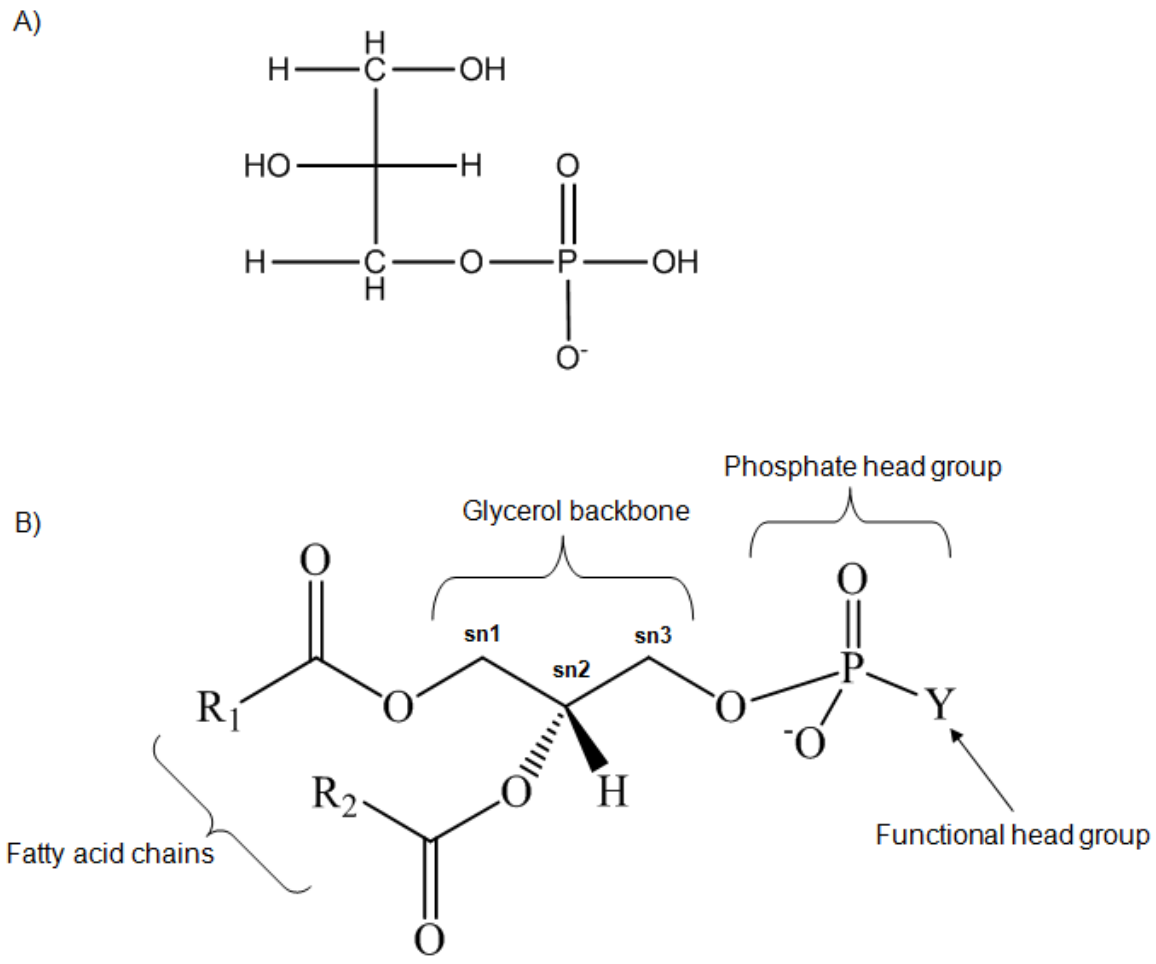

Figure 1-6. Chemical structure of A) *sn*-glycerol-3-phosphate B) the general anatomy of glycerophospholipids

Table 1-1. Selected naturally occurring fatty acid chains

Chain	Chemical Formula	Systematic (Common) Name
14:0	$CH_3(CH_2)_{12}COOH$	*n*-Tetradecanoic (Myristic) acid
16:0	$CH_3(CH_2)_{14}COOH$	*n*-Hexadecanoic (Palmitic) acid
18:0	$CH_3(CH_2)_{16}COOH$	*n*-Octadecanoic (Stearic) acid
24:0	$CH_3(CH_2)_{22}COOH$	*n*-Tetracosanoic (Lignoceric) acid
16:1 (Δ^9)	$CH_3(CH_2)_5CH=CH(CH_2)_7COOH$	*cis*-9-Hexadecanoic (Palmitoleic) acid
18:1 (Δ^9)	$CH_3(CH_2)_7CH=CH(CH_2)_7COOH$	*cis*-9-Octadecanoic (Oleic) acid
18:2 ($\Delta^{9,12}$)	$CH_3(CH_2)_4CH=CHCH_2CH=CH(CH_2)_7COOH$	*cis*-,*cis*-9,12-Octadecanoic (Linoleic) acid

Table 1-2. Common glycerophospholipids with their net charge at acidic lysosomal pH

Functional Group (Y)	Chemical Formula	Net Charge at pH 4.5
Hydroxyl	-OH	-1
Choline	$-CH_2 – CH_2 - {}^+N(CH_3)_3$	0
Ethanolamine	$-CH_2 – CH_2 - {}^+NH_3$	0
Serine	$-CH_2 – CH(COO^-) - {}^+NH_3$	-1
Glycerol	$-CH_2 – CH(OH) – CH_2 – OH$	-1
Inositol	$C_6H_6(OH)_6$	-1

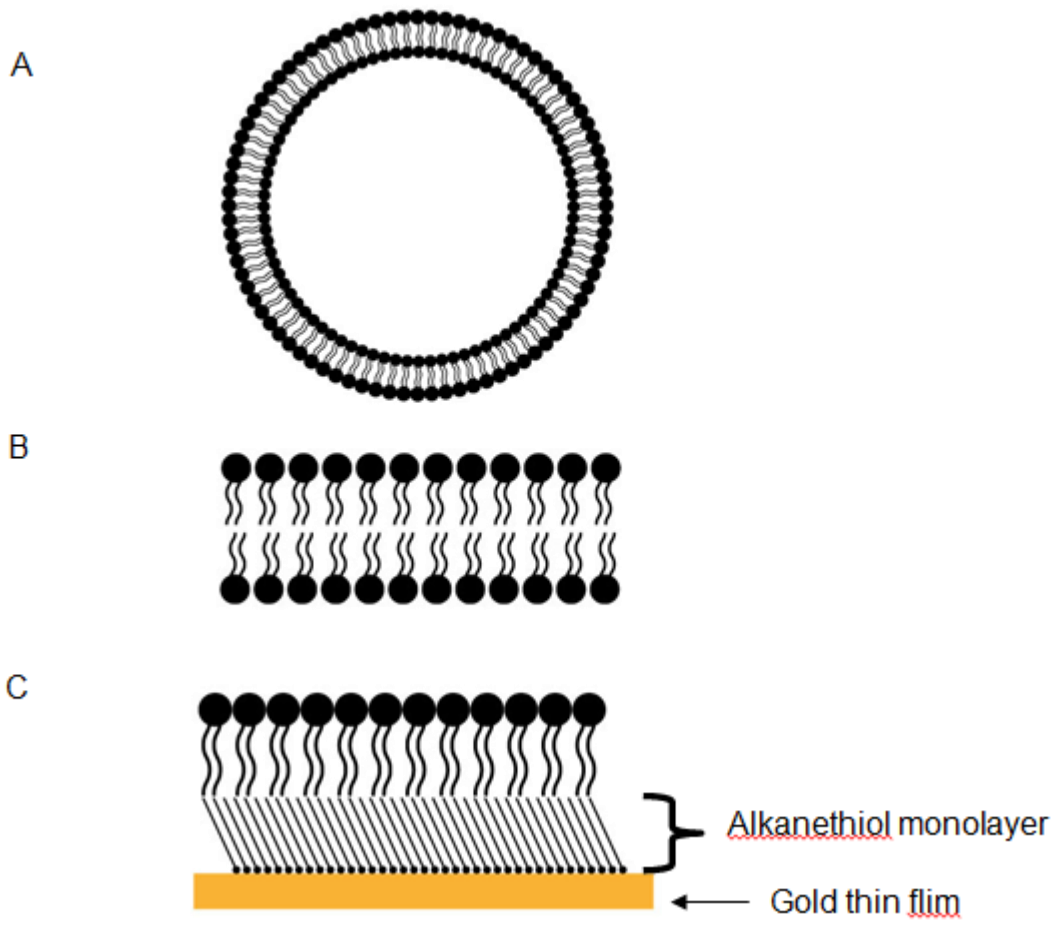

Figure 1-7. Biological membrane models. A) Lipid vesicles (liposomes). B) Lipid bilayer. C) Hybrid lipid bilayer

CHAPTER 2
THEORY OF TECHNIQUES

Circular Dichroism Spectroscopy

Circular dichroism (CD) spectroscopy is a powerful and technique used to monitor and study the secondary structure of proteins in solution. Using far UV absorption, CD spectra is extremely sensitive to the analysis of alpha helix, beta sheet, turn, and 'random' secondary types in proteins.[86] Advances in molecular biology have allowed proteins to be produced in a number of host systems in their native form, as site-directed mutants, or being engineered synthetically. Other techniques like X-ray crystallography and nuclear magnetic resonance spectroscopy are also capable of giving higher resolution structural information on proteins. However, CD is nondestructive, is able to study protein structure under a variety of experimental conditions, and good spectra can be obtained on less than 0.1 mg of samples in 30 minutes or less making it a useful technique for monitoring the structure of these proteins.[87,88]

Similar to ultraviolet-visible (UV-Vis) spectroscopy, CD spectroscopy is based on the absorption of light as a function of wavelength.[86] Absorption wavelength depends on the type of chromophore and/or arrangement of atoms in the sample. Proteins for example, absorb strongly in the UV region of the electromagnetic spectrum due to peptide bonds, amino acids with aromatic side chains (tyrosine, phenylalanine, and tryptophan), disulfide bonds, and any prosthetic groups.[89] For our purposes, we focus on contributions to CD spectra in the far-UV spectral region (190-250 nm) where secondary structural information can be obtained due to the electronic absorption of peptide bonds in the protein backbone.[87]

Polarized Light

Light is an electromagnetic wave comprising an electric, E, and a magnetic, B, field vector which are mutually perpendicular and also perpendicular to the direction of propagation of the wave.[90] We specifically consider the strength and direction of E because the specification of E completely determines B and it has a stronger interaction with matter than B. At any point in an electric field, light of a single wavelength can be resolved into three oscillations along an x, y, z-coordinate system. Figure 2-1 illustrates a light wave as a plane wave travelling along the z axis. The electric field is orthogonal to the z axis and the oscillations have the same frequency, but usually different amplitudes and phases.

Polarization is defined as the behavior with time of a vector field at a fixed point in space. Unpolarized light emits light that has components with electric fields oriented in all positions perpendicular to the direction of travel. However, if all of the photons in a light beam have the electric field oriented in the same direction, the light is said to be polarized. If the phase of the x and y oscillations are the same, the polarization is linear. If the phases differ by +/- 90° the polarization is circular. Light is elliptically polarized in all other cases where the phases are different. In fact, linearly and circularly polarized light are specific cases of the more general elliptically polarized state of light.

Principle of CD

Absorbance, A of electronic transitions in species is measured according to Beer-Lambert law

$$A(\lambda) = \varepsilon(\lambda)lc \qquad (2\text{-}1)$$

Where A has no units, ε is the molar extinction coefficient in liter mol^{-1} cm^{-1} at wavelength λ, l is the pathlength of the cell in cm, and c is the molar concentration of the

sample in mol liter^{-1}. Since ε is dependent on λ, A or ε can be plotted vs. λ to produce an absorption spectrum.

CD of a molecule is defined as the difference between the absorption of left and right circularly polarized light by a sample.[88] Plane polarized light is made up for two circularly polarized components with equal amplitudes: left- handed, L (rotating counter-clockwise), and right-handed, R (rotating clockwise). After passing through a chiral chromophore, L and R are absorbed to different extents thus yielding unequal molar coefficients. The resulting radiation no longer traces a circle, but now possesses elliptical polarization which can be monitored.

Proteins are chiral molecules with different ellipticity values for L and R circularly polarized light, ε_L and ε_R.[87,88] The difference between these quantities, $\Delta\varepsilon = \varepsilon_L - \varepsilon_R$, as a function of λ is plotted to produce a CD spectrum. CD bands may be either positive or negative depending on which type of light is absorbed more strongly. Ellipticity is historically the unit reported for the CD of samples, but others like mean residue ellipticity and delta epsilon have become more popular.[88] Ellipticites are typically in the range 10 mDeg. A CD signal is observed only if the chromophore in the sample molecule is intrinsically chiral, if it is covalently linked to a chiral center in the molecule, or if it is in an asymmetric environment.[88]

As was previously stated, CD signal due to the amide chromophores along protein backbones is sensitive to the various types of secondary structure.[87] Electronic absorption in the far UV region are due to the peptide bond which begins with a weak but broad $n \rightarrow \pi^*$ at 210-220 nm, followed by more intense $\pi \rightarrow \pi^*$ transition at 190 nm (Figure 2-2). CD signals that correspond to negative bands at 222 nm and 208 nm, and

a positive band at 198 nm are characteristic of α-helical proteins, whereas spectra for proteins with anti-parallel β-sheet structures exhibit negative and positive bands at 218 nm and 195 nm, respectively.[91] Disordered proteins with random coil conformations have very low ellipticity above 210 nm and negative bands near 195 nm.[91] Figure 2-3 shows the characteristic CD spectra of different secondary structural elements found in proteins. In our work, we use CD spectroscopy analysis to compare the secondary structure of our site-directed protein variants after they've been expressed and purified, to the spectrum of published wild-type,[92] to ensure that the protein is still properly folded.

Fluorescence Spectroscopy

Most biological processes with the exception of the storage of genetic information, involve proteins.[93] Proteins are extremely diverse in their secondary structure and function, and there always is ongoing interest in the relationship between the two. Specifically, researchers are interested in how proteins fold, how they recognize other molecules, and the mechanism involved when carrying out their particular function. While many analytical and biophysical techniques can be used to probe protein structure and function, no single one can provide a complete picture. X-ray crystallography and nuclear magnetic resonance provide detailed information about proteins that are essentially static, but fluorescence spectroscopy has the advantage of being able to study proteins in a more realistic dynamic state.

Fluorescence spectroscopy is a sensitive and selective optical technique that has been extensively used for many years in all scientific fields. With regard to protein fluorescence, the technique has been used to gain insight into the polarity of different regions of a protein, the flexibility of proteins, and the conformational transitions proteins

undergo.[93] In this work fluorescence quenching experiments were performed to determine the nature of the environment of tryptophan residues in GM2AP, and their accessibility to the quencher. Additionally, a dansyl based fluorescence assay was used to monitor the changes in the rates of lipid extraction by GM2AP from liposomes as a function of both pH and a series of tryptophan to alanine substituted constructs of the protein.

Principle of Fluorescence Spectroscopy

Photoluminescence, a process that occurs in fluorimetric analysis, is the emission of light from an atom or molecule in an electronically excited state. Depending on whether the analyte is in a singlet or triplet excited state, fluorescence or phosphorescence occurs. In a singlet excited state, the electron in the excited orbital is paired to an electron in the ground state of opposite spin. This permits return of the excited state electron to the ground state rapidly (10^8 s^{-1}) by emission of a photon.[94] Excitation to the singlet state followed by radiative relaxation of an electron between orbitals of different energies is illustrated by the Jablonski diagram (Figure 2-4). First, a molecule absorbs an incident photon of sufficient energy to promote an electron to a higher electronic state (for example S_2). Next, the molecule releases excess energy through vibrational relaxation and goes to the lowest energy of the excited state, S_1. The molecule then returns to the ground state (S_0) in a number of ways: 1. it fluoresces by emitting a photon, 2. It returns to the ground state nonradiatively through internal conversion, or 3. It transitions to the triplet state through intersystem crossing where it returns to the ground state via phosphorescence.[93] Phosphorescence is not discussed in this chapter.

Fluorescence emission can be characterized by its lifetime, quantum yield, anisotropy, or simply by its emission spectrum. Fluorescence lifetime, τ, is defined as the average time a molecule spends in the excited state before returning to the ground state and is defined by:

$$\tau = \frac{1}{\Gamma + k_{nr}} \tag{2-2}$$

where Γ and k_{nr} are both rate constants. Fluorescence lifetimes are usually close to 10 ns.[94] Fluorescence quantum yield, Q, is the ratio of the number of photons emitted to the number of photons absorbed and is given by:

$$Q = \frac{\Gamma}{\Gamma + k_{nr}} \tag{2-3}$$

Fluorescence anisotropy relates the orientation of the excitation light polarization to the absorption and emission dipoles which provides information about the size and shape of proteins, or the rigidity of various molecular environments.

An emission spectrum is a plot of fluorescence intensity vs. wavelength, and the spectrum is generally independent of excitation wavelength because vibrational relaxation is much faster than emission so excess energy is quickly dissipated (Kasha's rule).[94] Other nonradiative relaxation processes like solvent relaxation, complex formation, energy transfer, and excited state reactions lead to emitted photons of less energy than the energy associated with excitation. The photons subsequently emit at longer wavelengths, a phenomenon called Stoke's shift (Figure 2-5).[95] Note too that fluorescence absorption and emission spectra are generally symmetric because the vibrational energy levels in the ground and exited states are similar, and transitions being involved in both absorption and emission are also the same.[94]

Fluorescence Components and Configuration

All spectrofluorometers contain a light source, excitation and emission monochromators, a sample holder, and a detector. Figure 2-6 shows a block diagram with the essential components of a spectrofluorometer. The light source used must produce a constant photon output at all wavelengths. Common light sources include mercury lamps, xenon lamps, halogen lamps, light emitting diode sources, and laser diodes. The instrument used for this work is equipped with a xenon arc lamp mounted vertically in an attempt to increase stability and the useful life of the source.

For excitation and emission wavelength selection, monochromators must be able to pass all photons of all wavelengths with the same efficiency, and their efficiency must not be related to polarization.[94] Diffracting grating monochromators are suitable for this purpose. Photomultiplier tubes (PMTs) are used as the detector in commercial fluorescence instruments. PMTs are best described as current sources that detect individual photons that can be counted individually or as an average signal. Ideal photomultiplier tubes should be able to detect photons at all wavelengths with equal efficiency.

Biological Fluorescent Probes

Fluorescent chromophores used in biological studies can be intrinsic, extrinsic, or coenzymic. In proteins, intrinsic fluorophores are the amino acids tryptophan, tyrosine, and phenylalanine, with the indole group of tryptophan being the most dominant due to a higher quantum yield (0.13 in water), and a larger absorption cross section that the other fluorescent amino acids.[96] Tryptophan fluorescence is extremely dependent on polarity of its environment and its emission blue shifts as polarity decreases, while its quantum yield increases.[94] In our work, tryptophan is excited at 295 nm and maximum

fluorescence emission is observed at 346 nm. There are some proteins that contain fluorescent conenzymes like nicotinamide-adenine dinucleotide (NADH) and pyridoxal phosphate. Reports on studies of these chromophores have provided information about the structure and interactions of a number of proteins.[93]

Often times, analytes of interest do not possess fluorophores, and if they do, they are not located in the region of interest. To solve this problem, extrinsic fluorophores are bound or covalently attached to regions of interests in proteins or other biomolecules. In our work, we use a dansyl chromophore (Figure 2-8) covalently attached to a phosphatidylethanolamine lipid headgroup, to monitor protein-lipid extraction by GM2AP. When selecting extrinsic fluorophores special care should be taken in terms of ensuring that the chromophore should not disturb the structure or function of the molecule of interest, and that the probe is sensitive to its environment so that definitive interpretations can be made.[97] Dansyl is excited at 340 nm, where proteins do not absorb; hence there is no interference by tryptophan emission. The emission spectrum of dansyl is also highly sensitive to polarity of its environment with emission maxima at 518 nm when the chromophore is solvent exposed.

Quenching of Protein Fluorescence

Solute fluorescence quenching has widely been used in biophysical studies as a source of information for proteins. Polypeptide chains fold, forming secondary structure of protein, which results in some amino acid residues aqueous exposed on the surface, and others buried and inaccessible to the polar solvent. One method commonly used to study the structure of proteins in solution, is to identify amino acid residues that are aqueous exposed vs those that are buried via quenching of protein fluorescence.[1,98] Fluorescence quenching is defined as the decrease in fluorescence intensity of a

sample as a result of excited state molecular interactions, molecular rearrangements, energy transfer, ground state complex formation, or collisional quenching.[94] Since most proteins usually contain tryptophan residues, fluorescence quenching is employed to probe for the exposure of this intrinsic fluorophore. Quenching experiments are very popular in protein studies because of the value of the information that can be obtained, and the relative ease with which the experiments can be performed.

Various low molecular weight substances for example, oxygen, iodide ion, nitrate ion, amines, halogens, and cesium ion, act as quenchers of fluorescence. However acrylamide (neutral) and iodide (charged) have been successfully used as efficient quenchers of tryptophan fluorescence.[99] Iodide, being a charged and heavily hydrated quencher, can only quench aqueous exposed tryptophanyl residues on the surface of proteins,[100] while acrylamide, being an uncharged and polar quencher can quench any excited state tryptophanyl residue it collides with regardless of the nature of its environment.[101]

Collisional or dyanamic quenching involves the transient collisional interacton between a ground state quencher and an excited state fluorophore; upon contact, the fluorophore returns to the ground state without emitting a photon. A modified Jablonski diagram is shown in Figure 2-9 to illustrate this process. Static quenching, on the other hand, involves the formation of a ground state, nonfluorescent complex between the fluorophore and quencher.[94] The quenching experiements described in this dissertation utilizes collisional quenching. In general, fluorescence quenching occurring between the excited state of the indole ring in tryptophan, M*, and a quencher is described by:

$$M^* + Q \underset{k_{-d}}{\overset{k_d}{\rightleftharpoons}} (M^* \ldots Q) \xrightarrow{k_i} M + Q + heat \qquad (2\text{-}4)$$

where $M^*...Q$ is the fluorophore-quencher complex, k_d is the diffusional rate constant , and k_i is the dissipation rate constant. The Stern-Volmer equation, used to describe and interpret collisional quenching, is given by:

$$\frac{F_0}{F} = 1 + K_{SV}[Q] = 1 + k_q \tau_0 [Q] = \frac{\tau_0}{\tau} \qquad (2\text{-}5)$$

where F_0 and F are the fluorescence intensities in the absence and presence of quencher, T_0 and T are the fluorescence lifetimes in the absence and presence of quencher, and K_{sv} is the collisional quenching constant, which is equal to $k_q T_0$, where k_q is the bimolecular rate constant for the quenching process. Quenching data are usually plotted as F_0/F vs [Q] and the slope of the line gives K_{sv}, the degree of quenching of fluorophore. The inverse of K_{sv} is the quencher concentration at which 50% of the fluorescence intensity is quenched.[102]

Proteins can sometimes contain multiple tryptophan residues located in different environments, thus possessing unequal accessibility to quencher. A modified Stern-Volmer plot describes the fraction of total fluorescence accessible to quencher and is given by:

$$\frac{F_0}{F_0 - F} = \frac{1}{f_a} + \frac{1}{f_a K_a [Q]} \qquad (2\text{-}6)$$

where f_a is the fraction of the initial fluorescence accessible to quencher. Plots of $F_0/\Delta F$ vs 1/[Q] give a y-incercept of f_a^{-1}.

Sensitivity of Fluorescence Spectroscopy

Fluorescence spectroscopy is inherently as much as 1000X more sensitive than absorption spectroscopy.[95] One reason for high sensitivity of the technique is that intrinsic fluorescence is not common to most chemical species so fluorescence is

generally measured against a low or zero background.[95] The overall sensitivity of fluorescence is dependent on the fluorophore as well as the instrument. The molar absorptivity and quantum yield of a fluorophore will dictate it's response to excitation, and these factors cannot usually be controlled. Additionally, fluorescing power is dependent on protein concentration and the power of the source, unlike other absorbance methods where concentration is related to the ratio of the source power before and after sample interaction.[103]

In terms of the instrument, sensitivity can be expressed as the ratio of signal to noise at a particular set of conditions, or by determining the minimum detectable quantity of a fluorophore at a particular set of conditions. The components of the instrument that contribute to sensitivity include the intensity of the source, the efficiency of the optical system, the spectral bandpass of the monochromators, and the efficiency of the detector.[104]

Surface Plasmon Resonance Enhanced Ellipsometry

The study of biological molecules by way of biosensors is a key area of research in biology, chemistry and engineering. Several techniques have been employed to qualitatively and quantitatively detect biomolecular processes such as antibody-antigen, lipid-protein, and protein-protein interactions. A majority of techniques used today involve labels like fluorophores and radioactive isotopes to detect biomolecular interactions. Though sensitive, these techniques sometimes present concerns like the biomolecules not being able to react in their native states, the preparation time and expense associated with labeling, problems with photobleaching, and the precautions involved with handling radioactive material.[105]

There has been growing interest in employing label-free optical methods to monitor interactions because they are usually nondestructive and noninvasive techniques. Affinity optical biosensors are commonly used where biomolecules are immobilized on surfaces which are irradiated with light and then the reflected light is analyzed. The basis of analysis is the detection of changes in the refractive index of the sample(s) of interest near the reflecting surface as a result of the particular interactions.[105] Techniques like interferometry, ellipsometry, and surface plasmon resonance (SPR) are all capable of analyzing very thin films in the pm and low nm range (ranges of interest for the thickness of biomolecular layers).[106,107]

Surface plasmon enhanced ellipsometry (SPREE) is an optical technique that utilizes the combination of surface plasmon resonance (SPR) and ellipsometry to monitor and analyze adsorption and desorption of molecules on thin films. It is also referred to as total internal reflection ellipsometry (TIRE), which technique is based on the principles of ellipsometry under total internal reflection conditions.[108] With the use of appropriate thin metal films, the SPR effect gives high sensitivity to the real time monitoring of binding events, bond formations, and structural changes of biomolecules, among other things.[109] Here the theory behind both ellipsometry and SPR spectroscopy will be explained and the SPREE instrumentation used to combine these two techniques will be described. SPREE was used in this work to study phospholipid binding and extraction by GM2AP.

Ellipsometry

Ellipsometry is an old but very sensitive, nondestructive, and widely used optical technique used to study surfaces and thin films.[110] The technique of ellipsometry is based on the change in the polarization state of elliptically polarized light reflected from

a surface.[107] When a surface is covered with one or more layers of thin film and substrate, the optics of the entire system changes the polarization state. An ellipsometer measures ellipsometric angles Δ and Ψ, which can provide information about film thickness down to angstrom resolution and index of refraction out to the thousandth position.

Generation of Elliptically Polarized Light

Elliptically polarized light can be generated when linearly polarized light is passed through an optical element called a compensator which consists of a fast axis and a slow axis which are perpendicular to each other and the direction of the propagation of the wave. When linearly polarized light passes through a compensator, the two components that were in phase, will subsequently be out of phase, producing elliptically polarized light. Also, when linearly polarized light is reflected off a metal surface, it causes unequal phase shifts of both components that are perpendicular and parallel to the plane of incidence. The change in polarization results in elliptically polarized light and the amount of ellipticity depends on the physical and optical properties of the surface, and substrates being measured.

Reflection of Light off Surfaces

Ellipsometry involves the reflection of light off surfaces. Figure 2-10 illustrates a light beam being reflected from a film substrate. The incident beam, reflected beam, and the direction normal to the surface are perpendicular to the surface. This is known as the plane of incidence. The direction of x and y components are parallel and perpendicular to the plane of incidence, and are referred to as p and s components of the electric field respectively. When light is reflected by the surface, the sample may comprise various layers of different optical properties, resulting in a complex optical

system. The p and s components of the electric field will experience altered phase shifts, changing the state of polarization. The incident (E_{in}) and reflected (E_{out}) electric vectors are connected by the sample reflection matrix R:

$$\begin{bmatrix} \frac{E_{p,out}}{E_{s,out}} \end{bmatrix} = \begin{bmatrix} R_{pp} & R_{sp} \\ R_{ps} & R_{ss} \end{bmatrix} \times \begin{bmatrix} E_{p,in} \\ E_{s,in} \end{bmatrix} \tag{2-7}$$

When an incident beam interacts with a material, some of the light is reflected and some is transmitted at the interface between medium 1 and medium 2 (Figure 2-11). The complex index of refraction, Ñ, is the parameter used to describe the interaction of light with the material. Ñ is a combination of a real part (index of refraction, n) and an imaginary part as given by the equation:

$$\tilde{N} = n - ik \tag{2-8}$$

where *k* is the extinction coefficient and *i* is an imaginary number, the square root of -1. The theory for ellipsometry is contained in the Fresnel formalism. The Fresnel reflection coefficient, r, is the ratio of the amplitude of the reflected wave to that of the incident wave. r can be determined for the s and p components of the electric field as light travels from medium 1 to 2 by:

$$r_{12}^{p} = \frac{\tilde{N}_2 \cos\phi_1 - \tilde{N}_1 \cos\phi_2}{\tilde{N}_2 \cos\phi_1 + \tilde{N}_1 \cos\phi_2} \tag{2-9}$$

$$r_{12}^{s} = \frac{\tilde{N}_1 \cos\phi_1 - \tilde{N}_2 \cos\phi_2}{\tilde{N}_1 \cos\phi_1 + \tilde{N}_2 \cos\phi_2} \tag{2-10}$$

where $\tilde{N}_1$ and $\tilde{N}_2$ are the complex indices of refraction for mediums 1 and 2 respectively, and Φ_1 and Φ_2 are the angles of incidence and refraction, which are related by Snell's law.[111] The reflectance ratios, $\Re^p$ and $\Re^s$ are defined as the ratios of the reflected

intensity of light to that of the incident intensity, and is the square of the magnitude of the Fresnel reflection coefficients:

$$\Re^p = \left| r^p \right|^2 \tag{2-11}$$

$$\Re^s = \left| r^s \right|^2 \tag{2-12}$$

For light incident on one interface the light transmitted through the interface is neglected and the above is true. In this work however, as well as many real world situations, more than one interface is present. Figure 2-11 shows light interacting with three media. The resultant reflected light from medium 1 comprises a combination of the light reflected from the first interface and all the beams transmitted from medium 2 back into medium 1. The components of light will have different phases depending on the additional optical distances they travel, and for multiple interfaces, each successive transmission back to medium 1 is smaller. The ratio of the amplitude of the outgoing resultant beam to the amplitude of the incoming beam is now denoted as the total reflection coefficient, *R*. *R* is analogous to *r* and is given by:[107]

$$R^p = \frac{r_{12}^p + r_{23}^p \exp(-i2\beta)}{1 + r_{12}^p r_{23}^p \exp(-i2\beta)} \tag{2-13}$$

$$R^s = \frac{r_{12}^s + r_{23}^s \exp(-i2\beta)}{1 + r_{12}^s r_{23}^s \exp(-i2\beta)} \tag{2-14}$$

where r_{12} and r_{23} are the Fresnel reflection coefficients for the interface between media 1 and 2, and 2 and 3 respectively. R^p and R^s are generally complex numbers and β is the film phase thickness and:

$$\beta = 2\pi \left(\frac{d}{\lambda} \right) \tilde{N}_2 \cos \phi_2 \tag{2-15}$$

Where d is the film thickness. When multiple interfaces are present, R parallel and perpendicular to the plane of incidence now becomes:

$$\Re^p = \left|R^p\right|^2 \tag{2-16}$$

$$\Re^s = \left|R^s\right|^2 \tag{2-17}$$

Ellipsometric Parameters and Definitions

The ellipsometric angles Δ and Ψ are the parameters measured in ellipsometry. Recall that incident p-polarized light and s-polarized light are generally not in the same phase. When each component makes a reflection, the resulting phase shift for the different waves may not be the same. The phase difference between the p and s components of the incident wave is referred to as δ_1 and the difference after reflection is referred to as δ_2. Δ is the phase shift that occurs after reflection, determined as

$$\Delta = \delta_p - \delta_s \tag{2-18}$$

Similar to a phase shift, the amplitudes of the p and s components may change after reflection. Given that the total reflection coefficient for p and s is defined as the ratio of the reflected beam amplitude to that of the incident beam amplitude, Ψ is related to amplitude in a manner such that the tangent of Ψ gives the ratio of the amplitude change for the p and s wave components:

$$\tan\Psi = \frac{\left|R^p\right|}{\left|R^s\right|} \tag{2-19}$$

In ellipsometry, the two reflection coefficients R^p and R^s describe Δ and Ψ and are used to determine the complex reflectance ratio, ρ, of the total reflection coefficients

$$\rho = \frac{R^p}{R^s} = \frac{\left|R^p\right|}{\left|R^s\right|} \times e^{i(\delta_{pp} - \delta_{ss})} \tag{2-20}$$

The information about the system of interest is contained in ρ, and the parameters Δ and Ψ are measured directly by ellipsometers. Subsequently, the primary equation of ellipsometry is

$$\rho = \tan\Psi e^{i\Delta} \text{ or } \tan\Psi e^{i\Delta} = \frac{R^p}{R^s} \tag{2-21}$$

The ellipsometric parameters are related to the optical properties of the sample, that is, film thickness (due to mass change on the surface) and complex refractive indices, and are calculated from computerized optical models.[107]

Ellipsometric Components and Nulling Ellipsometry Configuration

The components used in ellipsometry include a monochromatic light source, polarizer, compensator, analyzer and a detector. The most common light sources used are lasers, arc lamps, or polychromatic sources and filtering. Typically, lasers are preferred because of their high output intensities as well collimated Gaussian beams.[90] In our work, an unpolarized laser beam at 532 nm laser is used. In cases where spectroscopic measurements are taken, arc lamps may be used because they have an output over a very broad wavelength range. Arc lamps however, are much less intense than lasers, resulting in decreased signal to noise ratios.

Polarizers are optical components that are used to convert any polarization state of a light beam to a single known and desired polarization state. The polarizer used in our work converts unpolarized light form our laser source, to linearly polarized light after transmission through the polarizer. Polarized light is produced when the electric field component of the light beam travels parallel to the optical axis of the polarizer. Beams

perpendicular to the optical axis are extinguished. In ellipsometry, polarizers are used in two different ways. When a polarizer is used to convert unpolarized light to linearly polarized light, it is known as a polarizer, with its angle position, P, located between the polarizing axis and the plane of incidence. Polarizers are also used to determine the polarization state of the already polarized reflected beam, and are called analyzers. In nulling ellipsometry, an analyzer locates the null, and its angle position is denoted A.

Another optical component of ellipsometry is the compensator, which is also known as a retarder or quarter-wave plate. Compensators alter the phase of one polarization component of a light beam with respect to another.[110] Compensators have a fast axis and a slow axis, both of which are perpendicular to the direction of propagation and each other. The difference in speeds leads to a phase shift of 90° in the components of the electric field along these axes. Since both components of linearly polarized light are in phase, the component of the wave aligned with the fast axis passes through the compensator faster than that of the slow axis, they will emerge out of phase, producing elliptically polarized light.

The three most common types of optical detectors used in ellipsometric measurements are photomultiplier tubes, semiconductor diodes, and charge-coupled device (CCD) cameras. Photomultiplier tubes are significantly sensitive to polarization sensitivity but they require high voltage power supplies and display nonlinearity.[90] Semi conductor diodes are inexpensive and linear over a broad range of intensities, but in our work, we utilize a CCD camera as our detection tool.

There is one basic ellipsometer configuration (light source – polarizer – sample – analyzer – detector) for all ellipsometric measurements. However, variation in

configurations can arise in the polarizing and analyzing regions of the incident and reflected beams respectively. In our work we employ the rotating analyzer nulling ellipsometry configuration. First monochromatic linearly polarized light is passed through a compensator to produce elliptically polarized light. Elliptically polarized light incident on the sample will result in the reflected light exhibiting a linear state of polarization. This is necessary because linearly polarized light is much easier to analyze after reflection.

After reflection the linearly polarized beam is extinguished by rotating the analyzer to a 90° position with respect to the axis of linear polarization. This is called finding the null. The CCD camera then detects the minimum in the signal. The polarizer – compensator – sample – analyzer (PCSA) configuration is used because the relationship between the settings of the optical elements and Δ and Ψ is simpler.[110] Figure 2-13 illustrates the set-up for nulling ellipsometry where we use a PCSA arrangement to determine the null. The polarizer - compensator combination produces elliptically polarized light incident on the sample, and the reflected linearly polarized light passes through the analyzer which rotates to find the null which is detected by the CCD camera. The angle combinations will change to determine the null depending on the change in the polarization state after reflection from different systems on the surface. Therefore calculations for Δ and Ψ can be made and based on optical models, information about biological interactions at the surface of our film may be acquired. One advantage of nulling ellipsometry is that in measuring angles, problems of stability of the light source, and nonlinearity of detectors is avoided.[108]

Surface Plasmon Resonance Spectroscopy

Surface plasmon resonance spectroscopy is an optical technique used to study interactions occurring at surface and interfaces.[112] SPR is based on the excitation of charge density oscillations called surface plasmons by light in thin layers of noble metals for example, gold, silver, and copper. Since the discovery of using SPR to characterize thin films and to monitor processes at metal interfaces in the late 1970s, the technique has been used in optical sensing devices for measuring physical, chemical, and biological quantities.[113] For biological systems, binding events of biomolecules can be studied using SPR which often requires the immobilization of the biomolecules on the surface of the metal via surface functionalization. The advantages of SPR are that it is extremely sensitive, and it is a label-free technique. SPR provides a powerful tool to investigate the dynamics and structural changes that are occurring in real time during biological interactions by monitoring the refractive index (n) changes at the surface of thin films that support surface plasmons due to total internal reflection.

Total internal reflection

Total internal reflection (TIR) occurs when light is reflected at an interface where the refractive index of the incident medium (n_0) is greater than the refractive index of the reflecting medium (n_1).[108] The incident light is usually passed through a dielectric medium like a prism (n = 1.72), and the reflecting medium is most likely a water based liquid (n = 1.33). As the angle of incidence is increased, the transmitted beam approaches a minimum angle called the critical angle, ϕ_c where the transmitted light is parallel to the interface, resulting in no energy crossing the interface. When n_0 is greater than n_1, TIR occurs if the angle of incidence is larger than ϕ_c and is described as

$$\sin \phi_c = \frac{n_1}{n_0} \quad (2\text{-}22)$$

and the beam is propagated back into the incident medium.

Although the reflected beam does not transfer energy across the interface, an electrical field intensity called an evanescent field wave is leaked into the reflecting medium. The evanescent wave decreases exponentially with increasing distance from the surface of the interface, decaying over a distance of about one light wavelength.[114] If the TIR interface is coated with a conducting metallic layer like gold with an appropriate thickness, the p-polarized component of the evanescent field wave penetrates the layer and excites electromagnetic surface plasmon waves within the layer that is in contact with the reflecting medium. Since gold is non-magnetic, the surface plasmon wave will also be p-polarized, and due to the nature of its propagation, an enhanced evanescent wave will be created. Since the electric field penetrates a short distance into the reflecting medium, SPR conditions are sensitive to the changes in refractive index at the gold surface.

Kretschmann configuration of SPR

There are three main configurations of SPR: grating coupled systems, optical waveguide systems, and prism coupled attenuated total reflection systems. In our work, the latter is used in the Kretschmann arrangement (Figure 2-14). The Kretschmann arrangement is the most widely used geometry in SPR as it has been found to be very suitable for sensing the change in refractive index on thin films.[106] In this configuration, a light wave passes through the high refractive index prism and is completely reflected at the interface between a prism and a thin metal layer. The evanescent wave that leaks

into the reflecting medium excites surface plasmon waves at the outer boundary of a metal.

The high refractive index prism modifies the wave vector of the light by decreasing the phase velocity of the photons. A matching condition occurs when the wave vector component of the incident beam parallel to the conductor surface, is equal to the wave vector of the surface plasmons which are bound to the conductor surface. The wave vector of the incident beam can be tuned to be equal to the surface plasmon wave vector by varying either the angle of incidence or the wavelength of the beam. If the wavelength of the beam is fixed, the reflectance of p-polarized light can be measured as a function of angle of incidence, and a sharp drop in the reflected light intensity will be observed and a phenomenon called surface plasmon resonance occurs.

Components of SPR measurement and sensitivity of the technique

The principal elements involved in SPR measurements are shown in Figure 2-15. First, a source which is converted to p-polarized light is used to excite the plasmon wave in the attenuated total reflectance configuration. Also, a prism is needed to couple light photons to the plasmons, and a thin metallic or semiconducting film is required on the surface of which plasmons can be excited. Finally, the SPR signal is detected by a CCD camera.

SPR is dependent on different parameters of the reflecting system which affects the spectral resolution and sensitivity of measurement. The parameters are: the refractive index (*n),* the extinction coefficient (k), and thickness of the different layers (d) on the surface. For improved sensitivity, the thickness of the metal should be a fraction of the wavelength of the incident beam. Thus, special consideration should be taken into account when selecting the type of metal and its thickness. For our purposes, the

metal chosen was gold with a thickness of 28.5 nm coupled to an adhesive 2 nm layer of chromium on SF10 glass slides. The incident beam is at a wavelength of 532 nm. Additionally, an increase in temperature can also affect the sensitivity of the technique.[106] SPR is very sensitive to molecular adsorption to the metal interface in the distance of the evanescent field wave, thus high sensitivity is achieved when monitoring the molecular adsorption of biomolecules on the surface of the gold.

SPREE Measurements

Under total internal reflection conditions, ellipsometric measurements and parameters obtain enhanced sensitivity and detection of interactions occurring at or near the surface of metallic (gold in this work) thin films. The increased sensitivity associated with the optical response of the technique comes from the efficiency of the collective excitation of conduction electrons near the metal surface. The resolution of SPREE is on the order of 5×10^{-7} refractive index units, compared to 10^{-5} and 2×10^{-6} to 10^{-5} for ellipsometry and SPR respectively.[115]

In this work, SPREE was used to measure the adsorption and desorption of lipid vesicles to form bilayers on functionalized gold surfaces. GM2AP was then flowed over the surface, and binding and/or extraction of lipid was observed by monitoring the change in the ellipsometric parameter, Ψ as a function of time. The change in resonance angle is proportional to the change in refractive index and thickness of the layers on the surface since the change in Ψ is related to the Fresnel R^p amplitude. The minimum detectable change in angle of the instrument used in this work is about 10 mDeg which corresponds to a change in thickness of 0.1 nm.[77]

Figure 2-16 illustrates the experimental set-up of SPREE. Measurements were taken using a commercial EP3-SW imaging system (Nanofilm Surface Analysis,

Germany). A SF10 glass slide coated with an adhesive chromium layer then gold layer is assembled on top of a 70 µL sample cell. A Peltier temperature control system (not shown) was linked to the sample cell to minimize baseline drift due to temperature fluctuations with time as data is being collected. A 60° SF10 prism is attached to the back side of the slide using diiodomethane as the refractive index matching fluid. A laser beam with wavelength of 532 nm produces elliptically polarized light incident on the sample by passing through a linear polarizer flowed by a compensator. The angles of the polarizer and compensator are fixed and set in a way to ensure that the reflected beam is linearly polarized. Once reflected off the sample, the beam is passed through a 10x working distance objective and the analyzer, which rotates until the null condition is obtained. This minimum light intensity is detected by the CCD camera and the angles of the different components are related to the optical properties of the sample.

The angle Ψ is plotted as a function of time in our experiments. Figure 2-17 shows a typical sensorgram of a protein being adsorbed to a lipid bilayer that was fused on a functionalized gold slide. The software, AnalysisR supplied by the instrument's company was used to fit the experimental data to a simple Langmuir model. Measurements began with injecting buffer in a flow cell and allowing it to come in contact with the surface (a). Next, lipid vesicles were injected and through vesicular fusion, lipid bilayers were adsorbed on the surface, resulting in an increase in Ψ (b). After the adsorption process was allowed to equilibrate, buffer was flowed through the cell to remove any free lipids. At (c) protein was injected into the flow cell, which resulted in adsorption to the surface, followed by a buffer wash to monitor desorption (d). In each adsorption or

desorption step, sufficient time was given for equilibration of substrates, and to allow for stable signal to be acquired.

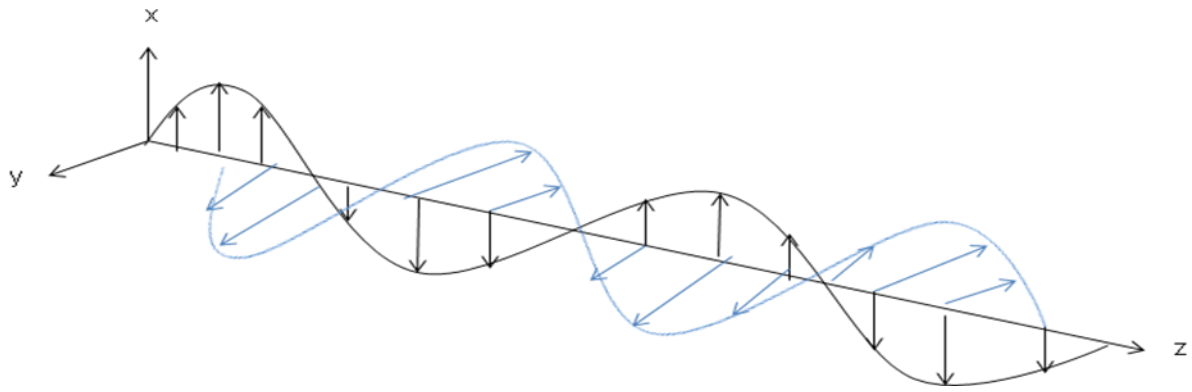

Figure 2-1 . Schematic representation of an electromagnetic wave showing the electric field as a function of position at constant time

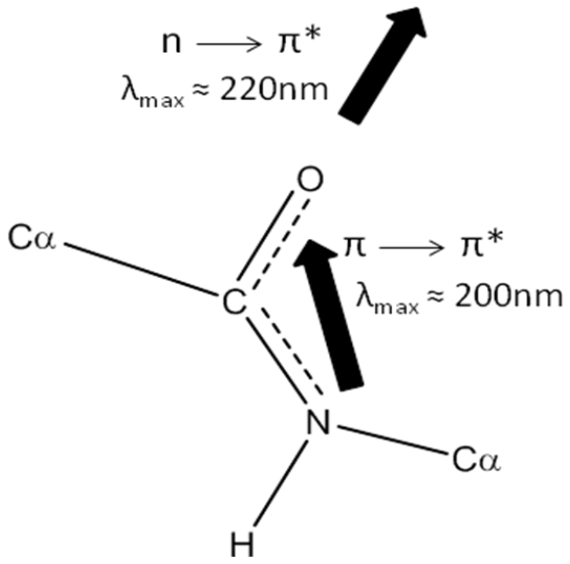

Figure 2-2. Peptide bond region of protein backbone showing electronic energy transitions associated with the absorption of amide chromophores

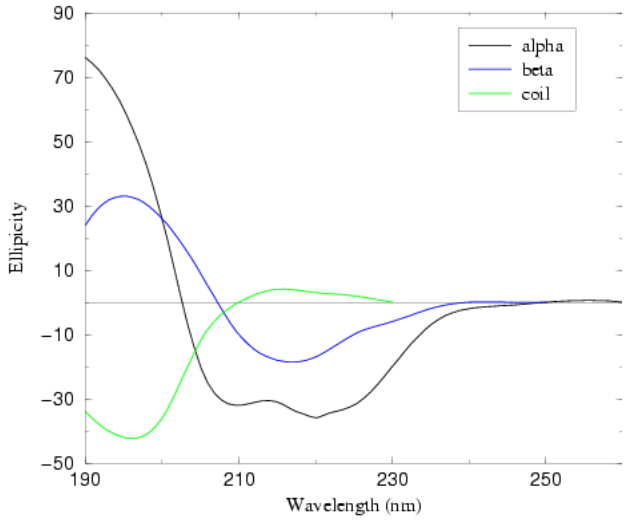

Figure 2-3. Far UV circular dichroism spectra showing the various types of secondary structure. Spectra show α-helical (black), β-sheet (blue), and random coiled (green) structures of proteins. Figure was reprinted from Besley *et al.*(http://besley.chem.nottingham.ac.uk/research/research-prospec.html) Accessed in May 2012

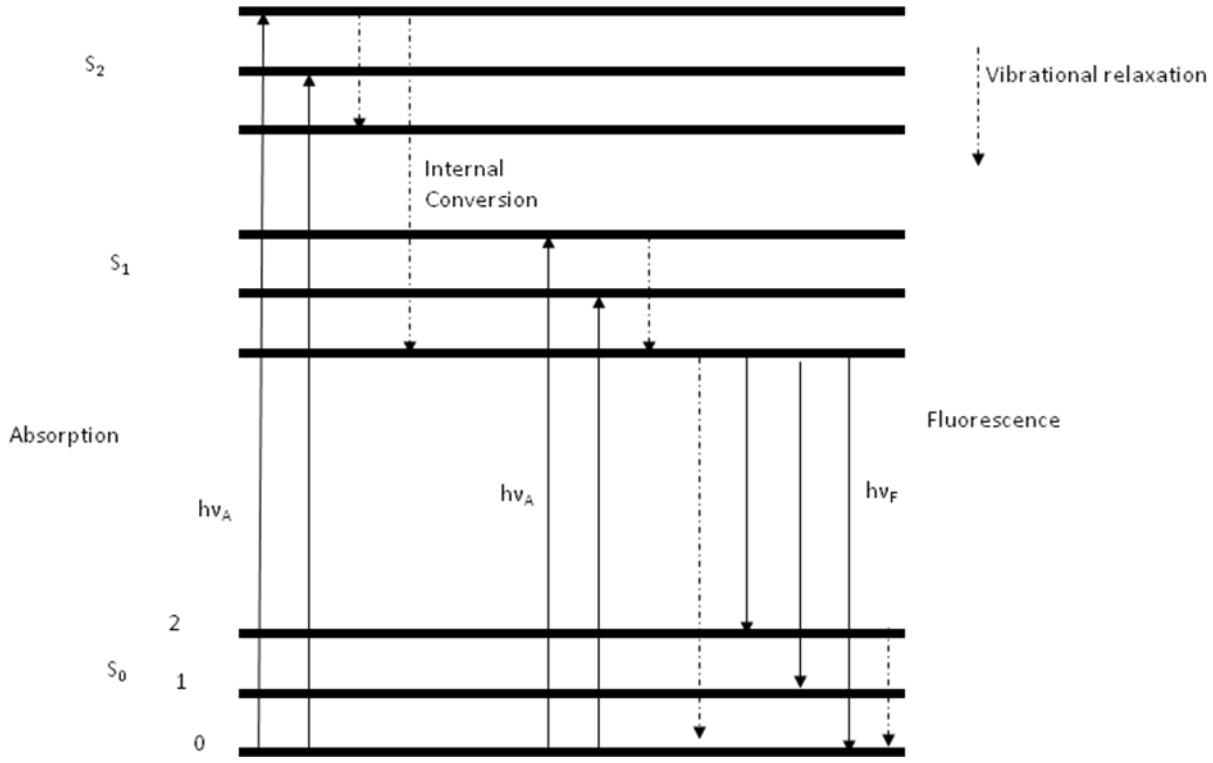

Figure 2-4. Jablonski diagram showing the energy level transitions involved in absorption and fluorescence emission. The solid lines represent radiative transitions while broken lines represent nonradiative transitions in the singlet state.

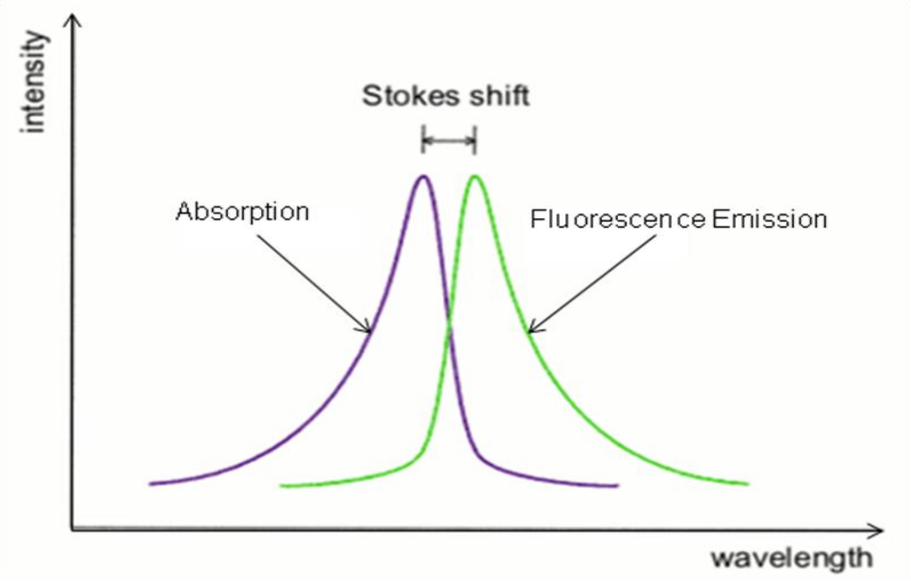

Figure 2-5. Representative absorption and fluorescence emission spectra

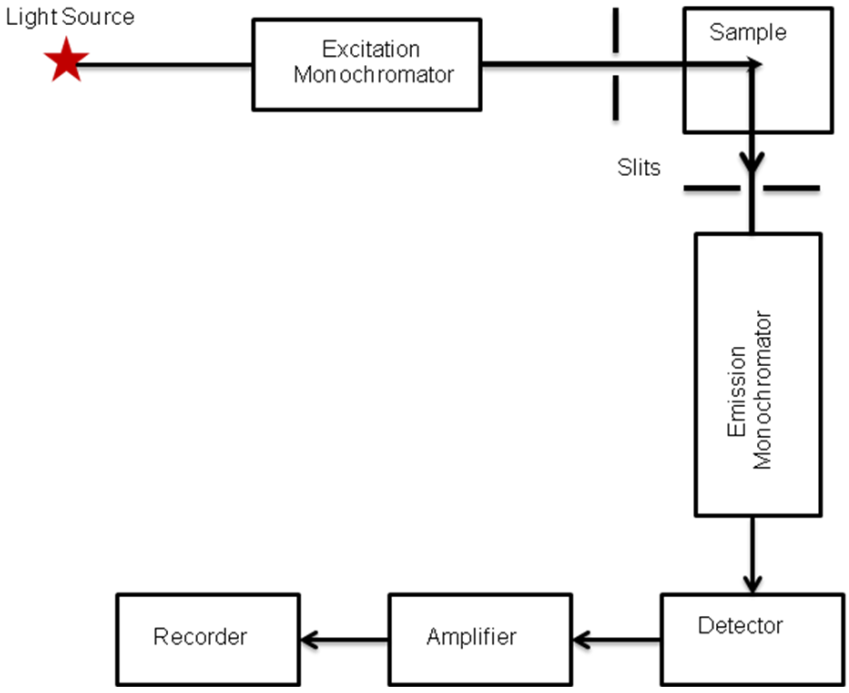

Figure 2-6. Block diagram illustrating the general schematic of a spectrofluorometer

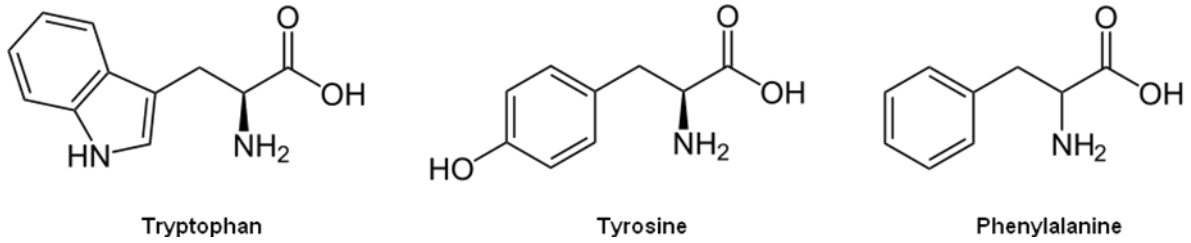

Figure 2-7. Chemical structures of the three intrinsic fluorescent amino acids: tryptophan, tyrosine, and phenylalanine

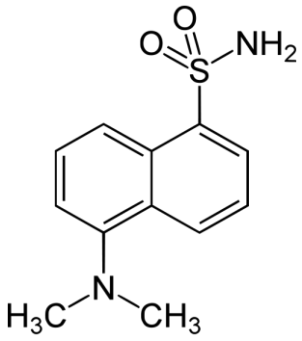

Figure 2-8. Chemical structure of the extrinsic fluorescent probe, dansyl amine

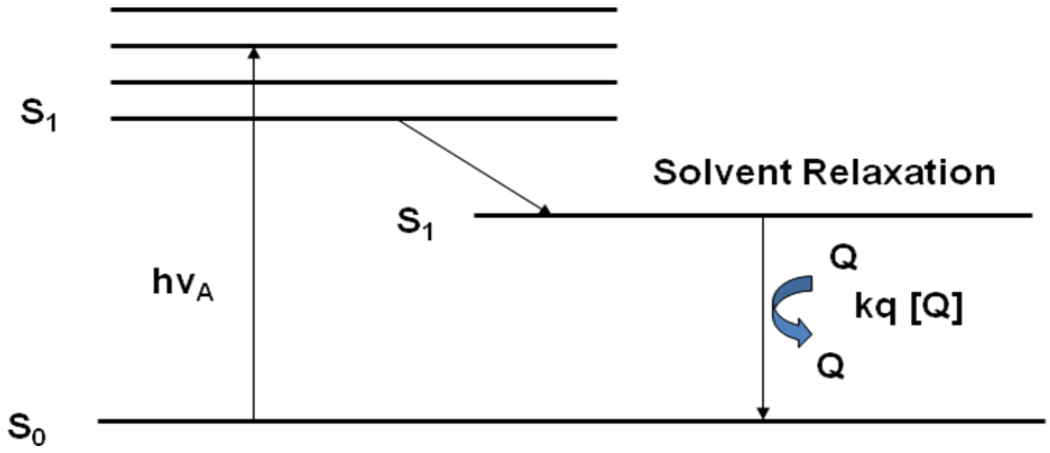

Figure 2-9. Modified Jablonski diagram showing the energy level transitions involved in collisional quenching

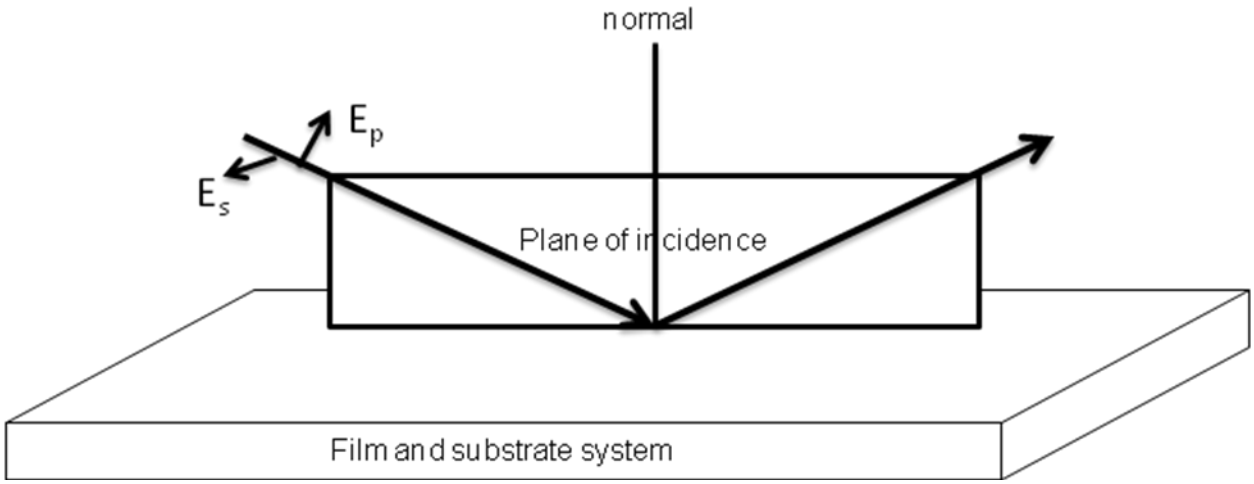

Figure 2-10. Reflection of a polarized light bean from a surface. The plane of incidence contains the incoming beam, the reflected beam, and the normal to the surface. E_p and E_s are the amplitudes of the electric field parallel and perpendicular to the plane of incidence

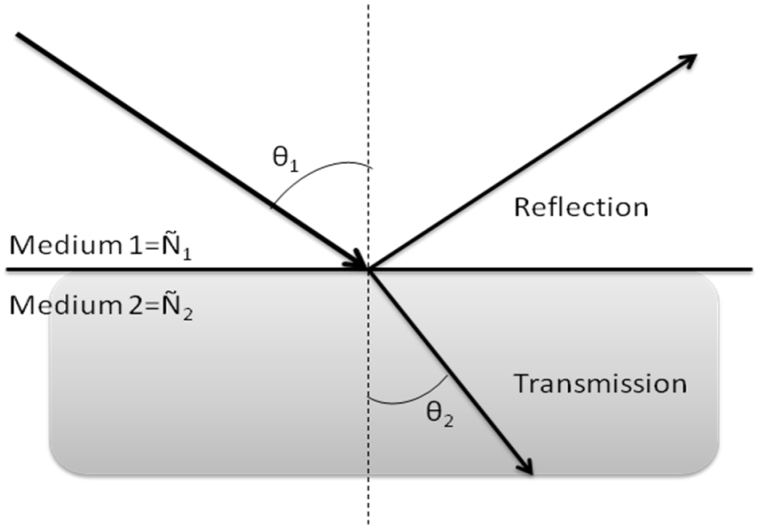

Figure 2-11. Interaction of light with a material at a single interface with complex index of refraction, $\tilde{N}_2$

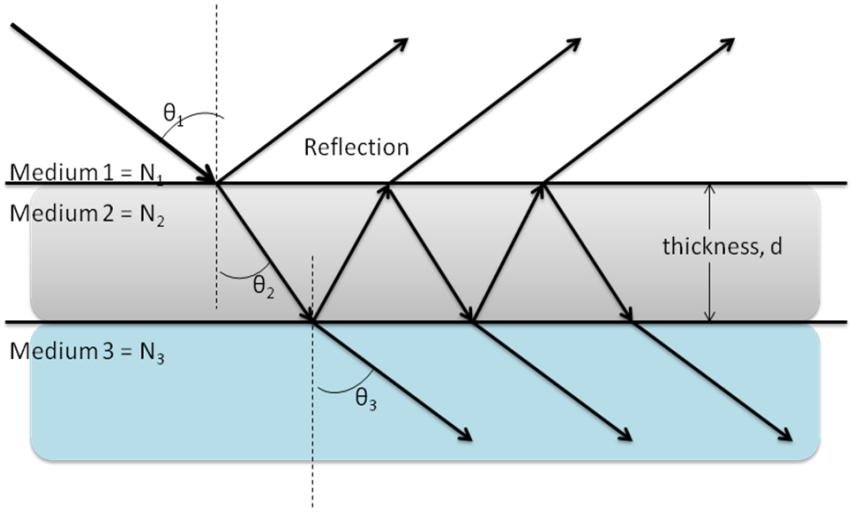

Figure 2-12. Interaction of light with a material showing reflections and transmissions through two interfaces

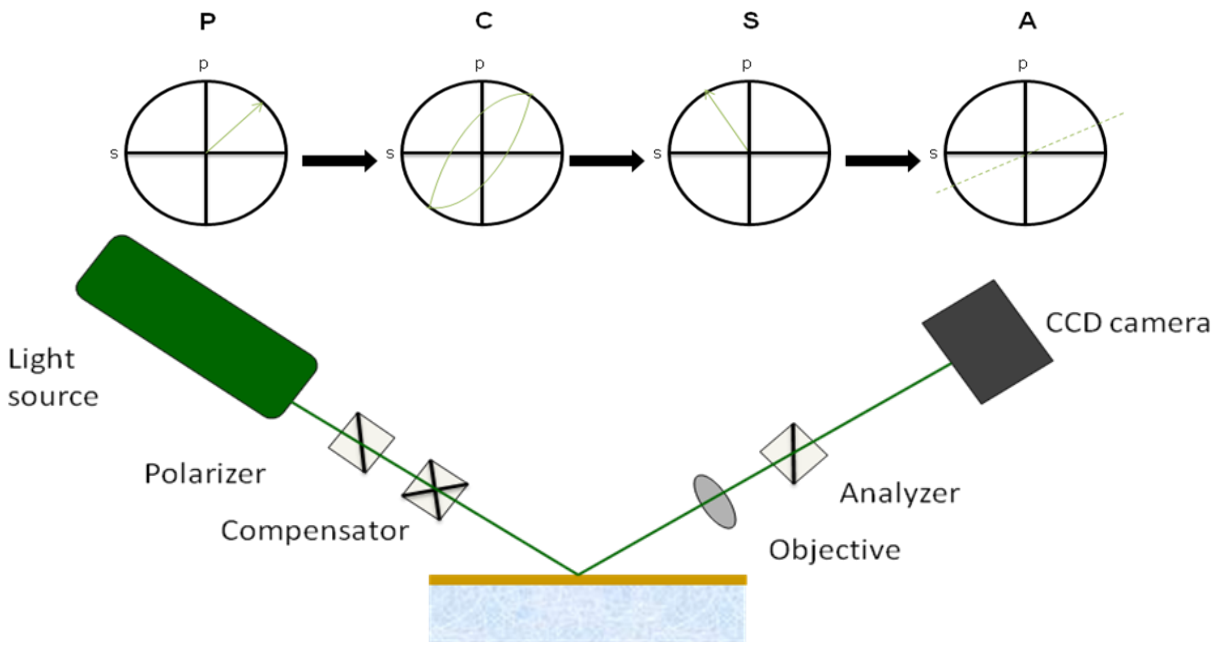

Figure 2-13 . Nulling ellipsometry configuration. The fixed polarizer-compensator combination before the reflection gives an elliptical polarization of light incident on the sample. The reflected beam is linearly polarized and the analyzer is rotated to find the null

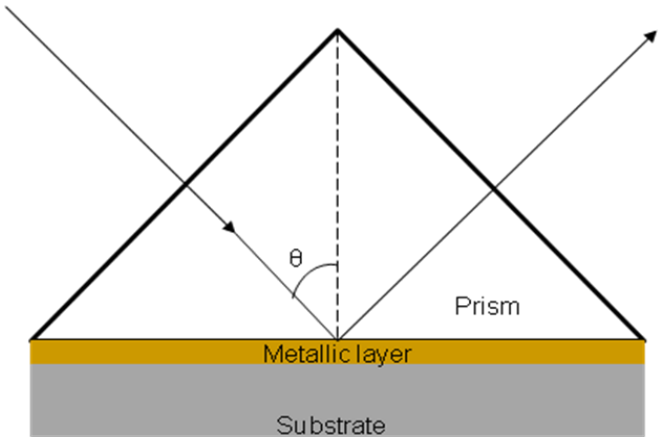

Figure 2-14. Kretschmann configuration of SPR showing a prism – metallic coating – substrate layer interface. θ is the angle of incidence

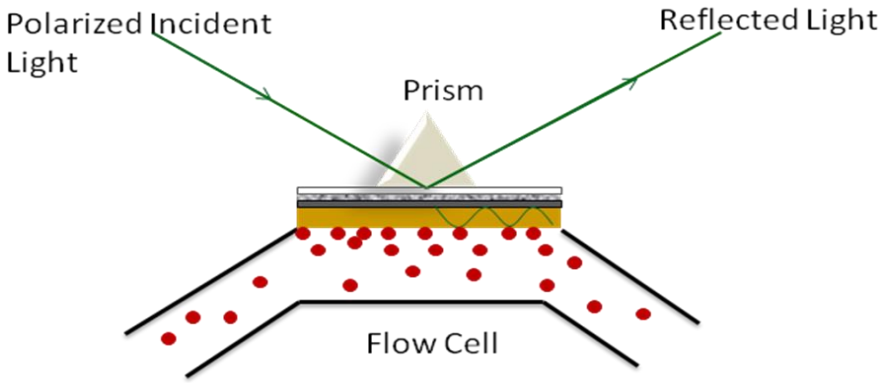

Figure 2-15. Illustration of the experimental set up used in surface plasmon resonance spectroscopy

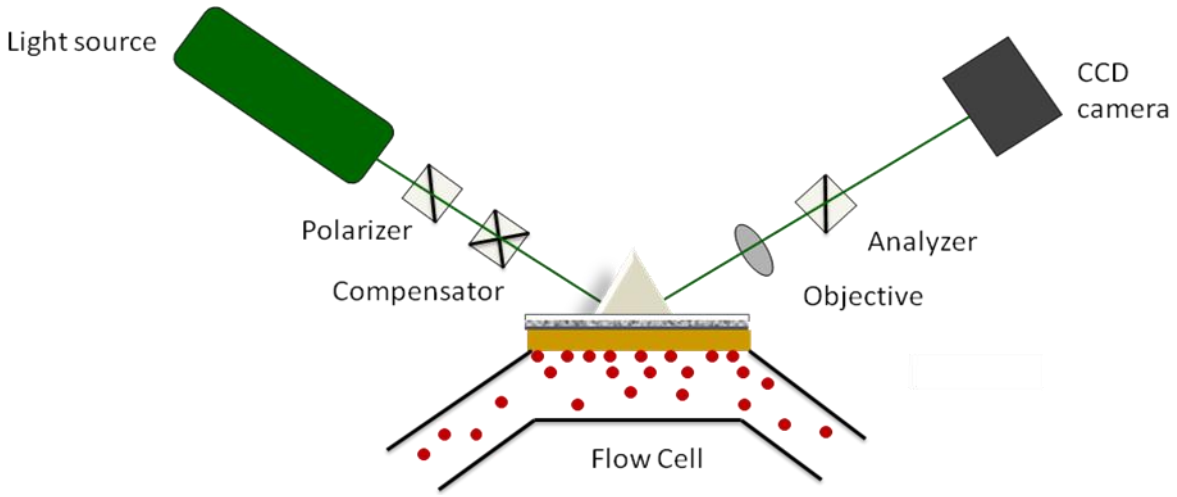

Figure 2-16. Schematic of a SPREE experimental setup. Ellipsometric measurements are taken under SPR conditions.The prism and surface are mounted on a flow cell for measurements under solution conditions

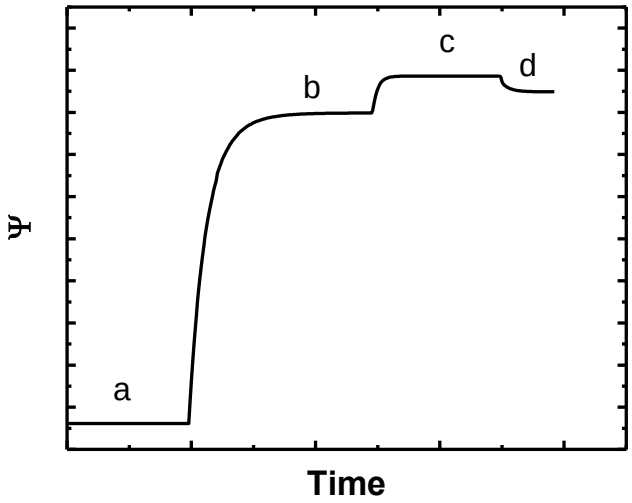

Figure 2-17. Typical SPREE sensorgram of protein adsorbing to a lipid bilayer that is functionalized on a metallic thin film. First, a buffer baseline is acquired (a) followed by the adsorption of lipid vesicles for bilayer fusion (b). Protein is then adsorbed (c), then buffer is flowed to wash away unbound protein

CHAPTER 3
CHARACTERIZATION OF GM2 ACTIVATOR PROTEIN CONSTRUCTS USING INTRINSIC TRYPTOPHAN FLUORESCENCE

Introduction

Glycosphingolipids are ubiquitous constituents of cell membranes in eukaryotic cells.[56] The catabolism of glycosphingolipids is an essential cellular process that occurs in the lysosome of cells. GM2 Activator Protein (GM2AP) is one of five nonenzymatic sphingolipid activator proteins (SAPs) required for the hydrolytic degradation of glycosphingolipids that contain four or fewer sugar head groups.[13] The other four SAPs, Saposins A-D, are encoded by a single gene mapped to chromosome 10 and are derived from the proteolytic processing of the precursor glycoprotein, prosaposin.[7,32] Saposins A-D are structurally homologous: existing as homodimers, sharing three disulfide bonds with the same connectivity, and possessing secondary structures of a predominantly alpha helical nature.[33,41] Conversely, GM2AP is encoded by an unrelated gene on chromosome 5, and is synthesized as a 193 amino acid prepro-polypeptide. The GM2AP sequence consists of an Asn-linked glycosylation site at Asn63-Val-Thr which targets the protein to the lysosome from the endoplasmic reticulum.[50] In its mature and deglycosylated form, GM2AP is an 18 kDa protein consisting of 162 amino acids.[25] GM2AP is structurally different from saposins A-D: it exists as a monomer, contains 4 disulfide bridges, and adopts an eight stranded β-cup topology instead of the predominantly α-helical secondary structure seen in the saposins.[13,25]

In vivo, GM2AP is required for the lysosomal catabolism of GM2 to GM3 by the exohydrolase β-hexosaminidase A (Hex A). The protein's role involves binding to, and extracting GM2 from intralysosomal vesicular membranes,[59] forming a protein-lipid complex where the ceramide moiety of the lipid is buried in the hydrophobic pocket of

the protein, and the bulky carbohydrate head group protrudes from the binding pocket and into the aqueous environment[57]. GM2 is then presented in the proper orientation to Hex A, which recognizes GM2's terminal sugar group GalNAc, for cleavage.[59] No other SAP can fulfill GM2AP's role and its physiological significance is evident by the occurrence of a fatal neurological disorder, AB variant of GM2 gangliosidoses, caused by the protein's deficiency or inability to function as a result of mutations.[116,117] Physiologically, GM2AP has also been found to be involved in CD1-mediated lipid antigen presentation to T-cells[118], to act as a factor that stimulates and enhances the association between phospholipase D and enzyme activators,[62,63] and to participate in the regulation of proton pumps in intercalated kidney cells.[119,120] In vitro, GM2AP acts as a general lipid transfer protein, where it is known to bind and extract other glycolipids and phospholipids.[25,57,121]

GM2AP has been isolated from natural sources and has been expressed in its glycosylated form from insect and yeast cells,[122,123] as well as in its deglycosylated form from *E. coli.* cells.[36,124] The revealed β-cup topology from x-ray crystallography of declycosylated protein provides a 12 Å x 14 Å x 22 Å hollow pocket lined with hydrophobic residues to carry out its function.[53] A 2.5-turn alpha helix at the rim of the hydrophobic cavity and two flexible loop regions were also identified in the resolved crystal structure of GM2AP.[53] Despite knowing the protein's function and structure, the precise molecular interactions of GM2AP are not yet well understood.

GM2AP contains three tryptophan residues in its 162 amino acid sequence – one residue (W5) is located on the backside of the binding pocket of the protein, and two residues (W63 and W131) are located in putative membrane binding loops of the

protein. Because tryptohan is an intrinsic fluorophore, fluorescence can be employed to study GM2AP. Fluorescence spectroscopy is a sensitive optical technique that has long been used to study proteins. Unlike other biophysical techniques, fluorescence spectroscopy has the advantage of studying proteins as dynamic systems as opposed to in their static form. Often times however, in order to use this technique, extrinsic fluorescent probes are needed for protein analysis either because the native protein does not contain tryptophan residues, or if they do, the residues are not located in regions of interest in the protein.

Here we report our findings from the characterization of the intrinsic fluorescence of the tryptophan residues in GM2AP. A series of tryptophan to alanine substitutions were constructed via site-directed mutagenesis of the recombinant protein. Fluorescence quenching experiments were employed to determine the nature of the environment of the tryptophan residues and their accessibility to the quencher. Tryptophan fluorescence of solvent exposed residues can be used to monitor GM2AP when investigating the regions of the protein involved in lipid binding and extraction. Furthermore, because W63 and W131 are natively located in regions thought to interact with the membrane surface, the need to attach extrinsic fluorescent labels would be eliminated when studying GM2AP interactions with lipid membranes via fluorescence spectroscopy.

Materials and Methods

Primers were obtained from Integrated DNA Technologies, Inc (Coralville, IA). 1kb standard DNA ladder was purchased from New England Biolabs (Ipswich, MA). SDS-PAGE Molecular Weight Standards broad range, and Biorad Criterion pre-cast 18% SDS-PAGE gel were purchased from BioRad (Hercules, CA).The Quikchange^{TM} site-

directed mutagenesis kit was purchased from Stratagene (Santa Clara, CA). The QIAprep spin miniprep kit was purchased from Quiagen (Valencia, CA). Factor Xa Cleavage Capture Kit was purchased from Novagen (Gibbstown, NJ). The Ni-NTA resin column, HiTrap Q HP Anion exchange column, HiPrep 26/10 desalting column, and Sephacryl S-200 High Resolution column were purchased from GE Healthcare (Pittsburg, PA). All other reagents and supplies were obtained from Fisher Scientific (Pittsburg, PA) and were used as received.

Site-Directed Mutagenesis of GM2AP Tryptophan to Alanine Constructs

The gene encoding the sequence for wild-type GM2AP, a gift from Christine Schubert Wright,[53] was constructed in pET16(b+) vector. The map of the plasmid pET16(b+) vector, containing cDNA sequence and the amino acid sequence of GM2AP wild-type are given in Figure 3-1 and Figure 3-2, respectively. A series of tryptophan (W) to alanine (A) variants designated as W5A, W5AW63A, W5AW131A, W63AW131A, and W5A/W63AW131A were engineered via several rounds of single point site-directed mutagenesis. First, a single amino acid mutation of tryptophan at position 5 to alanine using pET16b-GM2AP as the template was performed and the variant was designated W5A. Similarly, W63A was obtained by the single amino acid mutation of tryptophan at position 63 to alanine. The W5A variant was used to engineer additional amino acid mutations at residues 63 and 131 to produce W5AW63A, W5AW131A and W5AW63AW131A. The W63A variant was used to engineer W63AW131A. Primers for each mutation site were designed using the software, PrimerX (http://www.bioinformatics.org/primerx/) and were obtained from Integrated DNA Technologies Inc.

Mutagenesis reactions were performed using the QuikChange™ Site Directed Mutagenesis Kit and protocol (Stratagene, La Jolla, CA). Each buffered reaction contained 20 ng or 50 ng of template DNA, 125 ng each of forward and reverse primer, deoxynucleotide triphosphate (dNTP) mix, 2.5 units (U) PfuTurbo DNA polymerase, and 3-5% (v/v) dimethylsulfoxide. The reaction mixtures were vortexed and centrifuged for a few seconds before subjection to polymerase chain reaction (PCR).

PCRs were conducted in an Eppendorf (Hauppauge, NY) automated thermal cycler, for seventeen cycles. Each cycle consisted of 30 seconds at 95°C for denaturation of the double stranded DNA, one minute at 55°C for annealing of the primers, and a six minute extension at 68°C. After PCR, the reaction mixture was treated with 10 U *Dpn* I endonuclease for one hour at 37°C in order to digest the original, unmutated DNA template on the basis of methylation. After digestion, each reaction was checked for mutated DNA via a 1% polyacrylamide gel electrophoresis using 10 µL of the product. The resulting nicked vector DNA which contained the desired mutated sequence was then transformed into *E. coli* XL1-Blue supercompetent cells via the heat-shock method. The plasmid containing the mutated DNA sequence was subsequently isolated and purified using a QIAprep Spin Miniprep Kit (Qiagen, Valencia, CA), and submitted for DNA sequencing.

Expression and Purification of GM2AP TRP to ALA Constructs

Recombinant GM2AP expression and purification procedures were modified from the protocol reported by Wright et al.,[53] and originally published by Wu et al.[124] Plasmids containing the W to A mutations were transformed in *E. coli* BL21(DE3) cells using the heat-shock method. 5mL sterile pre-culture of Luria-Bertani (LB) media (tryptone, yeast extract and sodium chloride) with 100 mg/mL ampicillin were each inoculated with a

single colony of cells and grown for approximately 5 hours (to OD_{600} = 0.6) at 37°C, while shaking at 250 rpm. The pre-culture was then used to inoculate 1L LB media containing 100 mg/mL ampicilin and the cells were allowed to grow (OD_{600} ~0.8) with shaking at 250 rpm at 37°C for 3 hours. The temperature was reduced to 20°C and expression was induced with 0.8 mM isopropyl-β-D-thiogalacatopyranoside (IPTG), while shaking at 250 rpm overnight for 8 hours. Following induction, cells were pelleted by centrifugation at 5,000 rpm for 10 minutes at 4º C using a Sorvall RC6 centrifuge with SLA-3000 rotor.

The cell pellet was resuspended in 25 mL lysis buffer (0.1M phosphate, 0.1M NaCl, 1% Triton-X-100, 0.3M PMSF, 0.5mM Benzamidine,pH 8.0). The cells were tip sonicated for two minutes and then passed through a French pressure cell (Thermo Scientific, Waltham, MA) three times at 20,000 psi. The lysed cells were centrifuged at 12,000 rpm for 20 minutes at 4°C. The pellet was resuspended in lysis buffer, after which the previously mentioned sonication, french pressure, and centrifugation steps were repeated to pellet inclusion bodies and other cell debris. Inclusion bodies in the pellet were denatured by resuspension in 5 M urea buffer (5M urea, 0.1M phosphate, 10mM Tris-HCl, 5% glycerol, TCEP, pH 8.0), homogenized using a Dounce Tissue glass homogenizer, tip sonicated for 5 minutes (5 second on and off time intervals), and centrifuged at 12,000 rpm for 20 minutes at 4°C.

The supernatant containing denatured GM2AP was passed through a prepacked Ni-NTA resin column (GE Healthcare, Piscataway, NJ), pre-equilibrated with urea buffer. The N-terminal fused histidine tag on GM2AP allows for separation of the protein by Ni-chelating chemistry. The column was then washed with 10 column volumes (CV)

5 M pH urea buffer pH 8.0; 10CV 6M Guanidine HCl pH 8.0 followed by 10 CV 6M Guanidine HCl pH 7.0 (6M GuHCl, 0.1M phosphate, 10mM Tris-HCl, 5% glycerol). GM2AP was eluted with 6M Guanidine HCl pH 4.5.

GM2AP eluate fractions were pooled and the protein was refolded by drop-wise dilution overnight in a 20-fold volume of slow stirring refolding buffer (50mM Tris-base, 1mM EDTA, 0.05% Tween-20, 10% glycerol, 2mM Glutathione reduced, 0.2mM Glutathione oxidized pH10) at 4°C. The solution containing the protein was subsequently buffer exchanged by way of dialysis (25mM Tris base, 0.05% Tween-20, 2.5%; glycerol pH 8.0) for 2 days to get rid of guanidine hydrochoride, after which the protein was concentrated by anion exchange chromatography by loading the sample unto a 5 mL HiTrap^{TM} Q-Column (GE Healthcare, Piscataway, NJ) and eluting q-column elution buffer (200mM NaCl, 25mM Tris base, 2.5% glycerol, 0.05% Tween-20; pH 8.0).

It has been reported that the histidine tag fused to GM2AP alters the intrinsic fluorescence spectra under acidic conditions,[125] so the tag was removed by Factor Xa cleavage. The Q-column eluate containing GM2AP fractions was buffer exchanged into Factor Xa cleavage buffer (100mM NaCl, 50mM Tris HCl, 5mM $CaCl_2$, pH 8.0) using a HiPrep^{TM} 26/10 desalting column that was pre-equlibrated with Factor Xa cleavage buffer. His-tag cleavage was performed using a Factor Xa Cleavage Capture Kit (Novagen, Gibbstown, NJ). Briefly, Factor Xa enzyme was mixed with GM2AP in cleavage buffer at a 2:1 ratio (units of enzyme: mg protein) and the mixture was incubated at 4°C for 48 hours. The enzyme was subsequently quenched and removed using Xarrest agarose at a ratio of 100 µL Xarrest agarose : 8 units Factor Xa. GM2AP

was separated from Xarrest Agarose and cleaved enzyme by centrifugation at 1000 x g for five minutes. Cleaved protein was separated from uncleaved protein by passing the supernatant through a Ni-NTA resin column, with the flow through containing cleaved protein.

As a final purification step, GM2AP was concentrated to less than 5 mL and was loaded to a Sephacryl S-200 High Resolution column for size exclusion chromatography at a flow rate of 0.5 mL/min. Here residual detergent was removed and the protein was equilibrated in the appropriate buffer for spectroscopic measurements. The isolated sample was concentrated using Amicon Ultra-15 centrifugal filter units (EMD Millipore, Billerica, MA) and protein concentration was determined by Bradford assay and by UV absorption at 280 nm on a Cary 50 Bio UV-Visible spectrophotometer (Varian, Palo Alto, CA) using the appropriate extinction coefficient depending on the particular variant. Protein purity was evaluated by SDS-PAGE using 18% pre-casted polyacrylamide gels and Coomassie Brilliant Blue detection. Post purification, protein was stored at -20°C.

Circular Dichroism (CD) Spectroscopy Measurements

Circular dichroism spectra of 0.5 mg/mL of each GM2AP variant was obtained to ensure proper protein folding and to compare the relative secondary structure of the variants to that of the reported wild-type spectrum.[92] All measurements were collected on an Aviv 215 CD spectrometer using Hellma cuvettes with a 1 cm path length. Spectra were reported from 260 – 190 nm, collecting data at every nanometer. Temperature was 25°C and each spectrum is the average of four scans, corrected for buffer absorption and normalized to $\Delta\varepsilon = 0$ at 280 nm.

Intrinsic Fluorescence Quenching Measurements

Steady-state fluorescence experiments were carried out on a FluoroMax-3 fluorimeter (Jobin Yvon Horiba, NJ) with a temperature controlled sample cell (at 20± 0.1 °C) and a HAAKE K20 temperature controller (Thermo Electron Corporation, Waltham, MA). Measurements were made using a 4 x 4 mm light path quartz cuvette (Starna, Atascadero, CA). The excitation and emission slits were set to 2 nm and 5 nm respectively for optimal intensity measurements.[126] All samples were excited at 295 nm in order to eliminate contributions from amino acid residues other than tryptophan, and also to minimize absorbance by acrylamide. Emission spectra were collected between 300 nm and 450 nm for 1 µM protein in 50 mM ammonium acetate buffer (pH 4.5 and pH 7.0),

Collisional quenching experiments with acrylamide (neutral) and iodide (charged) were employed to analyze tryptophan accessibility of the GM2AP variants. 4 M stock solutions of KI and acrylamide were made fresh, with the addition of 0.1 M sodium thiosulfate to the KI stock solution to prevent triiodide formation given it absorbs in the same region that tryptophan fluoresces.[127] Emmission spectra were collected for 1µM GM2AP variant solutions in 50 mM sodium acetate at pH 4.5 and 7.0 in the absence of, and after each titration of quencher. All measurements were collected in triplicate. Quenching data was analyzed using the Stern-Volmer equation

$$\frac{F_0}{F} = 1 + K_{SV}[Q] \qquad (3\text{-}1)$$

where F_0 and F are the fluorescence intensities in the absence and presence of quencher respectively, [Q] is the quencher concentration, and K_{SV} is the Stern-Volmer quenching constant. The Stern-Volmer quenching constant was obtained from plots of

the ratio of fluorescence intensity at 344nm in the absence of quencher to fluorescence in the presence of quencher vs quencher concentration, and it provided information about the degree of quenching of tryptophan fluorescence. The fraction of total fluorophore accessible to quencher was determined using the modified Stern-Volmer equation

$$\frac{F_0}{F_0 - F} = \frac{1}{f_a} + \frac{1}{f_a K_a [Q]} \qquad (3\text{-}2)$$

where f_a is the fraction of the initial fluorescence accessible to quencher, K_a is the modified quenching constant and F_0, F and Q represent the same variables described in equation 3-1. Plots of F_0/F_0-F vs the reciprocal of quencher concentration were generated and the reciprocal of the y-intercept gave f_a.

Results and Discussion

Site-Directed Mutagenesis

The QuikChange site-directed mutagenesis kit was used in this work to construct a series of tryptophan to alanine substitutions. W5A, W5AW63A, W5AW131A, and W63AW131A were constructed using pET16b-GM2AP wild-type as the DNA template. The mutagenesis method employed the use of mutagenic primer-directed GM2AP gene amplification using polymerase chain reaction. Agarose gel electrophoresis was performed after *Dpn*I digestion of the methylated parent plasmid and selection of mutation-containing amplified DNA[128], to verify successful DNA amplification. Verification of site-directed mutagenesis was obtained by the observation of the *Dpn* I digested PCR products of W5AW63A (Lanes 1, 2, and 3) and W5AW131A (Lanes 4, 5, 6, and 7) analyzed in 1% agarose gel depicted in Figure 3-3. Lane 8 shows pET16b - GM2AP wild-type as a reference. The bands are approximately 6kb in size which

represent plasmid DNA containing nicks, and are at the expected position for linear pET16b plasmid with the GM2AP insert. The absence of bands in lanes 2 and 7 were indicative of a failed PCR amplification reaction. Adding DMSO to the mutagenesis reaction mixture resulted in positive results as it prevented primers and the DNA template from annealing to itself by disrupting base pairing.[129]

After PCR, the resulting mixtures from mutagenesis were transformed into XL-1 blue E. *coli* cells in order to seal nicks in the plasmid DNA and to enhance the stability of the gene in the plasmid. The cells were grown on ampicilin-containing LB agar plates, to allow for the selection of cells that have taken up plasmid possessing our gene of interest. Colonies on the agar plates were selected and the DNA was harvested using a QIAprep spin miniprep kit. Confirmation of amino acid mutations was done by submitting purified plasmid DNA for DNA sequencing at the University of Florida's sequencing facility. Figure 3-4 shows a sample agarose gel picture of the purified products which were submitted. Results from DNA sequencing show the DNA and corresponding amino acid sequences of the GM2AP variants in Figures 3-5, 3-6, 3-7, 3-8, and 3-9. Tryptophan was successfully mutated to alanine as depicted by TGG→GCG conversions at the respective positions in the sequences highlighted in red. Sequence analysis showed that all desired variants were obtained, and their corresponding plasmids containing the mutated genes were transformed into *E. coli* BL21 DE3 cells (a host which allows for high level protein expression and easy induction) for protein expression and purification.

Protein Expression and Purification

GM2AP expression and purification were performed based on modifications reported by Wright et al.[53], and were optimized in our lab. During the purification

process, guanidine HCl and urea buffers were prepared fresh because urea decomposes to form cyanate ions, which can covalently modify primary amines on the target protein. For urea buffer, any degradation products were removed by ion-exchange with AG501-X8 mixed-ion bed resin to prevent protein carbamylation. Glutathione oxidized and reduced were added to the refolding buffer to assist with the formation of the 4 disulfide bonds in the protein. Figure 3-10 shows sample chromatographs after the Ni affinity (A), anion exchange Q (B), buffer exchange (C) Ni after his tag cleavage (D), and size exclusion (E) columns throughout the purification process. Protein was detected by monitoring UV absorption at 280 nm (blue traces). Conductivity of the solution was also monitored (brown traces).

The purity and molecular weight of the various GM2AP variants were monitored by running SDS-PAGE, and comparing the bands to known molecular weight standards (Figure 3-11). Bands appeared near the 20 kDa marker which corresponds closely to the 18kDa molecular weight of GM2AP. The W5AW63A variant in lane 4 showed another band of approximate size 15 kDa. This band possibly suggests the presence of degraded protein. The protein sample was re-run through a size exclusion column in efforts to separate properly folded protein from degraded protein.

Circular dichroism spectra were collected to ensure that the secondary structure of GM2AP variants was conserved after the tryptophan to alanine mutations. Figure 3-12 shows CD spectra of all the protein variants overlaid and compared to the published spectrum for GM2AP wild-type.[92] All variants show a similar profile in agreement with that of the published wild-type, where the secondary structure of the protein predominantly consists of β sheets.

Intrinsic Fluorescence Quenching

Native GM2AP is instrinsically fluorescent because it contains three tryptophan, three tyrosine, and five phenylalanine residues. Our goal was to determine the environment of the tryptophan residues in GM2AP to explore the potential of studying the mechanism of this protein using intrinsic protein fluorescence. For multi-tryptophan proteins, fluorescence studies can be complicated because each fluorescing residue may have its own fluorescence yield, spectral position, and may not contribute equally to the observed fluorescence emission.[130] A series of tryptophan to alanine amino acid substitutions were constructed, allowing for single (W5AW63A, W5AW131A, W63AW131A) and one double (W5A) tryptophan residues to remain in the amino acid sequence of GM2AP. The degree of quenching of the GM2AP variants was investigated using neutral and charged quenchers. Two (W63 and W131) of the three tryptophan residues are located in the putative membrane binding regions of GM2AP. If the residues are accessible for fluorescence quenching, then the sites are exposed and suitable for monitoring changes in protein fluorescence as a result of lipid binding and/or extraction.

To selectively excite the tryptophan residues and not phenylalanine or tyrosine, an excitation wavelength of 295 nm was used and emission peaks were obtained. Maximal emission wavelength was observed at 346 nm for each variant (Figures 3-13 to 3-16). Total concentrations of 0 – 0.31 M neutral quencher acrylamide, and charged quencher KI, were titrated in GM2AP solutions. Figure 3-13 shows the total emission spectra at 20 °C associated with quenching of tryptophan residues in GM2AP W5A at pH 4.5 (A, C) and pH 7.0 (B,D). Similar results were observed for all other variants (Figures 3-14 to 3-16). Fluorescence intensity decreases with increasing amounts of both quenchers. It

must be noted that the overall quenching of protein by acrylamide was greater than that by KI. Total tryptophan fluorescence intensity was quenched on average by 80% with acrylamide, and 55% by iodide. Acrylamide and iodide are known to quench the fluorescence of indole derivatives that have aqueous exposure, but the charge and large size of KI due to hydration, restricts it from accessing buried residues in hydrophobic environments.[98,131] Thus, being a charged species electrostatic effects may affect the quenching action of KI.

Stern-Volmer plots (Figure 3-17) were generated and quenching constants (Table 3-1) were obtained to determine the degree of tryptophan quenching by acrylamide and iodide. The classic interpretation F_0/F vs. [Q] dictates that upward curvature or linear plots indicate that all tryptophan residues are homogeneous and are nearly equally accessible to quencher, while downward curvature results from tryptophan residues are in different environments.[131] Plots at acidic and neutral pH for both quenchers suggested that the tryptophan residues in the GM2AP variants were accessible to quencher, though not to the same degree. For iodide, it was observed that at neutral pH the Stern-Volmer quenching constants for all protein variants were lower than those at acidic pH. This may be explained by the glutamic acid (Glu) and aspartic acid (Asp) residues located in the putative membrane binding loops of the protein – the same regions where W63 and W131 are also present. At neutral pH Glu and Asp are expected to be negatively charged (side chain pKa values of 4.07 and 3.90 respectively) which should generate electrostatic repulsions with the negatively charged iodide ions, resulting in lower Ksv values.

Conversely, tryptophanyl quenching by acrylamide was lower at acidic pH than at neutral pH. The resolved crystal structure of GM2AP shows two conformations of the mobile loop containing W131 – one where the loop is aqueous exposed, and another where the loop was tucked into the protein.[53] The decrease in degree of quenching by acrylamide at acidic pH may be due to a stabilized 'tucked in' or more 'closed' conformation at acidic pH of the region of GM2AP where W131 resides, as was evident by a lower K_{SV} value when W131 is present (W5AW63A) in the protein. GM2AP W63AW131A displayed lower degrees of quenching by both acrylamide and iodide. W5A is located on the backside of the protein, in the region of the hydrophobic binding pocket. Predictably, W5A was not as accessible to quencher as W63 and W131 and this site did not show a pH dependence for acrylamide.

Figure 3-18 shows modified Stern-Volmer plots, which by calculating the reciprocal of the y-intercept for each plot, information about the fraction of accessible fluorophore to quencher at acidic and neutral pH can be obtained. Table 3-1 summarizes the fractional accessibility, f_a to tryptophan fluorescence of the GM2AP variants. The accessibility of the tryptophan residues to both quenchers were approximately 1.This indicates that the residues were accessible for quenching regardless of quencher or pH. However, it must be noted that while f_a tells the fraction of total fluorescence accessible to quencher, it does not mean that all tryptohan residues are equally accessible for quenching.[98]

Conclusions

Here we described the site-directed mutagenesis and protein expression and purification methods W to A constructs of GM2AP. CD spectroscopy revealed that the amino acid substitutions did not alter proper protein folding. The variants were then

used to characterize the intrinsic tryptophan fluorescence of the protein. Quenching results suggest that while the tryptophan residues were accessible to acrylamide and iodide, the degree of quenching varied. W63 seemed to be most accessible, followed by W131, and W5 was not as accessible due to its location in the hydrophobic region of GM2AP. These findings insinuate that since W63 and W131 are located in putative membrane binging regions of the protein, and are solvent exposed, intrinsic tryptophan fluorescence may be a useful technique for the further investigation of the precise molecular mechanism of GM2AP function without the need for attaching fluorescent probes to the protein.

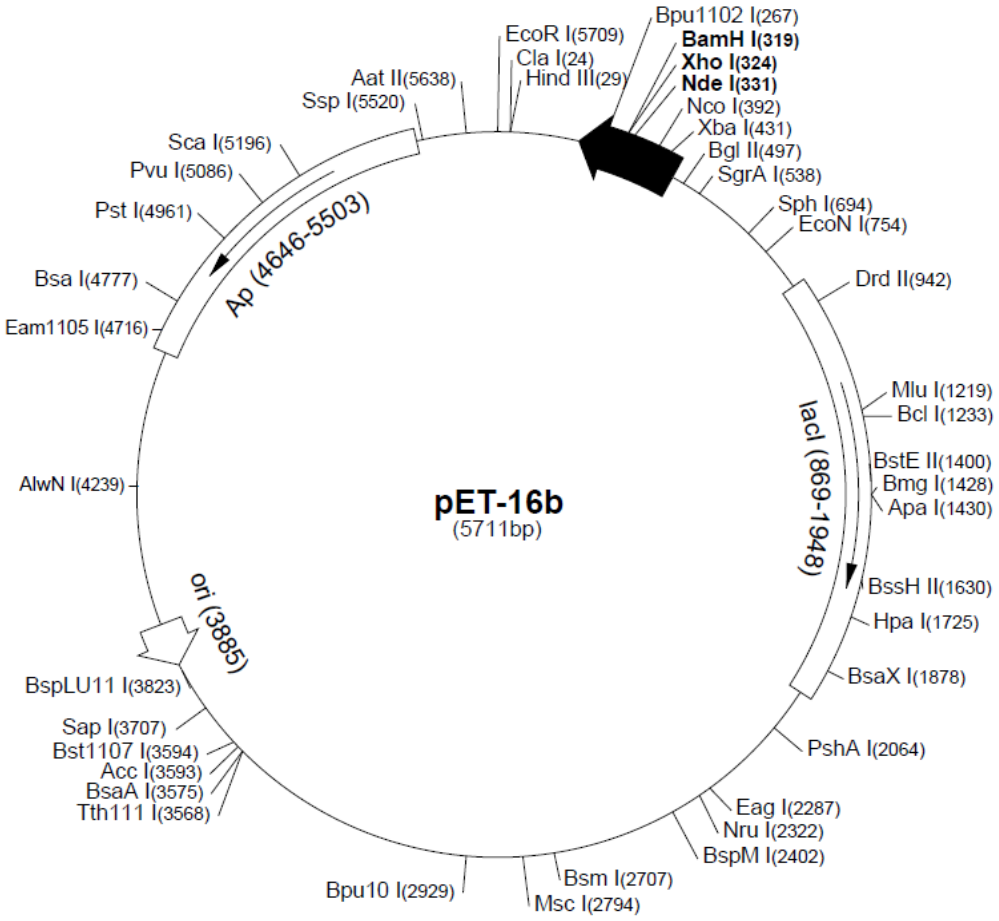

Figure 3-1. pET16b vector map. The T7 promoter region is depicted by the thick black arrow. This region contains the site for insertion of the gene encoding GM2AP DNA. Figure was reprinted from https://wasatch.biochem.utah.edu/chris/links/pET16b.pdf. Accessed May 2012

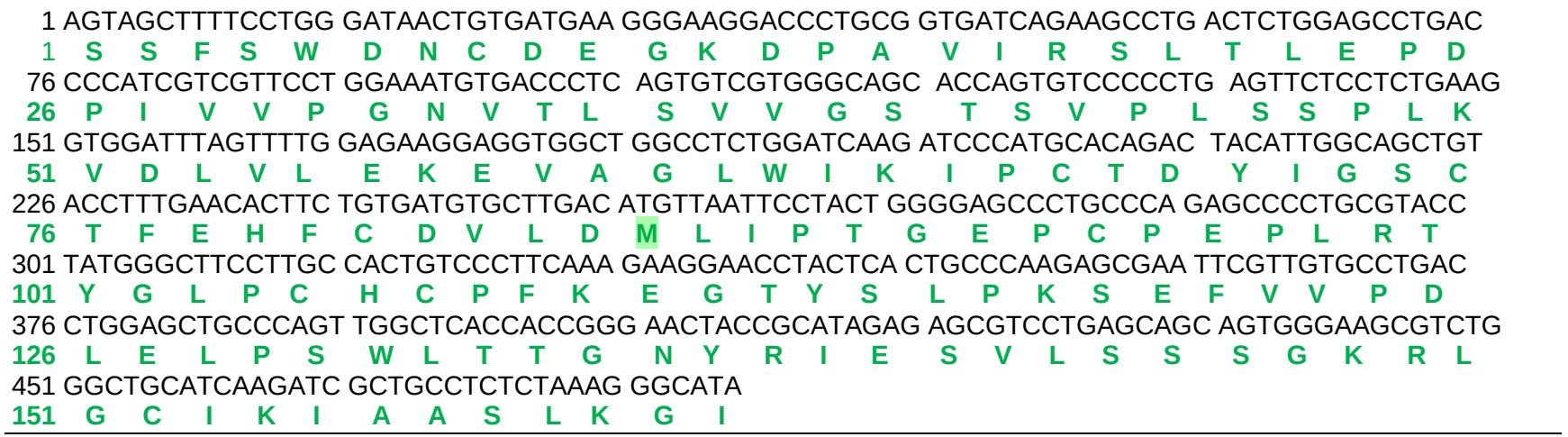

Figure 3-2. *E. coli* codon-optimized DNA and amino acid sequence of GM2AP wild-type protein

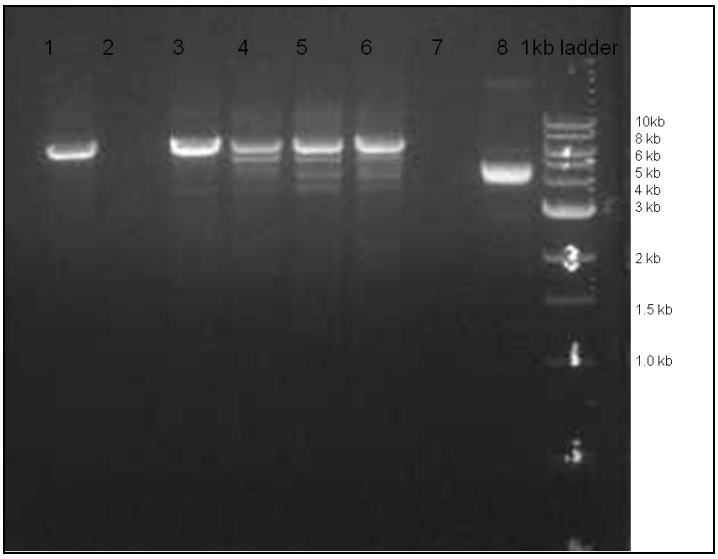

Figure 3-3. Sample agarose gel picture of GM2AP variants after *DpnI* digestion. Lanes 1, 2, 3 W5AW63A; 4, 5, 6, 7 W5AW131A; 8 pET16b-GM2AP wild-type as a reference; 9 1 kb standard DNA ladder from NEB (Ipswich, MA)

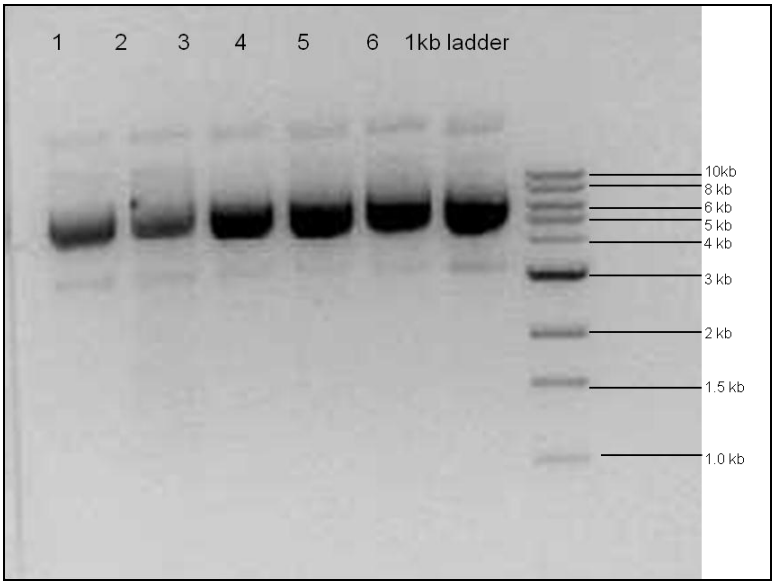

Figure 3-4. Sample agarose DNA gel of pET16b-GM2AP variants after plasmid purification. Lanes 1, 2, 3 W5AW63A; 4, 5, 6 W5AW131A; 7 1 kb standard DNA ladder from NEB (Ipswich, MA)

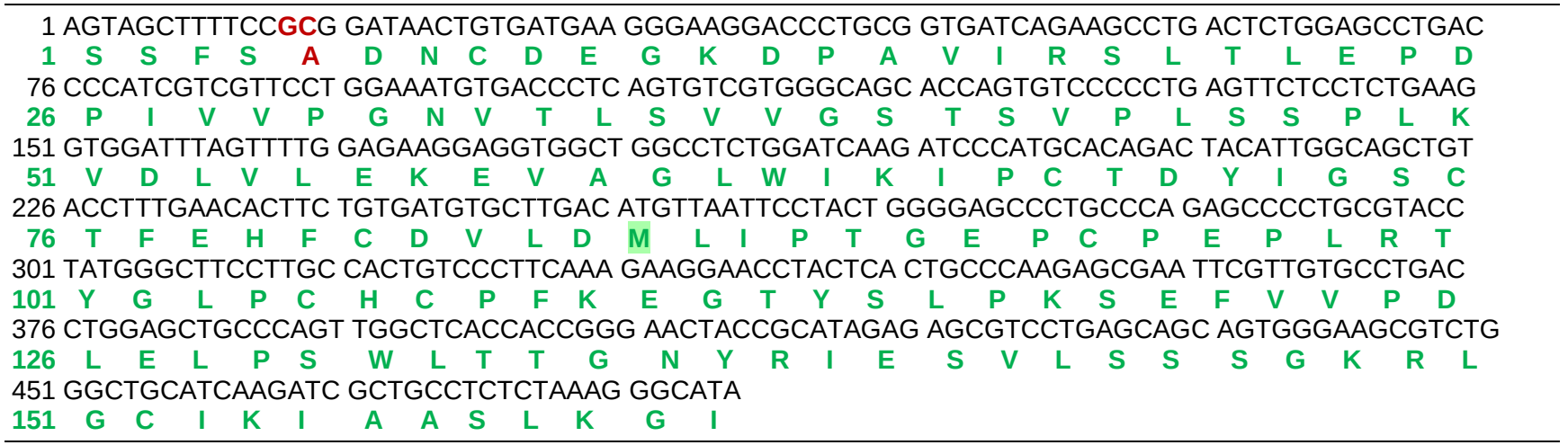

Figure 3-5. E. *coli* codon-optimized DNA and amino acid sequences of GM2AP W5A. The amino acid mutation site is colored red

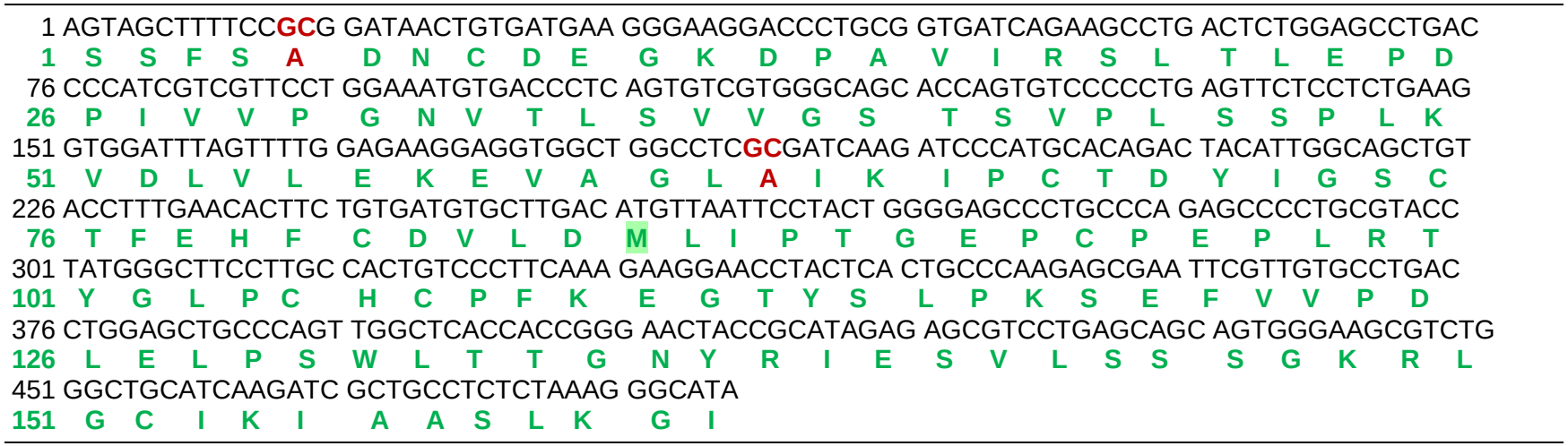

Figure 3-6. E. *coli* codon-optimized DNA and amino acid sequences of GM2AP W5AW63A. The amino acid mutation sites are colored red

```
  1 AGTAGCTTTTCCGCG GATAACTGTGATGAA GGGAAGGACCCTGCG GTGATCAGAAGCCTG ACTCTGGAGCCTGAC
  1  S  S  F  S  A  D  N  C  D  E  G  K  D  P  A  V  I  R  S  L  T  L  E  P  D
 76 CCCATCGTCGTTCCT GGAAATGTGACCCTC AGTGTCGTGGGCAGC ACCAGTGTCCCCCTG AGTTCTCCTCTGAAG
 26  P  I  V  V  P  G  N  V  T  L  S  V  V  G  S  T  S  V  P  L  S  S  P  L  K
151 GTGGATTTAGTTTTG GAGAAGGAGGTGGCT GGCCTCTGGATCAAG ATCCCATGCACAGAC TACATTGGCAGCTGT
 51  V  D  L  V  L  E  K  E  V  A  G  L  W  I  K  I  P  C  T  D  Y  I  G  S  C
226 ACCTTTGAACACTTC TGTGATGTGCTTGAC ATGTTAATTCCTACT GGGGAGCCCTGCCCA GAGCCCCTGCGTACC
 76  T  F  E  H  F  C  D  V  L  D  M  L  I  P  T  G  E  P  C  P  E  P  L  R  T
301 TATGGGCTTCCTTGC CACTGTCCCTTCAAA GAAGGAACCTACTCA CTGCCCAAGAGCGAA TTCGTTGTGCCTGAC
101  Y  G  L  P  C  H  C  P  F  K  E  G  T  Y  S  L  P  K  S  E  F  V  V  P  D
376 CTGGAGCTGCCCAGT GCGCTCACCACCGGG AACTACCGCATAGAG AGCGTCCTGAGCAGC AGTGGGAAGCGTCTG
126  L  E  L  P  S  A  L  T  T  G  N  Y  R  I  E  S  V  L  S  S  S  G  K  R  L
451 GGCTGCATCAAGATC GCTGCCTCTCTAAAG GGCATA
151  G  C  I  K  I  A  A  S  L  K  G  I
```

Figure 3-7. E. *coli* codon-optimized DNA and amino acid sequences of GM2AP W5AW131A. The amino acid mutation sites are colored red

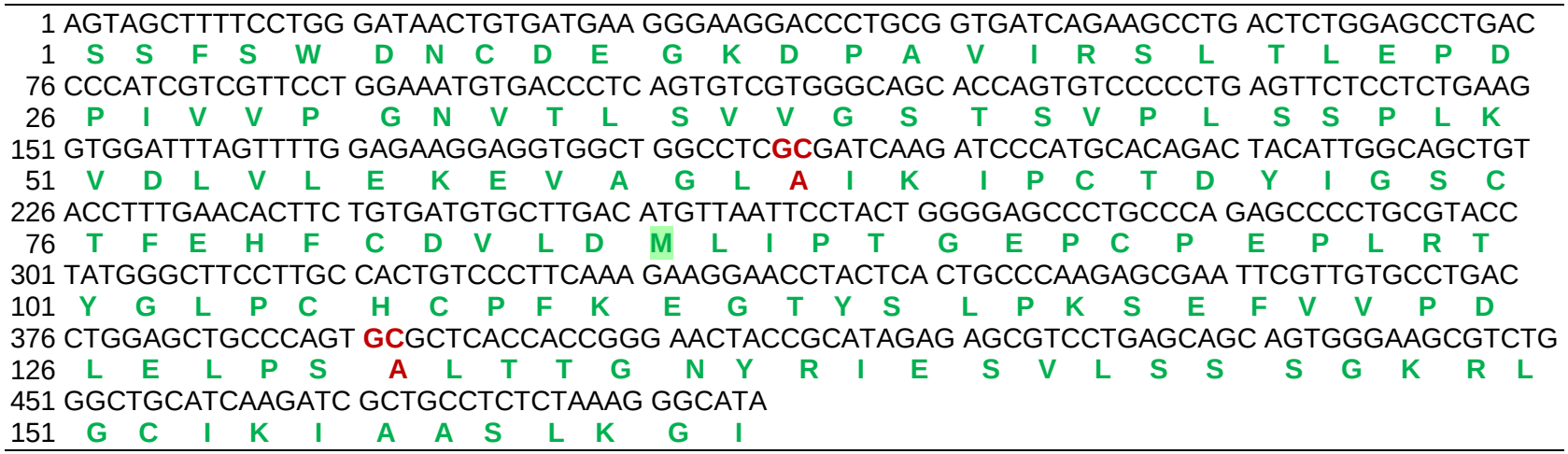

Figure 3-8. E. *coli* codon-optimized DNA and amino acid sequences of GM2AP W63AW131A. The amino acid mutation sites are colored red

```
  1 AGTAGCTTTTCCGCG GATAACTGTGATGAA GGGAAGGACCCTGCG GTGATCAGAAGCCTG ACTCTGGAGCCTGAC
    1  S  S  F  S  A     D  N  C  D  E     G  K  D  P  A     V  I  R  S  L     T  L  E  P  D
 76 CCCATCGTCGTTCCT GGAAATGTGACCCTC AGTGTCGTGGGCAGC ACCAGTGTCCCCCTG AGTTCTCCTCTGAAG
   26  P  I  V  V  P     G  N  V  T  L     S  V  V  G  S     T  S  V  P  L     S  S  P  L  K
151 GTGGATTTAGTTTTG GAGAAGGAGGTGGCT GGCCTCGCGATCAAG ATCCCATGCACAGAC TACATTGGCAGCTGT
   51  V  D  L  V  L     E  K  E  V  A     G  L  A  I  K     I  P  C  T  D     Y  I  G  S  C
226 ACCTTTGAACACTTC TGTGATGTGCTTGAC ATGTTAATTCCTACT GGGGAGCCCTGCCCA GAGCCCCTGCGTACC
   76  T  F  E  H  F     C  D  V  L  D     M  L  I  P  T     G  E  P  C  P     E  P  L  R  T
301 TATGGGCTTCCTTGC CACTGTCCCTTCAAA GAAGGAACCTACTCA CTGCCCAAGAGCGAA TTCGTTGTGCCTGAC
  101  Y  G  L  P  C     H  C  P  F  K     E  G  T  Y  S     L  P  K  S  E     F  V  V  P  D
376 CTGGAGCTGCCCAGT GCGCTCACCACCGGG AACTACCGCATAGAG AGCGTCCTGAGCAGC AGTGGGAAGCGTCTG
  126  L  E  L  P  S     A  L  T  T  G     N  Y  R  I  E     S  V  L  S  S     S  G  K  R  L
451 GGCTGCATCAAGATC GCTGCCTCTCTAAAG GGCATA
  151  G  C  I  K  I     A  A  S  L  K     G  I
```

Figure 3-9. E. *coli* codon-optimized DNA and amino acid sequences of GM2AP W5AW63AW131A. The amino acid mutation sites are colored red

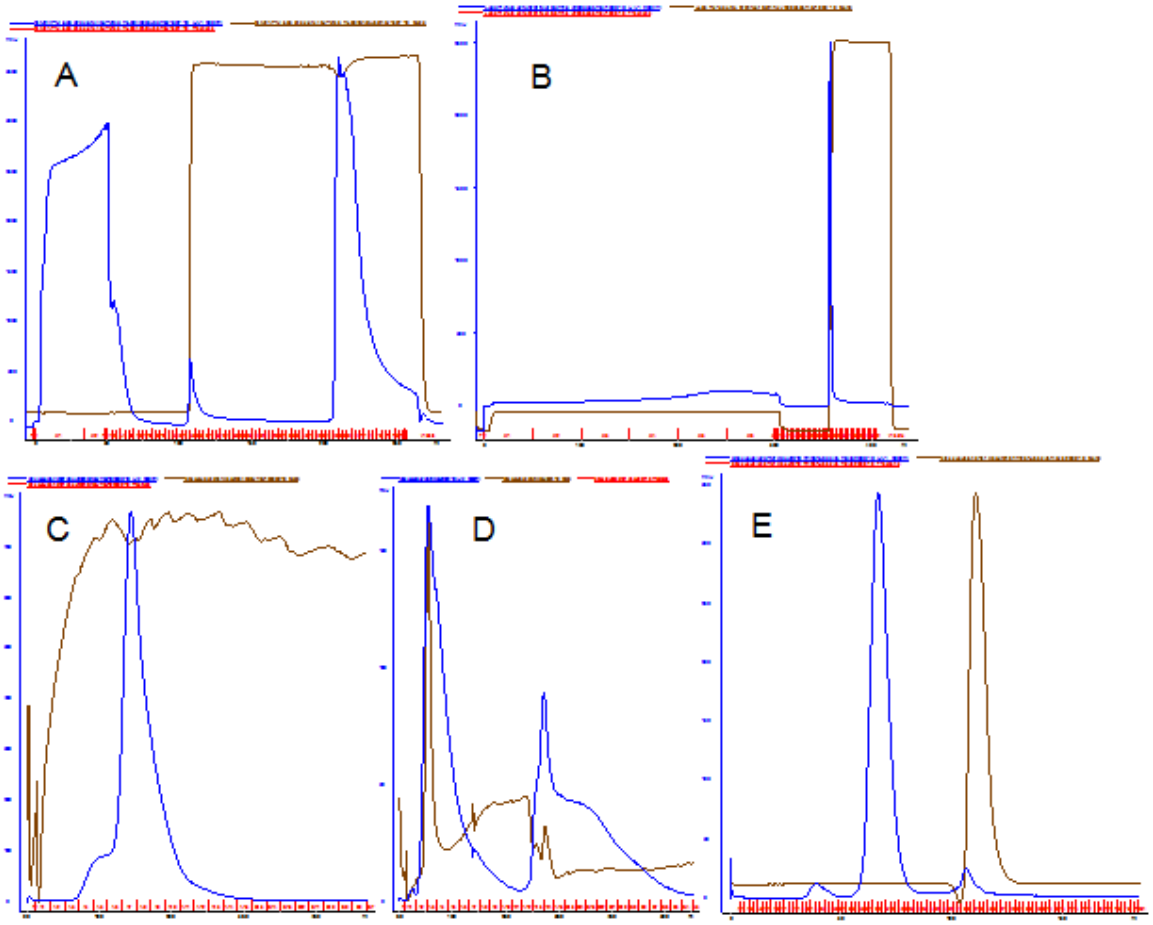

Figure 3-10. Sample column chromatographs during GM2AP purification. UV absorption at 280 nm (blue traces) was used to detect protein after (A) Ni-NTA column, (B) anion exchange Q column, (C) buffer exchange column, (D) Ni-NTA column after histag cleavage, and (E) S200 size exclusion column. The brown traces show solution conductivity

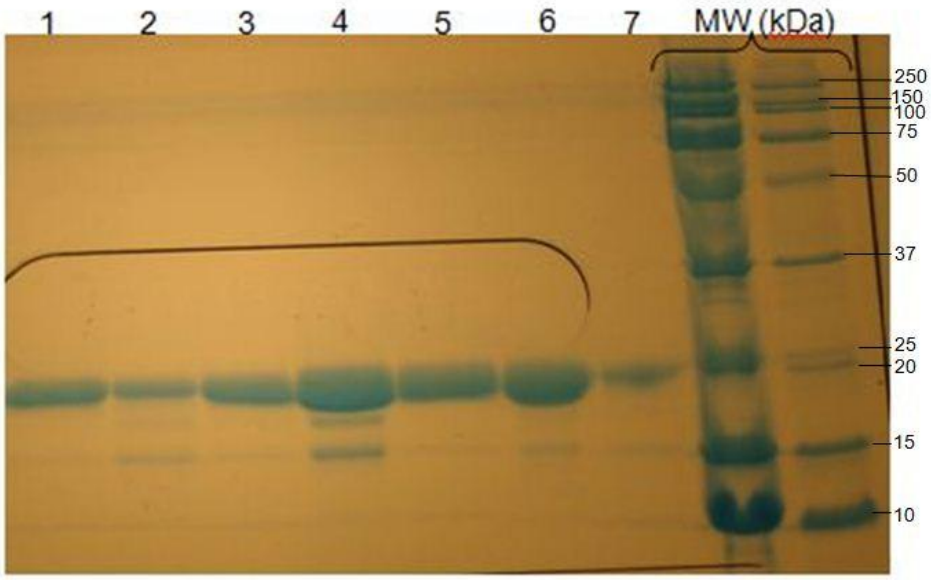

Figure 3-11. 18% SDS-PAGE gel of 15 µL samples of purified GM2AP protein and variants after size exclusion chromatography: Lane 1 Wild-type; 2 W5A; 3, 4 W5AW63A; 5, 6 W5AW131A; 7 W63AW131A. The two MW weight lanes correspond to precision plus protein standards from BioRad (Hercules, CA)

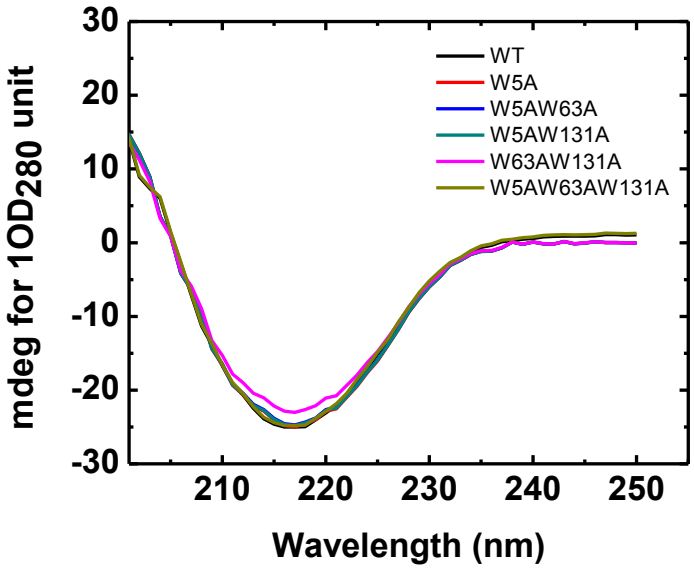

Figure 3-12. Circular dichroism spectra of GM2AP wild-type (black) and 0.5 mg/mL samples of GM2AP variants: W5A (red), W5AW63A (blue), W5AW131A (green), W63AW131A (fuchsia), and W5AW63AW131A (olive)

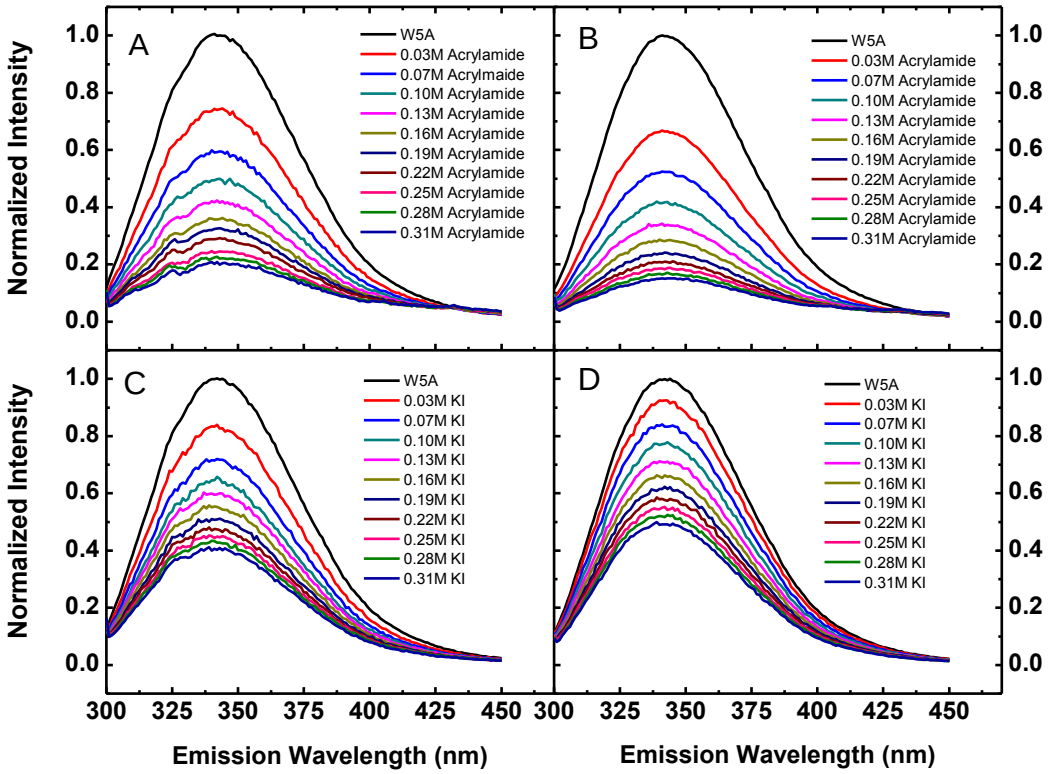

Figure 3-13. Fluorescence emission spectra of 1 µM GM2AP W5A showing results from the titration of increasing amounts of acrylamide at A) pH 4.5, B) pH 7.0, and KI at C) pH 4.5 and D) pH 7.0 as described in the text. Emmision scans were recorded using 2 nm and 5 nm excitation and emission slits while exciting at 295 nm

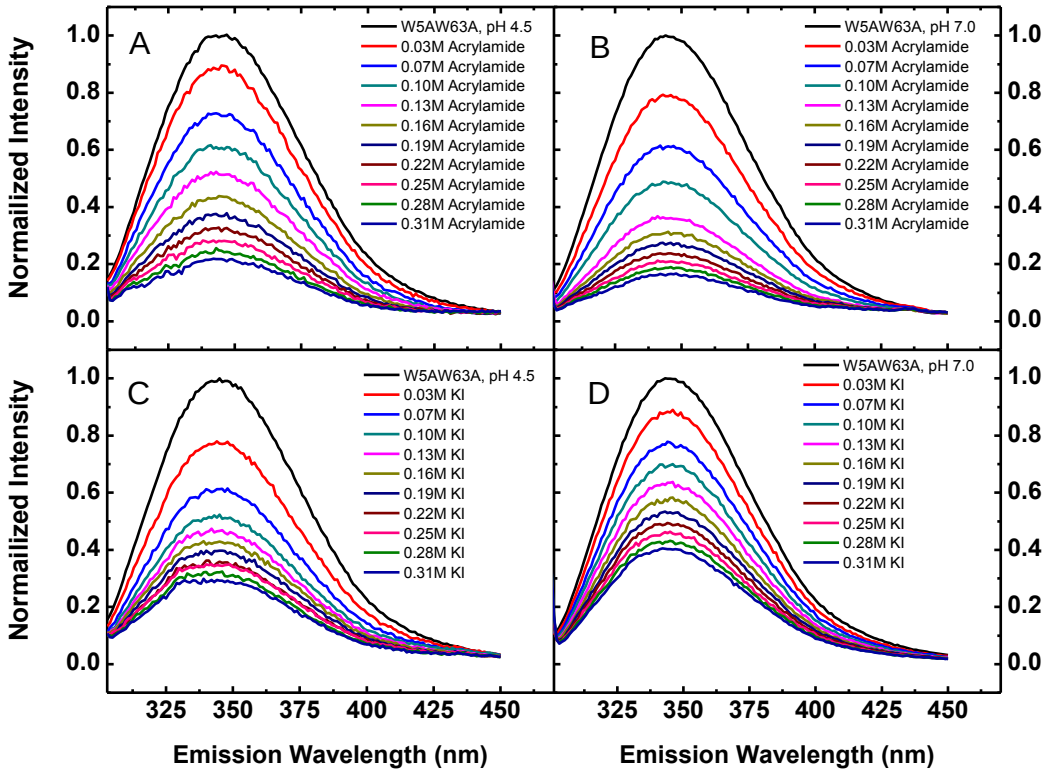

Figure 3-14. Fluorescence emission spectra of 1 µM GM2AP W5AW63A showing results from the titration of increasing amounts of acrylamide at A) pH 4.5, B) pH 7.0, and KI at C) pH 4.5 and D) pH 7.0 as described in the text. Emmision scans were recorded using 2 nm and 5nm excitation and emission slits while exciting at 295 nm

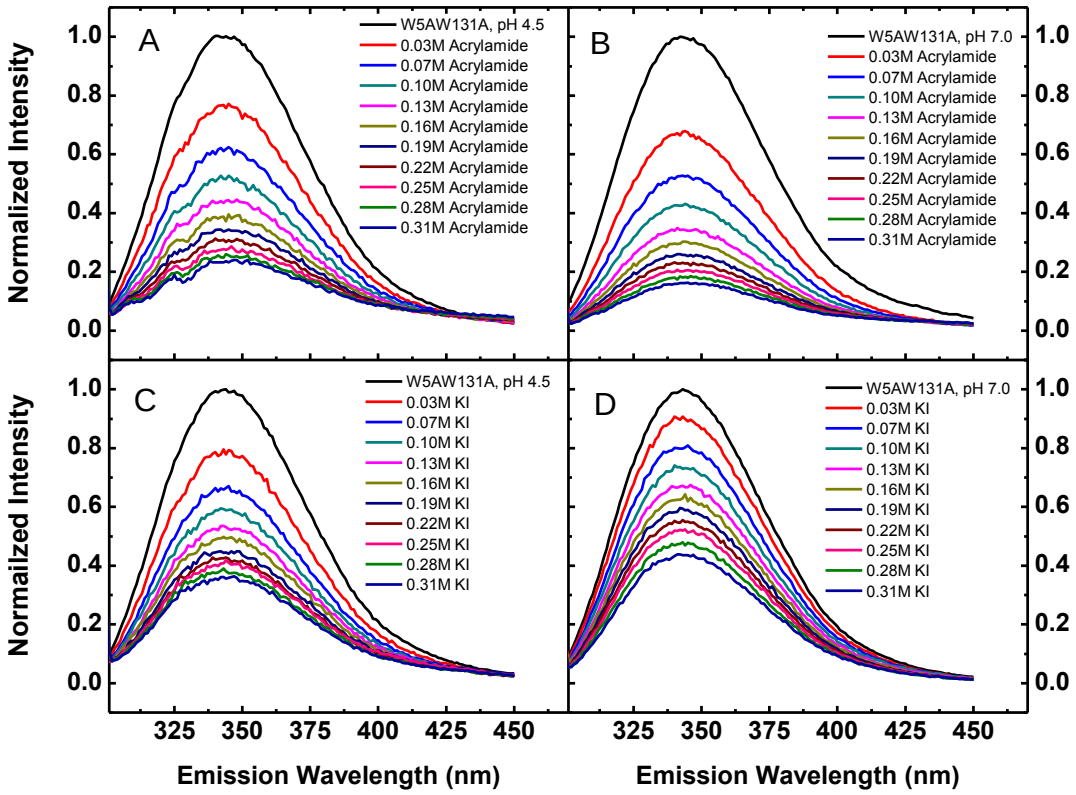

Figure 3-15. Fluorescence emission spectra of 1 µM GM2AP W5AW131A showing results from the titration of increasing amounts of acrylamide at A) pH 4.5, B) pH 7.0, and KI at C) pH 4.5 and D) pH 7.0 as described in the text. Emmision scans were recorded using 2 nm and 5nm excitation and emission slits while exciting at 295 nm

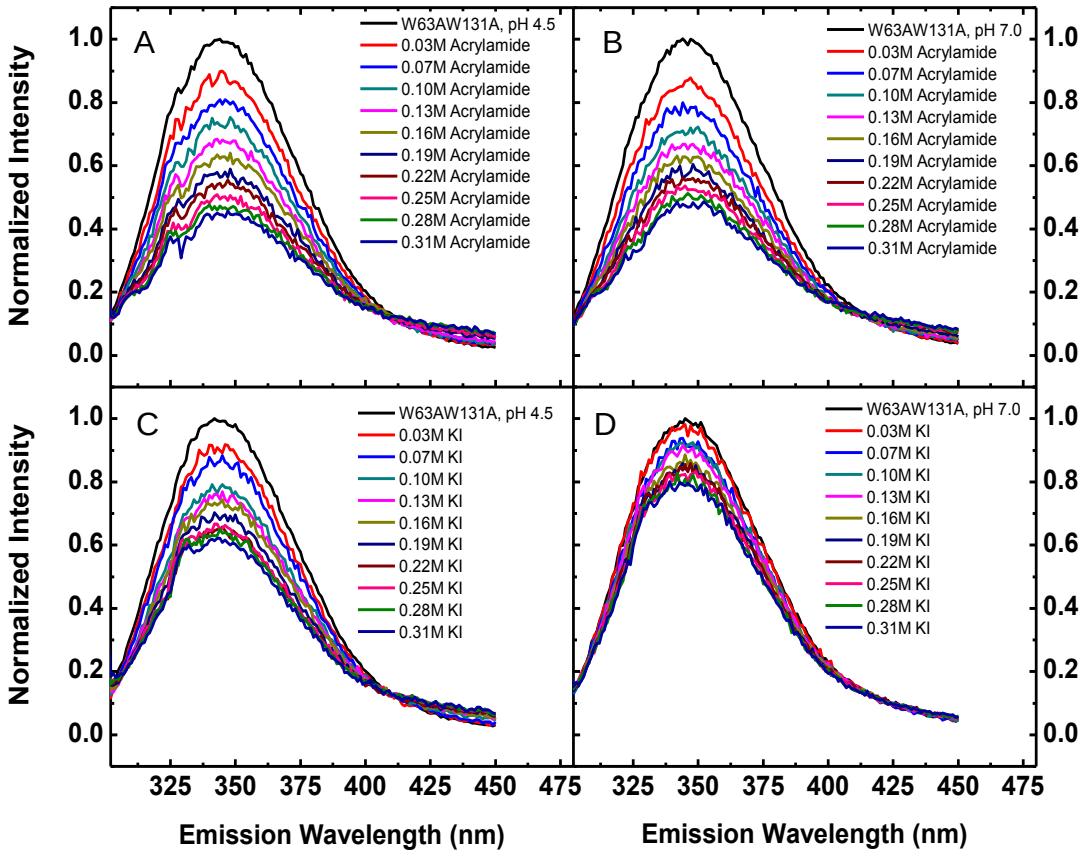

Figure 3-16. Fluorescence emission spectra of 1 µM GM2AP W63AW131A showing results from the titration of increasing amounts of acrylamide at A) pH 4.5, B) pH 7.0, and KI at C) pH 4.5 and D) pH 7.0 as described in the text. Emmision scans were recorded using 2 nm and 5nm excitation and emission slits while exciting at 295 nm

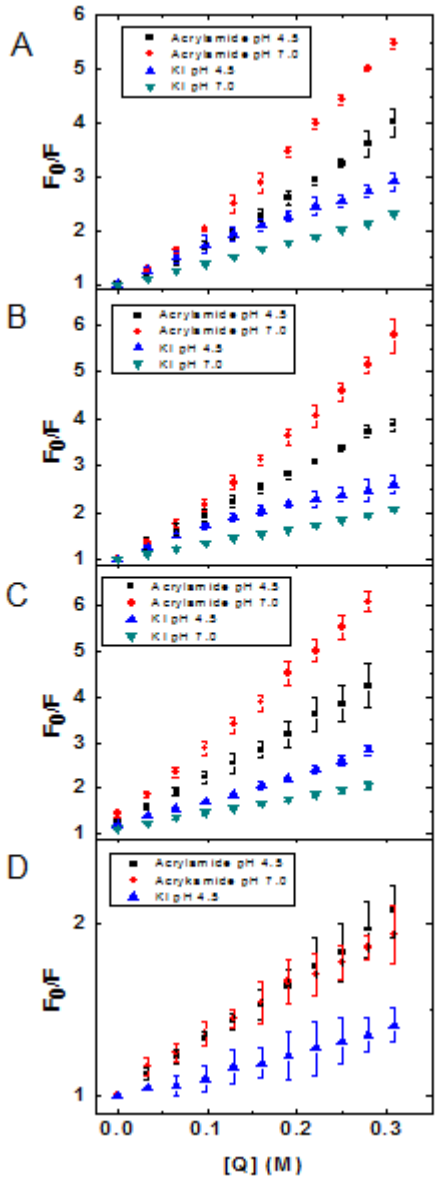

Figure 3-17. Stern-Volmer plots of GM2AP A) W5A, B) W5AW63A, C)W5AW131A, D) W63AW131A quenching by 0 – 0.31 M acrylamide at pH 4.5 (black square); and pH 7.0 (red circle); KI at pH 4.5 (blue triangle) and pH 7.0 (green inverted triangle). All titrations were performed at 20°C with an initial protein concentration of 1 µM; excitation and emission wavelength of 295 nm and 346 nm respectively. Data calculations were corrected for dilution and experiments were done in triplicate

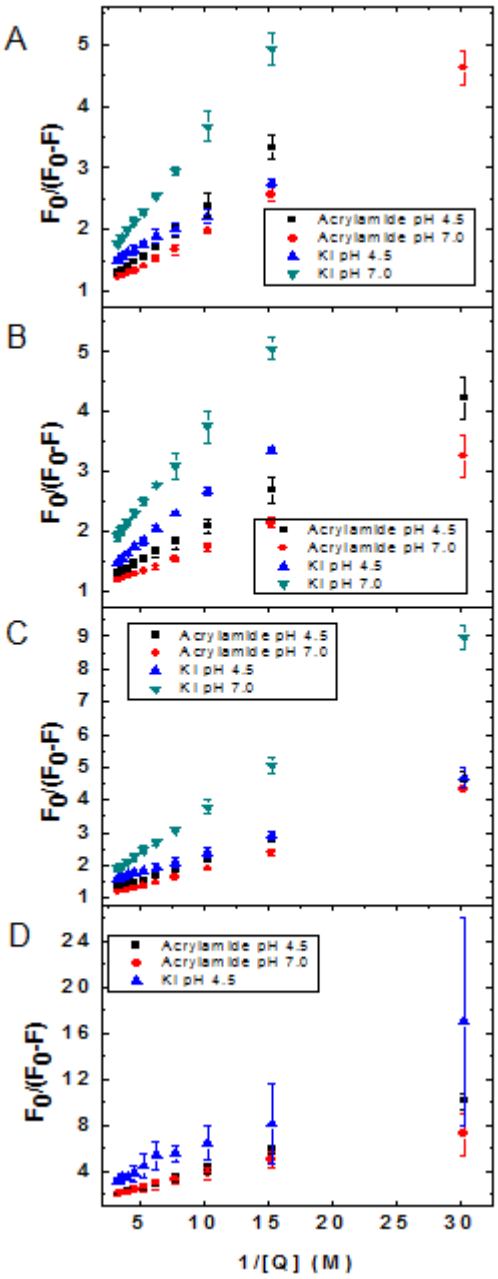

Figure 3-18. Modified Stern-Volmer plots of GM2AP A) W5A, B) W5A/W63A, C)W5AW131A, D) W63AW131A quenching by 0 – 0.3M acrylamide at pH 4.5 (black square) and pH 7.0 (red circle); 0 – 0.31 M KI at pH 4.5 (blue triangle) and pH 7.0 (green inverted triangle). All titrations were performed at 20°C with an initial protein concentration of 1 µM; excitation and emission wavelength of 295 nm and 346 nm respectively. Data calculations were corrected for dilution and experiments were done in triplicate

Table 3-1. Stern-Volmer quenching constants (K_{SV}) and fraction of total tryptophan accessible (f_a) to acrylamide and potassium iodide at acidic and neutral pH

	ACRYLAMIDE			
	pH 4.5		pH 7.0	
Tryptophan Mutant	K_{SV} (M^{-1})	f_a	K_{SV} (M^{-1})	f_a
W5A	10.5 ±0.1	0.97 ±0.01	16.7 ±0.3	0.95 ±0.01
W5AW63A	8.4 ±0.1	0.81 ±0.02	12.9 ±0.1	0.90 ± 0.02
W5AW131A	9.5 ± 0.1	1.10 ± 0.02	13.8 ± 0.1	0.99 ± 0.02
W63AW131A	3.42 ± 0.03	1.03 ± 0.03	3.3 ± 0.10	1.01 ± 0.05
	IODIDE			
W5A	5.6 ±0.1	1.00 ±0.02	3.5 ±0.1	1.11 ±0.2
W5AW63A	6.5 ±0.1	1.00 ±0.02	4.1 ±0.1	1.00 ±0.2
W5AW131A	6.5 ± 0.1	1.21 ± 0.02	3.4 ± 0.1	1.20 ± 0.2
W63AW131A	1.38 ± 0.01	1.30 ± 0.01	-	-

CHAPTER 4
VESICLE BINDING AND LIPID EXTRACTION STUDIES OF GM2 ACTIVATOR PROTEIN VARIANTS

Introduction

Gangliosides are a group of sialic acid-containing glycosphingolipids (GSLs) that are primarily found in the outer leaflet of neuronal cell membranes, where they function as cell markers and are available for cell-signaling events.[1,53] Ganglioside catabolism takes place in the lysosomal compartments of cells and degradation, which entails a stepwise cleavage of oligosaccharide groups, occurs by acidic hydrolases.[59] For GSLs with fewer than four oligosaccharide head groups, hydrolases require non-enzymatic accessory proteins called sphingolipid activator proteins (SAPs) for cleavage.[13,132]

GM2 Activator Protein (GM2AP), one of the five SAPs, is an essential accessory protein for the degradation of the ganglioside GM2 to form GM3 (which is further broken down into reusable components of sphingosine by numerous other enzymes). GM2AP function involves extraction of GM2 from intralysosomal vesicles, followed by a protein-lipid leaving the cell membrane where GM2 is presented to the enzyme β-hexosaminidase A (HexA) for cleavage in solution.[1,51,52] Disruptions in the degradation process lead to the accumulation of harmful quantities of GM2 ganglioside in the neuronal cells, resulting in a collection of diseases called GM2 gangliosidoses—disorders that cause physical and mental disorders in infants that usually resulting in death by age four.[3]

The mature form of GM2AP has been isolated from natural sources and expressed as a glycosylated protein from insect[133] and yeast[56] cells. The nonglycosylated protein has been expressed in *Escherichia coli,*[124] and will be the form used in this study. GM2AP is an 18-kDa protein whose crystal structure of has been

resolved via X-ray crystallography. Studies of the wild type protein have revealed three distinct monomers in the 11-monomer unit cell.[53] The secondary structure of GM2AP comprises an eight-stranded β-cup fold forming a hollow hydrophobic pocket suitable for binding GM2 and contains approximately one half of the 162 total amino acid residues in the protein.[53] The cavity is accessible from one end of the protein only and is lined by surface loops and a 2.5-turn alpha helix at its rim.[53] Analyses of the protein conformations in crystal structures of GM2AP show that one of the two putative membrane binding loops of GM2AP, containing W131, and referred to as the flexible loop - has one conformation where the loop is more structured with W131 tucked into the protein, and two other unstructured conformations where W131 is aqueous exposed.[53]

In addition to taking part in the conversion of GM2 to GM3, GM2AP also functions as a lipid transfer protein. The protein is known *in vitro* to bind and extract several GSLs and phospholipids such as phosphatidylglycerol (PG) and phopsphatidylcholine (PC) from micelles or liposomes and transfer them as soluble 1:1 complexes between membranes.[1,57,60] Phospholipids bind to GM2AP in a different orientation from GM2. GM2 binds in a way that the ceramide tails are tucked in the hydrophobic pocket of the protein and the bulky carbohydrate head group protrudes from the surface of the protein and into the aqueous environment. Phospholipids like PG however, bind in such a way that the entire lipid is buried in the hydrophobic cavity of GM2AP.[60] Figure 4 -1 shows a ribbon structure of GM2AP showing the modeled binding modes of GM2 and PG adopting different orientations within the hydrophobic pocket of the protein.

Despite the fact that the crystal structure and function of GM2AP have been determined, little is known about the specific mechanism involving the interaction with vesicular surfaces, extraction of lipids, and transfer of these lipids between membranes. Studies on the interaction of GM2AP with its specific ligand GM2 have been performed utilizing several techniques such as sucrose density ultracentrifugation, sucrose density isoelectric focusing, polyacrylamide gel electrophoresis, circular dichroism, and steady-state fluorescence spectroscopy.[51,52] Additionally, GM2AP's role as a lipid transfer protein has also been investigated using gel filtration chromatography, thin-layer chromatography (TLC), fluorescence resonance energy transfer (FRET), fluorescence dequenching assays and surface plasmon resonance.[27,51,57,82] GM2AP contains three native tryptophan residues (Figure 4-1), two of which are located in mobile regions of the protein thought to be involved in vesicular membrane binding. We can therefore mutate the more hydrophobic tryptophan residues to a less hydrophobic residue in efforts to modulate effective membrane partitioning and protein activity in order to further understand the molecular mechanism of GM2AP binding and extraction.

Here, a series of single, double, and triple point tryptophan (W) to alanine (A) mutations have been engineered in GM2AP to investigate the changes in lipid extraction from vesicles as a result of decreasing the hydrophobicity of the regions of the protein where the residues are located. The ability of each tryptophan variant to extract and transfer phospholipids from liposomes was investigated by utilizing a fluorescence assay containing dansyl-labeled phospholipids.[134] Additionally, the extraction efficiency of GM2AP in a POPC:GM2 mixture was determined by physical separation and direct measurement of the amount of protein bound to GM2 in solution

after separation.[135] Changes in extraction efficiency, and by extension, the ability of GM2AP to bind and extract GM2 was investigated for each protein variant containing the W to A substitutions.

Materials and Methods

1-Palmitoyl-2-Oleoyl-sn-Glycero-3-Phosphocholine (POPC) in chloroform was purchased from Avanti Polar Lipids (Alabaster, AL) and used without further purification. *N*-(5-dimethylaminonaphthalene-1-sulfonyl)-1, 2-dihexadecanoyl-sn-glycero-3-phosphoethanolamine (Dansyl-DHPE) was purchased from Molecular Probes (Eugene, OR) in the form of powder. Monosialoganglioside GM2 was purchased from Sigma-Aldrich (St. Louis, MO) as a powder. Unless otherwise stated, all other reagents were purchased from Fisher Scientific (Pittsburg, PA).

GM2 Activator Protein Expression and Purification

The DNA of recombinant GM2AP was cloned in pET16b vector and site-directed mutagenesis was performed to acquire the desired protein variants. The protein was over expressed in BL21 (DE3) *E. coli* cells and purified as previously described.[134] A more detailed description of protein purification can be found in Chapter 3. Purity of final protein samples was identified via SDS-PAGE using 18% pre-casted polyacrylamide gels and Coomassie Brilliant Blue detection. To ensure the protein was properly folded, circular dichroism spectra were obtained to verify secondary structure was analogous to published circular dichroism spectra of GM2AP wildtype.[92] Protein concentration was determined by Bradford assay and by UV absorption at 280 nm on a Cary 50 Bio UV-Visible spectrophotometer (Varian, Palo Alto, CA). The appropriate extinction coefficient for each protein variant was provided by the ExPASy website (http://expasy.org) and is listed in Table 4-1.

Lipid Preparation

Mixtures of the appropriate volumes of each lipid in chloroform were prepared and dried under a stream of nitrogen gas. The mixture was further dried overnight for at least 8 hours in a desiccator to produce a film. For fluorescent vesicles (those containing dansyl-DHPE), the tubes containing the films were wrapped with aluminum foil due to fluorophore sensitivity to light. The dried films were rehydrated into appropriate volumes of 50 mM NaOAc, pH 4.8 at room temperature, followed by vortex mixing for one hour and five freeze-thaw cycles using liquid nitrogen. Each lipid mixture was extruded by 55 passes through 100 nm polycarbonate filters using an Avanti handheld mini-extruder (Avanti Polar Lipids) to produce large unilamellar vesicles (LUVs).

Fluorescence Spectroscopic Measurements

Steady-state fluorescence experiments were carried out using a FluoroMax-3 fluorimeter (Jobin Yvon Horiba, NJ) with a temperature controlled sample cell (at 20± 0.1°C) and a HAAKE K20 temperature controller (Thermo Electron Corporation, Waltham, MA). Measurements were made using a 4 mm light path quartz cuvette (Starna, Atascadero, CA). The excitation and emission slits were set to 2 nm and 5 nm respectively and GM2AP in solution was excited at 295 nm. For experiments involving the use of lipids, the excitation and emission polarizers were configured to 90°C and 0°C, respectively in order to provide maximal suppression of scattering artifacts associated with lipid vesicles, which can affect emission intensity and spectral measurements.[126] Fluorescence intensities were corrected for dilution before final analyses.

Dansyl-DHPE Extraction Assay

1 mM stock samples of 4:1 molar ratio POPC:dansyl-DHPE LUVs were diluted with 50 mM sodium acetate buffer pH 4.8 to give a final concentration of 1 µM LUVs in 300 µL solution. Emission spectra were collected between 400 and 600 nm with a dansyl excitation of 340 nm and excitation and emission slit widths set to 8nm and 5 nm respectively. Protein was added to the LUVs to give a final concentration of 5 µM and the fluorescence emission intensity and maximal wavelength change as the GM2AP:dansyl complex was being formed, was monitored over time. Spectra were collected until the maximum intensity was constant at or near 484 nm. Transfer rates of DANSYL-DHPE by the different W to A variants monitored at 484 nm and were determined according to Equation 4-1 and plots of relative transfer of dansyl-DHPE from liposomes as a function of time were generated.

$$\text{Relative transfer of dansyl-DHPE} = \frac{I_t - I_0}{I_f - I_t} \times 100 \qquad (4\text{-}1)$$

where I_t is the fluorescence emission intensity at 484 nm at time t, I_0 is the fluorescence emission intensities at 484 nm in the absence of protein, and and I_f is the constant maximum fluorescence intensity at 484 nm after dansyl-DHPE had been sequestered from liopsomes.

GM2 Extraction

10 nmol GM2AP variants were mixed with 300 nmol POPC: GM2 (9:1) vesicles in 50 mM sodium acetate buffer pH 4.8. Mixtures of GM2AP variants with vesicles had a final volume of 100µL and were incubated at room temperature for 60 minutes before loading onto a 1.6 x 500 mm Sephacryl S-200 self-packed column (GE Healthcare, Piscataway, NJ). With the aid of a peristaltic pump the vesicles and GM2AP-GM2

complexes were separated by size exclusion chromatography (SEC). 200 µl eluate fractions were collected. GM2AP concentrations in fractions that did not contain vesicles (did not scatter light) were determined by measuring UV absorbance at 280 nm in a 1-cm path length cuvette on a Cary 50 Bio UV-Vis spectrophotometer (Varian, Palo Alto, CA). GM2 concentrations in each fraction were measured by a resorcinol assay previously described.[18,136] Breifly, the collected fractions were mixed with an equal volume of resorcinol reagent, and then the mixture was incubated in boiling water for 15 minutes. The tubes containing the fractions were then cooled and 60 µL of 85:15 n-butyl acetate:n-butanol were added to each tube. The mixture was centrifuged at 4000 rpm for 2 minutes using a benchtop centrifuge (Beckman, Fullerton, CA) to separate the phases. GM2 ganglioside concentrations from the GM2-resorcinol complex were determined by measuring UV absorbance at 580 nm, using a 1-cm path length cuvette and an extinction coefficient of 5700 $mol^{-1}cm^{-1}$. The amount of GM2AP variant bound to the vesicles and hence, extraction efficiency of the protein was determined by subtracting the concentration of the protein in fractions that did not contain vesicles from the total protein concentration in the mixture prior to gel filtration.

Results and Discussion

In addition to extracting and forming a complex with its functional ligand GM2, GM2AP is known to bind and extract other lipid ligands.[12,25,60] Unlike GM2, where the sugar head group of the ligand is solvent exposed while the acyl chains are buried inside the hydrophobic cavity of the protein, GM2AP has been crystallized with phosphoglycerol lipids showing the entire lipid structure oriented in the binding pocket of the protein.[60,137] It has been shown that GM2AP forms a 1:1 protein-ligand complex with *N*-(5-Dimethylaminonapthalene-1-sulfonyl)-1, 2-dihexadecanoyl-*sn*-glycero-3-

phosphoethanolamine (DANSYL-DHPE), a dansyl labeled glycerophospholipid, which is suspected to adopt a binding mode similar to that of PG.[134] When the dansyl fluorophore is in a non-polar environment, the wavelength of maximal emission is blue-shifted when compared to being in a polar environment.[97] Fluorescence intensity is also increased. Figure 4-3 shows how this fluorescent property of dansyl is used to observe a wavelength shift from 518 nm - when dansyl-DHPE is incorporated in100 nm large unilamellar vesicles consisting of 4:1 POPC:dansyl DHPE vesicles - to 484 nm, when dansyl-DHPE is sequestered by GM2AP for form the protein-lipid complex.[134] 5 μM GM2AP wildtype was added to 1 μM POPC:dansyl-DHPE (4:1) vesicles and emission spectra were obtained every 15 seconds until there was no change in wavelength shift. The molar ratio of GM2AP to total dansyl-DHPE was 25:1 in order to ensure complete sequestration of dansyl-DHPE from the outer lipid bilayer. Plots showing the change in wavelength intensity at 484 nm as a function of time while GM2AP was extracting dansyl-DHPE were recorded and fit to appropriate curves (Figure 4-4B).

Ganglioside degradation occurs in the acidic lysosomal compartment of cells where pH is around 4.8. Figure 4-3A shows the rate of transfer at 484 nm as wild-type GM2AP extracts dansyl-DHPE over time at different pHs. Data collected for pHs 4.8 and 5.5 were fit to single exponential first order curves (Equation 4-2), the data for pH 6.0 was fit to a Boltzmann function curve (Equation 4-3), and the data for pHs 6.5 and 7 were fit to linear curves.

$$y = y_0 + Ae^{-\frac{x}{t}} \tag{4-2}$$

$$y = \frac{A_1 - A_2}{1 + e^{(x - x_0)/dx}} + A_2 \tag{4-3}$$

$$y = ae^{-e^{(-k(x-x_c))}} \quad (4\text{-}4)$$

For data fit by first order exponential curves, the half lives, defined as the time required for one half of the total dansyl-DHPE to be sequestered by GM2AP, were determined. At pH 4.8, the half life was found to be 1.5 ±0.2 minutes (Figure 4-4A). The rate of lipid extraction decreases with increasing pH. At pH 5.5 the observed time for one half of total dansyl-DHPE extraction was 4.3 ± 0.3 minutes and at pH 6.0, 16.4 ± 1 minutes were required. For data collected at pH 6.0, we defined the half life as the time when half of the total amount was extracted, where the total value was taken as the equilibrium value after 60 minutes. No appreciable lipid extraction was observed at pH 6.5 or 7.0.

Although GM2AP can function as a lipid transfer protein where binding, extraction, and transfer of lipids other than GM2 can occur, acidic pH conditions (optimal at 4.8) seem to be required for extraction to proceed. Note, we have found that ligand binding is not pH dependent, but membrane binding, and thus lipid extraction and transfer are. The pH dependence of membrane binding can be understood by considering the electrostatic potential of the surface of GM2AP as the pH changes. There are a number of aspartic acid (D) and glutamic acid (E) residues around the binding pocket of GM2AP and at acidic pH, these amino acid residues likely become protonated. We can postulate that protonation of D and E reduces the charge lining the pocket and exposes the hydrophobic residues in the binding cavity to accommodate lipid binding and extraction.

Figure 4-4B shows plots of the relative transfer of dansyl-DHPE from liposomes to GM2AP monitored at 484 nm vs. time for the W to A variants in comparison with wild-

type (WT) GM2AP. Plots for W5A, W5AW63A, W5AW131A, W5AW63AW131A were fit to single exponential first order curves (Equation 4-2), and the W63W131A plot was fitted to a SGompertz sigmoidal curve (Equation 4-4). When tryptophan is substituted with alanine at amino acid position 5 (W5A), similar extraction rates to WT were observed where the time for one half of total dansyl-DHPE extraction for each were 1.5 ± 0.2 minutes and 2.2 ± 0.1 minutes; respectively. This result is not unexpected given that W5 is located on the back side of the protein's beta sheet and not in the region of the protein thought to be involved in binding to the lipid membrane surface for ligand extraction. An amino acid residue substitution at that site should not affect GM2AP transfer rates.

For W5AW131A a half life of 2.7 ± 0.2 minutes was observed, which is approximately 2x slower than WT. Resolved crystal structures of GM2AP show two different conforms of the W131 flexible loop of the protein in the 11 monomer unit cell, where the loop is solvent exposed in one conformation and tucked in the other.[53] Based upon results of cross-linking studies of this loop (Jeff Carter PhD dissertation 2012), we believe that the flexibility of this loop regulates access to the hydrophobic cavity where extracted lipid resides. Interestingly, the alanine substitution at this site does not dramatically alter the rate of ligand extraction; implying that the hydrophobicity of this loop does not regulate membrane binding.

In comparison, for all constructs containing W63A, lipid extraction rates werefour or more times lower compared to WT. For the W5A/W63A variant, a half life of 6.0 ± 0.3 minutes was observed. With the W63AW131A and W5AW63AW131A constructs, the kinetics of dansyl-DHPE sequestration slowed further, to 8.0 ± 0.1 and 10 ± 0.4

minutes; respectively. Based upon X-ray structures and results from our lab using power saturation spin labeling electron paramagnetic resonance (EPR), a model of how GM2AP interacts with the membranes to extract lipids has been proposed. From X-ray models alone, GM2AP was proposed to sit “upright” on the bilayer with the hydrophobic loop that contains W63 protruding into the membrane surface. Contrary to this orientation, powere saturation data suggest a model where the face of GM2AP has the opening to the lipid cleft, which includes the flexible loop containing W131 juxtaposed on the bilayer surface.[138] Results from these W/A mutagenesis studies indicate that it is likely that GM2AP first binds to the membrane via the hydrophobic loop, with then rotation to the orientation suggested by EPR results (Figure 4-5). Hence the hydrophobicity of W63 is critical for the initial membrane binding event, whereas W131 is likely only involved in modulating the mobility of the flexible loop.

These results indicated that although the W/A variants are still able to extract dansyl-DPHE from vesicles, removal of the tryptophan residues from the apolar and flexible loops decreased initial extraction rates, providing insights into the molecular steps of membrane binding, lipid recognition, and extraction. Wimley and White developed a hydrophobicity scale to determine the contribution of whole amino acid residues to the partitioning of lipid membranes.[139] The scale ranks the interfacial hydrophobicity for the 20 natural amino acids, and it is shown that aromatic residues like tryptophan are more favored at the membrane interface due to high hydrophobic interactions. The hydrophobicity scale supports our claim that substituting alanine residues for tryptophan would disrupt the hydrophobic interactions at the membrane interface, weakening GM2AP’s ability to bind lipid.

The results described above assay the effects of the mutations on GM2AP's ability to bind lipid membranes and extract modified phospholipid. Given that the binding pocket in GM2AP differs for phospholipids and gangliosides, we investigated the effects of the W/A substitution on the ability of GM2AP to mobilizes its functional ligand, GM2 from vesicles. To determine how GM2 extraction efficiency was altered as a result of the W to A amino acid substitutions, an equilibrium gel filtration assay was used. Extraction efficiency is described as the ratio of the molar amount of GM2 relative to GM2AP recovered after gel filtration in non-vesicle fractions.[125] Figure 4-6 shows the elution profiles of the amounts of GM2 and GM2AP measured in the collected fractions after gel filtration. GM2AP was allowed to incubate for 60 minutes with 100 nm extruded 9:1 POPC:GM2 vesicles in 50 mM NaOAc buffer at pH 4.8. The measured concentrations of GM2 and GM2AP were used to determine the extraction efficiency of each protein variant. Due to light scattering resulting in high absorbance readings at 280 nm, protein concentrations could not be determined in eluted fractions containing vesicles. However, the total protein concentration was known for each experiment, so the total amount of protein bound to GM2 was determined by subtracting the protein concentration measures from fractions without vesicles from the initial total protein concentration.

WT and W5A constructs showed the largest ratio of about 0.5, meaning that approximately one half of the protein added to vesicles formed a complex with GM2. The W5A/W131A variant had a ratio of 0.43, while W5A/W63A and W63A/W131A had ratios of 0.40 and 0.37 respectively. Within error, these ratios are similar indicating that the equilibrium extraction of GM2 is not affected by making W to A substitution in the

putative membrane binding loops of the protein. Results from this assay support the idea that the point mutations made in the mobile loops of the protein did not hinder lipid extraction ability, but rather affected the protein's efficiency at binding to the vesicular membrane prior to lipid extraction.

Conclusions

GM2AP is essential for GM2 degradation in neuronal cells and also functions as a phospholipid transfer protein. As shown here, a dansyl based fluorescence assay to determine changes in lipid transfer, and a gel filtration assay to determine lipid extraction efficiency of a series of W to A GM2AP constructs was used to study the protein's molecular interactions with liposomes. Removal of tryptophan residues from the mobile loops of GM2AP resulted in slower lipid binding, but did not affect lipid extraction. Binding to lipid vesicles becomes more difficult because the hydrophobic characteristic of tryptophan residues located in the apolar and hydrophobic loops of GM2AP is favored for hydrophobic interactions at the lipid membrane interface. Our results corroborate previous findings that it is likely that GM2AP first binds to the membrane via the hydrophobic loop, with then rotation to the orientation that has the opening to the lipid cleft, which includes the flexible loop containing W131 juxtaposed on the bilayer surface, allowing lipid to be extracted into the binding pocket of the protein. Additionally, while GM2AP also functions as a lipid transfer protein, an acidic environment (near pH 4.8) seems to be required for optimal protein function.

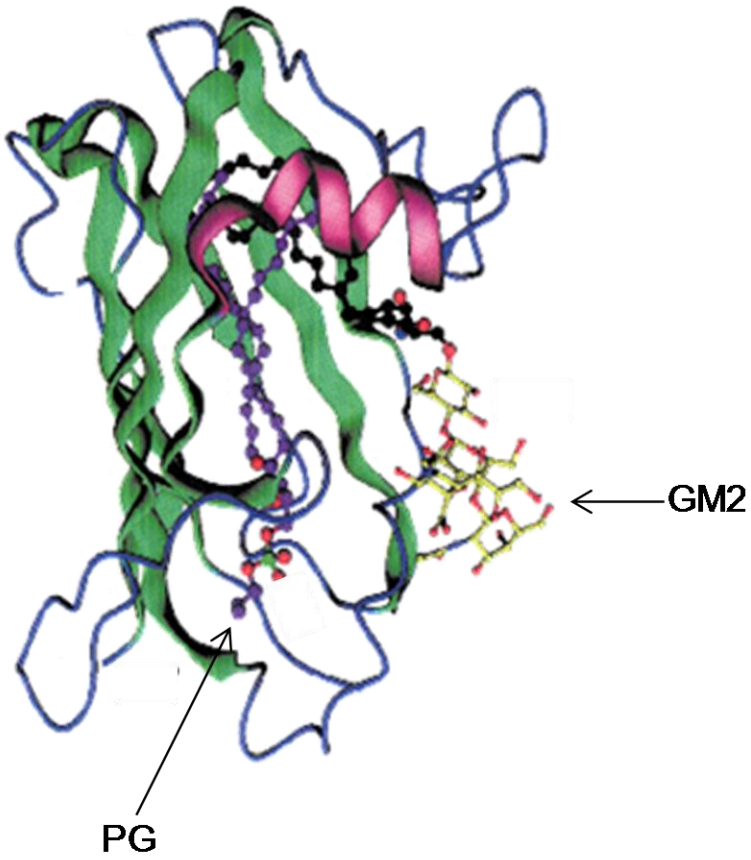

Figure 4-1. Ribbon structure of GM2AP showing the modeled binding modes of GM2 and PG adopting different orientations within the hydrophobic pocket of the protein. The carbohydrate head group of GM2 protrudes from the surface of the protein, while PG is entirely buried in the hydrophobic cavity. Reprinted from *Journal of Molecular Biology*, *331*, Wright, C.S.; Zhao, Q.; Rastinejad, F., Structural Analysis of Lipid Complexes of GM2-Activator Protein, 951-964., Copyright (2003), with permission from Elsevier

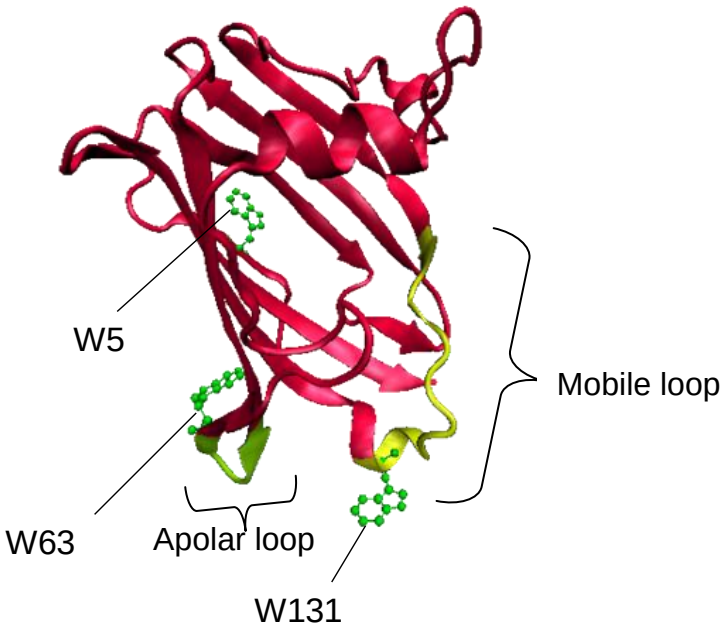

Figure 4-2. Ribbon structure of GM2AP (PDB ID IG13) showing the location of the three native tryptophan residues (green) and the two putative binding loops (yellow highlights). Figure made via VMD

Table 4-1. Extinction coefficients of GM2AP wildtype and its W to A variants

Protein Variant	Extinction coefficient ($M^{-1}cm^{-1)}$
WT	23000
W5A	17460
W5AW63A	11960
W5AW131A	11960
W63AW131A	11960
W5AW63AW131A	6460

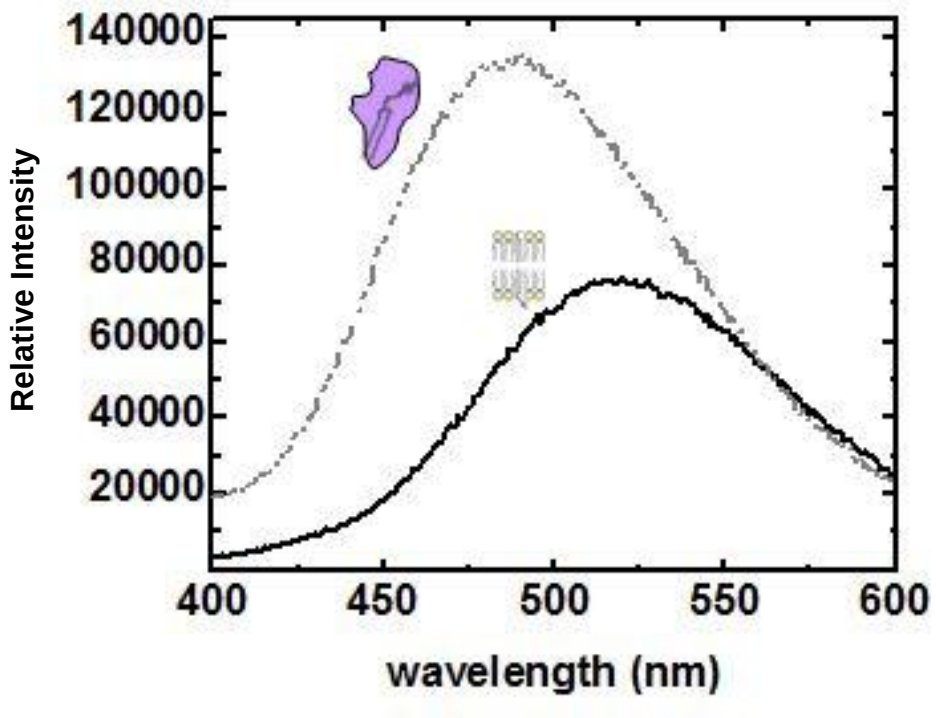

Figure 4-3. Fluorescence emission spectra of 1μm 4:1 POPC:dansyl-DHPE (black solid line) and 0.2 μM 1:1 wild-type GM2AP:dansyl-DHPE (grey dashed line) complexes after 16 minutes. The blue shift in maximal emission wavelength and increase in intensity suggests the dansyl headgroup is located in a more hydrophobic environment. Both protein and lipid vesicles were in 50 mM NaOAc, pH 4.8. The spectra were taken at 20°C on a FLUOROMAX-3 with an excitation wavelength of 340 nm. The excitation polarizer was set to 90° and the emission polarizer was set to 0°

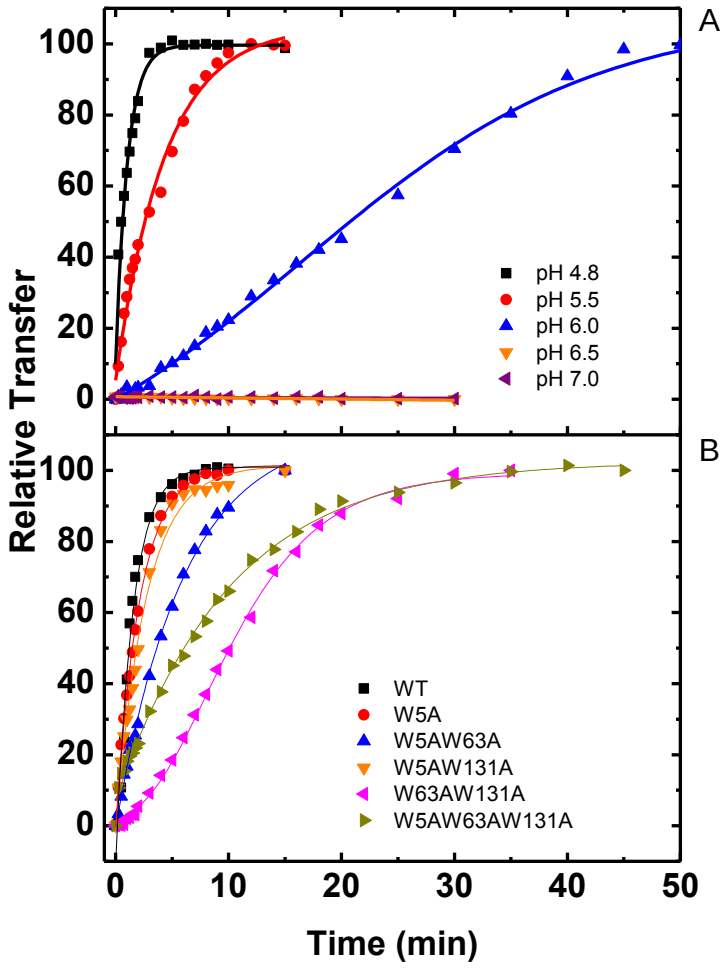

Figure 4-4. Changes in relative transfer as dansyl is being sequestered from 1 mM 4:1POPC:dansyl-DHPE vesicles at 484 nm by (A) 5 μM WT at different pHs as a function of time, and (B) 5 μM protein variants at pH 4.8 as a function of time

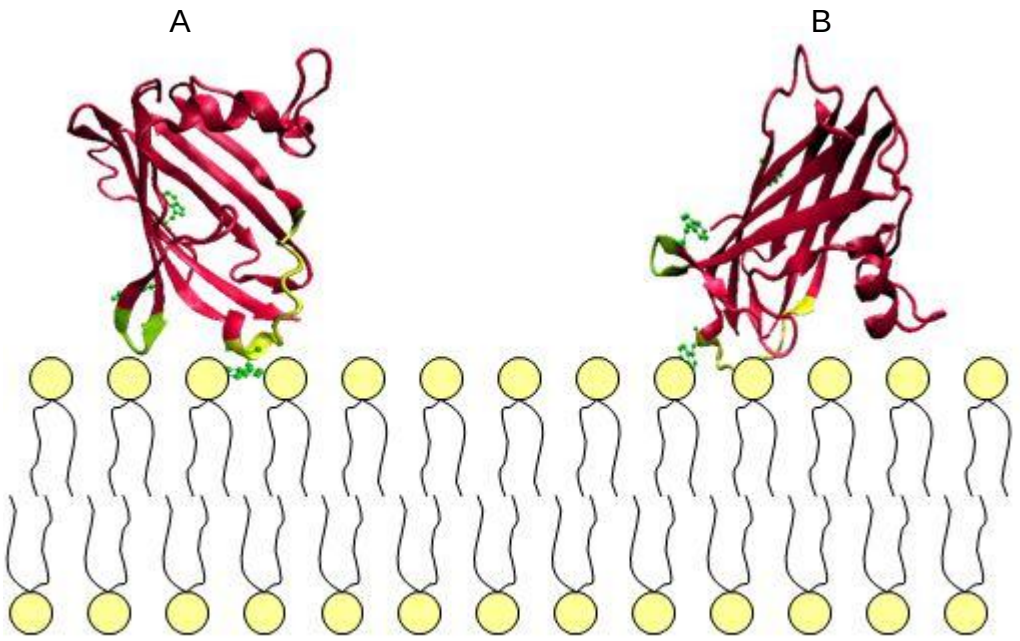

Figure 4-5. Proposed model of the membrane bound orientation of GM2AP. GM2AP first binds to the membrane via the hydrophobic loop (A),then rotates to the orientation that has the opening to the lipid cleft, which includes the flexible loop containing W131 juxtaposed on the bilayer surface(B)

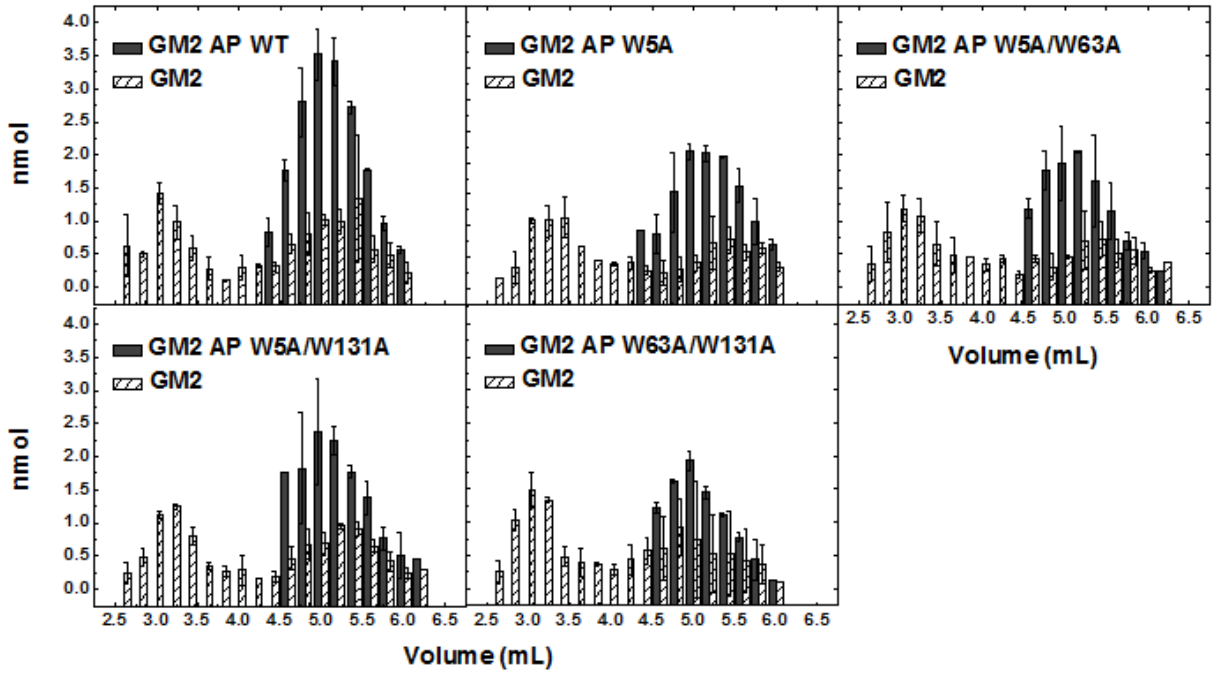

Figure 4-6. Elution profiles showing the extraction efficiency of GM2 extraction by a series of W to A GM2AP variants. 10 nmol protein was mixed with 300 nmol POPC:GM2 (9:1) vesicles in 50 mM NaOAc pH 4.8 buffer and allowed to react for 60 minutes before separation via SEC. The average fraction size was 200 µl. The striped columns show the amount of GM2 (determined by resorcinol assay) in each fraction. The grey columns show the amount of protein (determined by UV-Vis) in each fraction. Fractions containing vesicles were not assayed for protein concentration

Table 4-2. Half lives and extraction efficiencies of GM2AP variants and their ratios with respect to WT protein

Variant	Half life	Ratio of half life to WT	Extraction efficiency	Ratio of extraction efficiency to WT
WT	1.5 ± 0.2	-	0.50 ± 0.05	-
W5A	2.2 ± 0.1	1.5 ± 0.3	0.47 ± 0.07	1.0 ± 0.2
W5AW63A	6.0 ± 0.3	4.0 ± 0.7	0.40 ± 0.13	0.80 ± 0.34
W5AW131A	2.7 ± 0.2	1.8 ± 0.4	0.43 ± 0.09	0.90 ± 0.27
W63AW131A	8.0 ± 0.1	5.3 ± 0.8	0.37 ± 0.04	0.70 ± 0.15
W5AW63AW131A	10 ± 0.4	7 ± 1	-	-

CHAPTER 5
SURFACE PLASMON RESONANCE ENHANCED ELLIPSOMETRY STUDIES TO STUDY LIPID BILAYER INTERACTIONS BY GM2 ACTIVATOR PROTEIN

Introduction

GM2 activator protein (GM2AP) is an 18 kDa nonenzymatic sphingolipid activator protein (SAP) required for the lysosomal degradation of GM2 ganglioside by the exohydrolase, β-hexosaminidase A (Hex A) in neuronal cells.[3,25] In vivo, the protein binds to and extracts GM2 from intralysomal vesicles where the tetrasaccharide headgroup of the lipid is made accessible to Hex A for hydrolytic cleavage of the *N*-acetyl-glucosamine (GalNAc) group, to form GM3.[35,59] A deficiency or defect of GM2AP causes a buildup of GM2 in cells which leads to the fatal neurological disorder, AB variant, a form of GM2 gagliosidoses.[3] The mature form of GM2AP has been isolated from natural sources and has been expressed in its glycosylated form from insect and yeast cells.[122,140] The recombinant form of GM2AP has been expressed in and purified from *Escherichia coli*.[36,141] Resolved crystal structure of nonglycosylated GM2AP reveals a hollow, hydrophobic binding pocket for lipids, formed from eight β-strands in the protein.[53]

Lipid extraction studies have been performed on GM2AP in vitro, and it is known that the protein is not specific for GM2 only, but it can bind and extract other nonspecific glycolipids from micelles and lipid vesicles, forming 1:1 complexes in solution.[121] GM2AP can also bind and transfer phospholipids such as phosphatidylcholine (PC), phosphatidylglycerol (PG), and a dansyl-labeled phosphatidylethanolamie between membranes.[57,60,142] Additionally, a number of crystal structures have been published and deposited in the protein data bank showing binding modes of GM2AP-lipid complexes with GM2 and other phospholipids.[57,60] As such, GM2AP is referred to as a

lipid transfer protein. Despite knowledge about the crystal structure and function of GM2AP, details of the precise molecular process by which the protein binds and extracts lipids from vesicles are not well understood.

Most GM2AP interactions with lipids have been investigated where the lipids exist in solution as micelles or liposomes before extraction and transfer. A biomolecular interaction analysis of GM2AP via surface plasmon resonance on a Biacore Pioneer L1 chip has been reported, but the surface was functionalized with a hydrophilic dextran matrix and lipids were immobilized on the sensorchip in the form of large unilamellar vesicles (LUVs) for analysis.[27,92] It was discovered from sucrose loaded sedimentation assays that during lipid extraction less than 15% of GM2AP remained on the surface of liposomes in the presence and absence of GM2.[125] Results from the assay explain the reason why it is difficult to solely investigate the membrane binding step involved in the overall interaction of GM2AP with lipids. This finding, coupled with the fact that GM2AP also functions a lipid transfer protein lead us to pursue another system with which to study GM2AP: lipid membrane associated interactions – planar supported lipid bilayers (SLBs).

A typical SLB consists of a phospholipid bilayer that covers the surface of a planar solid support. Different solid substrates (glass, silicon, quartz, and mica) and surfaces (metal films and polymers) have been used to support the formation of the bilayers;[75] there are three main methods by which SLBs are formed: 1) The classical Langmuir-Blodgett technique where lipid monolayers are transferred onto a surface;[143,144] 2) the adsorption of liposomes on a surface for membrane vesicle fusion;[74] and 3) a combination of the two previous methods where the inner lipid monolayer is transferred

to a surface via the Langmuir-Blodgett method, followed by vesicle fusion of the outer lipid monolayer.[145] SLBs serve as membrane mimics to study a number of biological processes for example cellular signaling events,[146] cell adhesion,[147] ligand-receptor interactions,[148] membrane insertion of proteins,[149] and protein-lipid binding.[150]

In this work, planar supported lipid bilayers and surface plasmon resonance enhanced ellipsometry (SPREE) were used to examine the interaction of GM2AP with membranes. Alkanethiol self-assembled monolayer (SAM), and zirconium octadecylphosphonate modified surfaces on a thin gold film was used to form a lipid bilayer (the former forms a hybrid bilayer) by vesicle fusion.[77,79] The gold film provided an optically active and physiologically compatible coating for SPREE analysis of the protein-lipid membrane interactions.[151]

Surface plasmon resonance enhanced ellipsometry (SPREE) is an optical technique that utilizes the combination of surface plasmon resonance (SPR) and ellipsometry to monitor and analyze adsorption and desorption of molecules on thin films. The addition of the SPR effect gives high sensitivity to the real time monitoring of binding events of proteins to SPBs. The technique is non-destructive and does not require labeling probes unlike other surface analytical methods.

This chapter reports on the use of phosphatidylcholine (PC) and phosphatidylglycerol (PG) lipids in varying ratios to construct model membranes. The effect of pH, hydrophobicity, and anionic lipid on GM2AP's interaction with the supported hybrid bilayer is examined here. Additionally, the effect of anionic lipid and protein concentration on GM2AP's interaction with the zirconium octadecylphosphonate supported bilayer was also determined. The results revealed that in the absence of PG,

GM2AP extracts PC from the hybrid bilayer. Protein binds to the membrane in the presence of anionic lipid on both surfaces, and on the zirconium octadecylphosphonate surface, binding increases with increasing GM2AP concentration. Detailed results are discussed.

Materials and Methods

1-Palmitoyl-2-oleoyl-sn-glycero-3-phosphocholine (POPC) and 1-palmitoyl-2-oleoyl-sn-glycero-3-[phosphor-rac-(1-glycerol] (POPG) in chloroform were purchased from Avanti Polar Lipids (Alabaster, AL) and used without further purification. Octadecyl mercaptan, 98% was purchased from Aldrich Chemical Company Inc. (Milwaukee, WI). Diiodomethane and zirconyl chloride octahydrate, 98% were purchased from Sigma-Aldrich (St. Louis, MO). SF10 glass slides (25 mm x 25 mm) were purchased from Schott glass (Duryea, PA) then were subjected to metal deposition of a 4 nm chromium adhesive layer, and a 28.5 nm gold layer (LGA Thin Films, Santa Clara, CA). Unless otherwise indicated, all reagents and supplies were obtained from Fisher Scientific (Pittsburg, PA) and were used as received.

GM2 Activator Protein Expression and Purification

Recombinant GM2AP wild-type was over expressed in *E. coli* BL21 (DE3) cells and purified as previously described in Chapter 3 and elsewhere.[125] A more detailed description of protein purification can be found in Chapter 3. Purity of final protein samples was identified via SDS-PAGE using 18% pre-casted polyacrylamide gels and Coomassie Brilliant Blue detection. The structural integrity of final protein samples was verified by circular dichroism spectra and comparison to published circular dichroism spectra of GM2AP wildtype.[92] Protein protein concentration was determined by Bradford

assay and by UV absorption at 280 nm on a Cary 50 Bio UV-Visible spectrophotometer (Varian, Palo Alto, CA) using an extinction coefficient of 23000 $M^{-1}cm^{-1}$.

Purity of final protein samples was identified via SDS-PAGE. To ensure the protein was properly folded, circular dichroism spectra were obtained to verify secondary structure analogous to published circular dichroism spectra of GM2AP wildtype.[92] Protein concentration was measured by Bradford assay and by UV absorbance at 280 nm absorption and an extinction coefficient of 23000 $M^{-1}cm^{-1}$ using a Cary 50 Bio UV-Vis Spectrophotometer (Varian, Palo Alto, CA).

Gold Slide Preparation

Gold slides were initially cleaned in a 3:3:15 v/v solution of ammonium hydroxide : hydrogen peroxide : nanopure water (18.1 MΩ) for 1 minute at 60 °C, then were rinsed with water and dried under a flow of nitrogen. The slides were further plasma cleaned for 10 minutes using a Harrick Plasma sterilizer. Slides were exposed to a 1 mM solution of octacecylmercaptan (ODM) in ethanol overnight to form a self-assembled alkanethiol monolayer, rendering the slides hydrophobic. The slides were rinsed with water and dried under nitrogen before use or further modification.

Surface Modification with Zirconium Phosphonate

Hydrophobic glass slides were modified with zirconium octadecylphosphonate monolayers using a Langmuir-Blodgett (LB) deposition technique.[152] Monolayers were transferred to the gold slides using a KSV 3000 Teflon-coated LB trough with hydrophobic barriers (KSV Instruments, Stratford, CT). The aqueous subphase comprised of 2.6 mM calcium chloride at pH 7.6. The surface pressure was measured by Wilhelmy plate filter paper. Concentrations of 0.3 mg/mL of octadecylphosphonic acid (ODPA) in chloroform were spread on the subphase in the trough and the solvent

was allowed to evaporate for 10 minutes. The monolayer was compressed linearly at a rate of 8 mN/min at room temperature to a target surface pressure of 20 mN/min. The monolayers were transferred by dipping the slides at a rate of 8 mN/min through the monolayer film, and into a vial that was submerged in the subphase. The vial containing the slide was removed from the trough and a final concentration of 3 mM zirconyl chloride solution was added to the vial in order to self-assemble Zr^{4+} ions at the organic template. The slides were incubated in the $ZrOCl_2$ solution for 4 days, then were rinsed with and stored in water until used.

Lipid Preparation

Lipid mixtures of the appropriate ratios in chloroform were prepared and dried under a stream of nitrogen gas. The mixture was further dried overnight for at least 8 hours in a desiccator to remove residual chloroform. The dried films were rehydrated into appropriate volumes of 50 mM NaOAc, pH 4.8 at room temperature, to obtain a final concentration of 1.0 mg/mL. The mixtures were mixed to yield multilamellar vesicles and then subjected to five freeze-thaw cylcles using liquid nitrogen. Each lipid mixture was extruded by 55 passes through 100 nm polycarbonate filters using an Avanti handheld mini-extruder (Avanti Polar Lipids) to produce large unilamellar vesicles (LUVs).

Formation of Lipid Supported Layers

Alkanethiol-phospholipid supported bilayers were formed by adding 1 mg/mL lipid vesicle solution to the ODM monolayered gold slides. Similarly, supported phospholipid bilayers were formed by adding 1 mg/mL lipid vesicles to the zirconium octadecylphosphonate surface. Through adsorption and rupture, the vesicles were

allowed to self-assemble onto the surface in a flow cell, forming either a hybrid bilayer with ODM (Figure 5-1), or a lipid bilayer on zirconated surfaces (Figure 5-2).

Surface Plasmon Resonance Enhanced Ellipsometry (SPREE) Measurements

Ellipsometry measurements under total internal reflection conditions were performed on a commercial EP3-SW imaging system (Nanofilm Surface Analysis, Germany). Briefly, an ellipsometer was coupled with a SPR cell which was mounted on top of a flow cell. The instrument was equipped with a frequency-doubled Nd.YAG laser (adjustable power up to 20 mW) at 532 nm. By way of a polarizer and quarter-wave plate, elliptically polarized light was directed through a 60° equilateral prism coupled to each functionalized gold slide in the Kretschmann configuration. To keep good optical contact between the prism and slide, diiodomethane, an index matching fluid was used. For maximum sensitivity, the angle of incidence (AOI) was set to 64°. Buffer, lipid vesicles, and GM2AP were injected into the flow cell via a peristaltic pump at a flow rate of 50 µL/min. The sample cell was kept at a constant temperature of 24 °C using a peltier temperature control system linked to the cell. After the addition of vesicles (to form supported lipid layers), and protein (to monitor membrane binding or extraction), buffer was flowed through the cell to remove substrate that didn't adsorb to the surface. Figures 5-3 and 5-4 illustrate how typical SPREE measurements are taken for both types of SLBs.

The change in the ellipsometric parameter Ψ was recorded as a function of time as each substrate was flowed over the surface. The time step in recording for all experiments was 30 seconds. The minimum detectable signal change of the instrument used in this work was about 10 millidegrees which gives a thickness precision of 0.1 nm. The experimental data for adsorption and desorption of layers on the surface was fit

by the curve fitting analysis program AnalysR (Nanofilm, Germany) to a Langmuir model called the law of mass action where the equations for change in ellipsometric signal (Δf) are given by:

Baseline equation: $\Delta f_{base}(t) = t * 0 + cstA$ (5-1)

Adsorption equation: $\Delta f_{adsorb}(t) = f_1 * (1 - e^{-\frac{t}{\tau}}) + cstA$ (5-2)

Desorption equation: $\Delta f_{desorb}(t) = f_2 * e^{-(k_{off} \cdot t)} + cstB$ (5-3)

Results and Discussion

The interaction of GM2AP with SLBs was successfully monitored by SPREE. Lipid vesicles were prepared and adsorbed to the solid supports by vesicle fusion prior to addition of protein. Two types of solid supports were used to monitor lipid membrane interaction – a phospholipid/ODM hybrid bilayer, and a zirconium octadecylphosphonate modified SLB. Both solid supports are said to form stable solid supports with which to study protein-lipid interactions.[76,77,79] Reported monolayer studies of protein – lipid interaction showed that GM2AP is surface associated with phospholipid bilayers and does not penetrate into the lipid bilayer,[1] so the motivation behind using stable, planar SLBs to monitor interactions with GM2AP was based on the hopes of finding a stable system with which to study membrane binding.

Interaction of GM2AP with Phospholipid/ODM Hybrid Bilayers

Hybrid bilayers were formed by functionalizing gold slides with a self-assembled ODM monolayer, and by adsorbing phospholipid vesicles by vesicle fusion in the flow cell of the instrument. One advantage of using an alkanethiol modified surface to form bilayers is that alkanethiols can form a complete hydrophobic surface on metals, thus providing the driving force for vesicle fusion to form complete bilayers on the solid

supports.[76] It was reported that the covalent association between the outer phospholipid monolayer with the inner ODM layer is insensitive to changes in buffer, pH, and ionic strength,[79] so any changes in the ellipsometric parameter, psi, can be interpreted to be as a result of adsorption of GM2AP.

Figure 5-5 shows SPREE sensorgrams of the interaction of GM2AP with POPC/ODM hybrid bilayers. For all experiments, upon addition of GM2AP to the membrane, lipids were extracted from the surface. This result was not surprising, though disappointing, as GM2AP is known to be a phospholipid transfer protein.[153] At pH 4.8, approximately 55% of lipid was extracted from the bilayer (Figure 5-5A), while only about 20% of lipid was extracted at pH 5.5 (Figure 5-5B). Consistent with the dansyl based assay described in Chapter 4, increasing the pH of the protein environment changes the degree of interaction with lipids. Additionally, the GM2AP W63W131 variant produced 33% lipid extraction from the surface – a decrease in percentage when compared to wildtype protein. The fact that similar results to other assays performed allowed us to be confident with the SPREE results that were obtained.

POPG was added to the lipid mixture to investigate how the incorporation of anionic lipid would affect protein interaction with the membrane. In vitro studies revealed that in the presence of an anionic lipid, BMP, lipid extraction by GM2AP was enhanced.[83] SPREE results after incorporating different concentrations of POPG to the outer lipid monolayer are shown in Figure 5-6. With increasing POPG concentrations, the rates of lipid adsorption to the functionalized surface decreased. Similar results were observed elsewhere.[77,154] The slower rates of lipid adsorption onto the surface can be

attributed to different stiffness of the vesicles formed from different lipids, leading to thinning of the lipid layers.

Another interesting observation from incorporating POPG to the outer lipid monolayer was that instead of an enhanced extraction of lipid due to the incorporation of anionic lipid, protein bound to the membrane. The increase in binding signal was similar regardless of the concentration of anionic lipid in the membrane. The reason for membrane binding is currently not definitive, though it is believed that electrostatic interactions are playing a role in this phenomenon.

Interaction of GM2AP with Zirconium Octadecylphosphonate modified SLBs

A zirconium octadecylphosphonate modified substrate was developed, characterized, and shown to be an effective and stable solid support for lipid bilayers.[77] Herein, we took advantage of this stable SLB to investigate the binding of GM2AP to lipid bilayers. Figure 5-7 shows SPREE sensorgrams of the adsorption of GM2AP to POPC/POPG bilayers consisting of varying percentages of POPG on the zirconium octadecylphosphonate modified surfaces. Protein adsorbed to the lipid bilayers but was desorbed off the bilayer that contained no POPG, upon rinsing with buffer (Figure 5-7A). Unlike the observation for 100% POPC lipid layers on the hybrid bilayer, GM2AP was unable to extract lipid from the solid support. For bilayers containing POPG, the change in psi that corresponds with adsorption of protein to the membrane, were similar regardless of percent PG in the membrane. These results suggest that while the zirconium modified surfaces are stable enough to not be extracted from the membrane, some anionic lipid is needed for protein to remain bound to the bilayer. Zirconium ions are responsible for the stability of lipid layers formed on the surface and their restricted mobility.[77] Zirconium octadecylphosphonate surfaces are more stable than the hybrid

bilayers in this regard, though a lipid membrane containing only POPC is not sufficient for GM2AP to bind. Other studies of protein interactions with SLBs report that membrane binding increases with increasing concentrations of anionic lipids in the membrane, though that was not the case in our experiments. Further experiments on the zirconium modified surfaces, with combinations of other anionic lipids need to be performed to definitively say why addition of POPG induces membrane binding, especially since the amount of protein bound did not vary with the different concentrations of POPG.

The addition of POPG to zirconium octadecylphosphonate modified SLBs induce binding of GM2AP to the surface. The system allows for the investigation of GM2AP binding to planar membranes, which are more closely related to the cell membrane than lipsomes. Furthermore, because GM2AP also functions as a lipid transfer protein, membrane binding studies have not been successful with lipid vesicles in solution.[83] Different concentrations of GM2AP were adsorbed onto the lipid bilayers . Figure 5-8 shows that with increasing protein concentrations, the binding signal increased. For 5 uM protein the binding signal was 0.11 °, and the signal increased to 0.27 ° for binding of 25 uM GM2AP. Similar results were observed for 50 uM and 100 uM protein with binding signals of 0.45 ° and 0.60 ° respectively. These preliminary results are encouraging, showing that membrane binding events can be monitored on these surfaces by SPREE.

Conclusions

In this study, we were able to use planar solid supported lipid bilayers to monitor the interactions of GM2AP with lipid membranes. Because GM2AP functions as a phospholipid transfer protein with vesicles in solution, these systems provide a means

by which membrane binding can be studied using SPREE. The POPC/ODM hybrid bilayer allowed for lipid extraction from the membrane, but upon addition of POPC, and anionic lipid the membrane, GM2AP bound to the membrane. Membrane binding was also observed with zirconium octadecylphosphonate modifies SLBs. While binding signals were similar for protein regardless of POPG concentration with both supports, an increase in signal was observed with increasing GM2AP concentration on the zirconium modified surfaces.

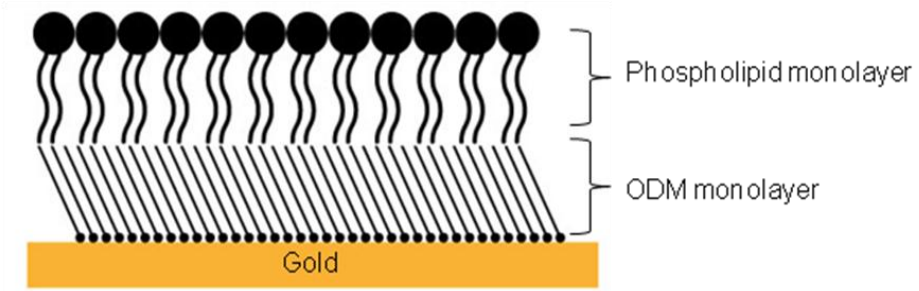

Figure 5-1. A schematic illustration of a hybrid lipid bilayer. An octadecylmercaptan monolayer is functionalized on a gold surface and a hybrid bilayer was formed by vesicular fusion of phospholipids

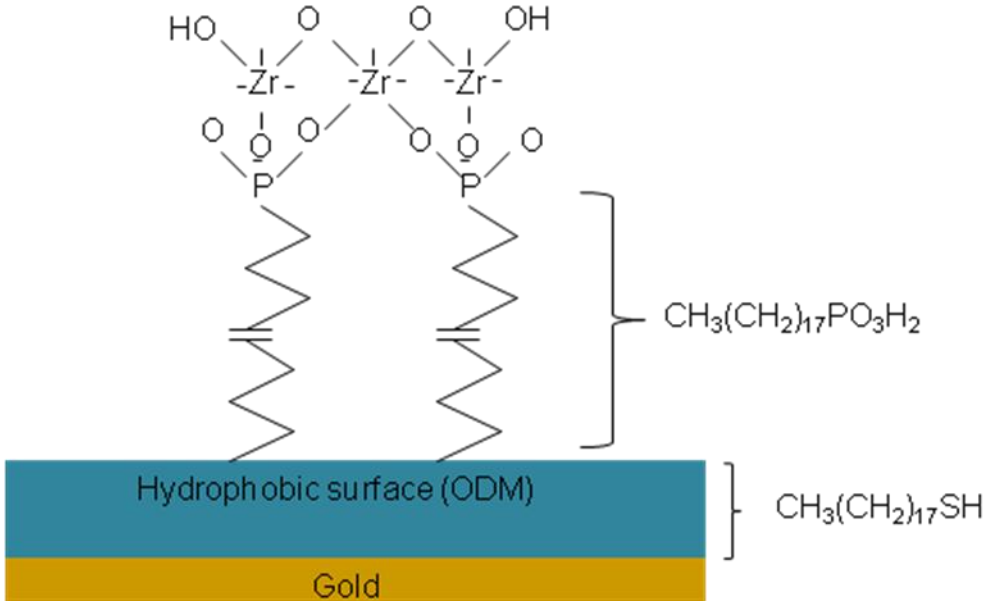

Figure 5-2. A schematic representation of a zirconium octadecylphosphonate modified surface for the formation of supported lipid bilayers

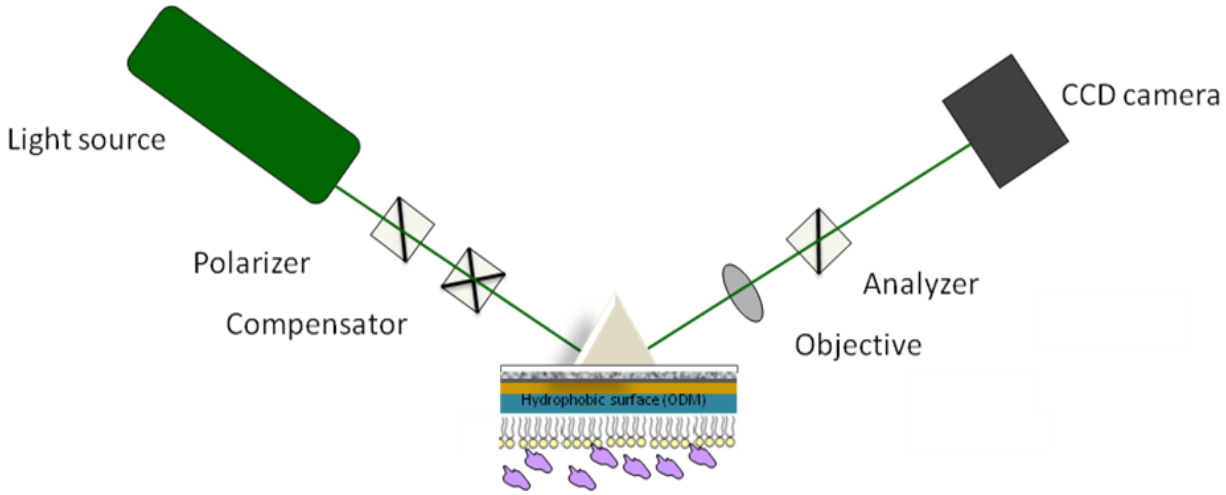

Figure 5-3. Illustration of the SPREE experimental set up showing the layers involved with the adsorption of GM2AP on the octadecyl mercaptan/phospholipid hibrid bilayer. The angle of incidence was set to 64° and psi values were recorded in 30 second increments

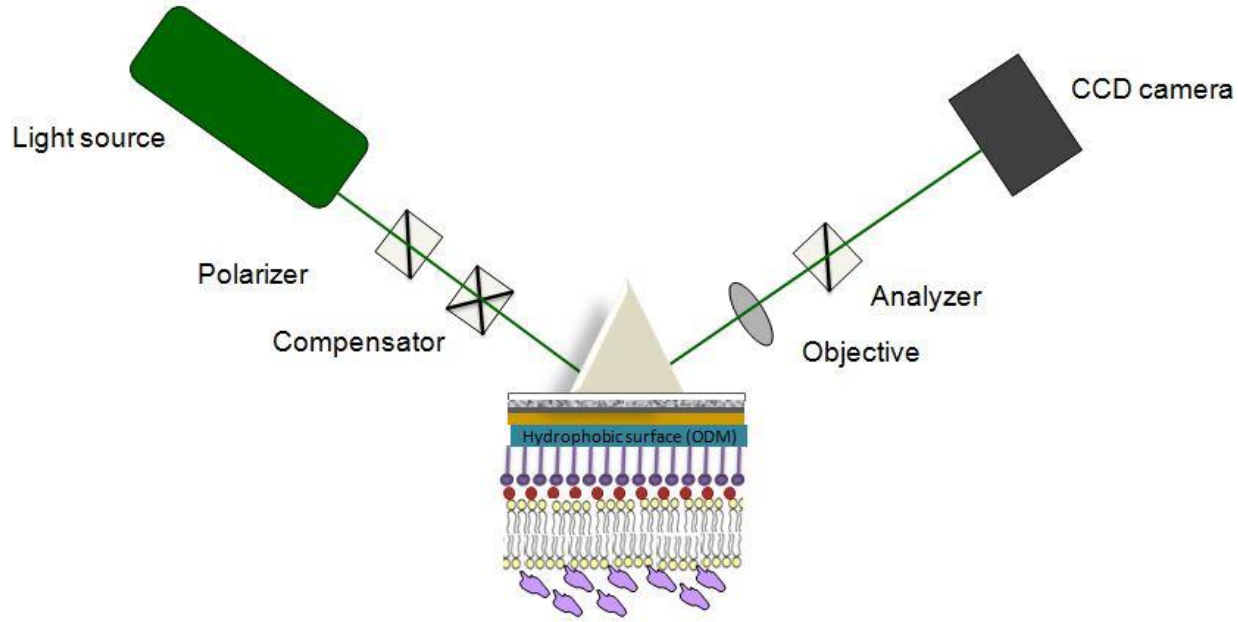

Figure 5-4. Illustration of the SPREE experimental set up showing the layers involved with the adsorption of GM2AP on the zirconium octadecylphosphonate supported phospholipid bilayer. The angle of incidence was set to 64° and psi values were recorded in 30 second increments

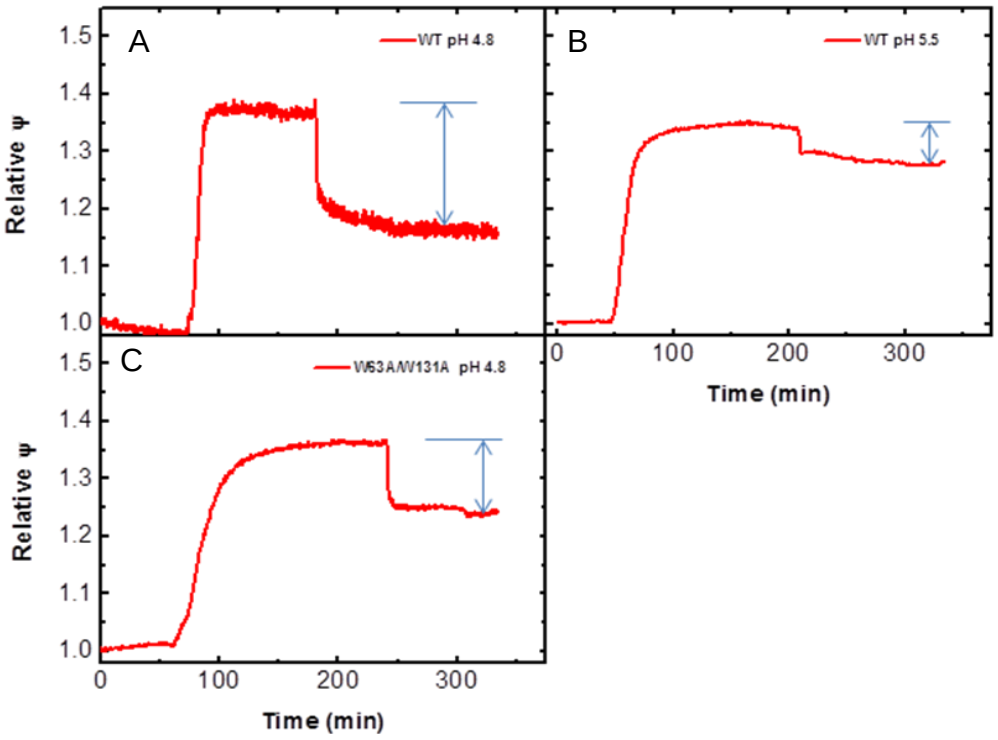

Figure 5-5. SPREE sensorgrams showing POPC extraction by 50 uM GM2AP at (A) pH 4.5 and (B) pH 5.5; and by (C) 50 uM GM2AP W63AW131A at pH 4.8 on octadecylmercaptan-POPC hybrid bilayers. Lipid concentration was 1 mg/L. The angle of incidence was 64° and measurements were taken at 24 °C

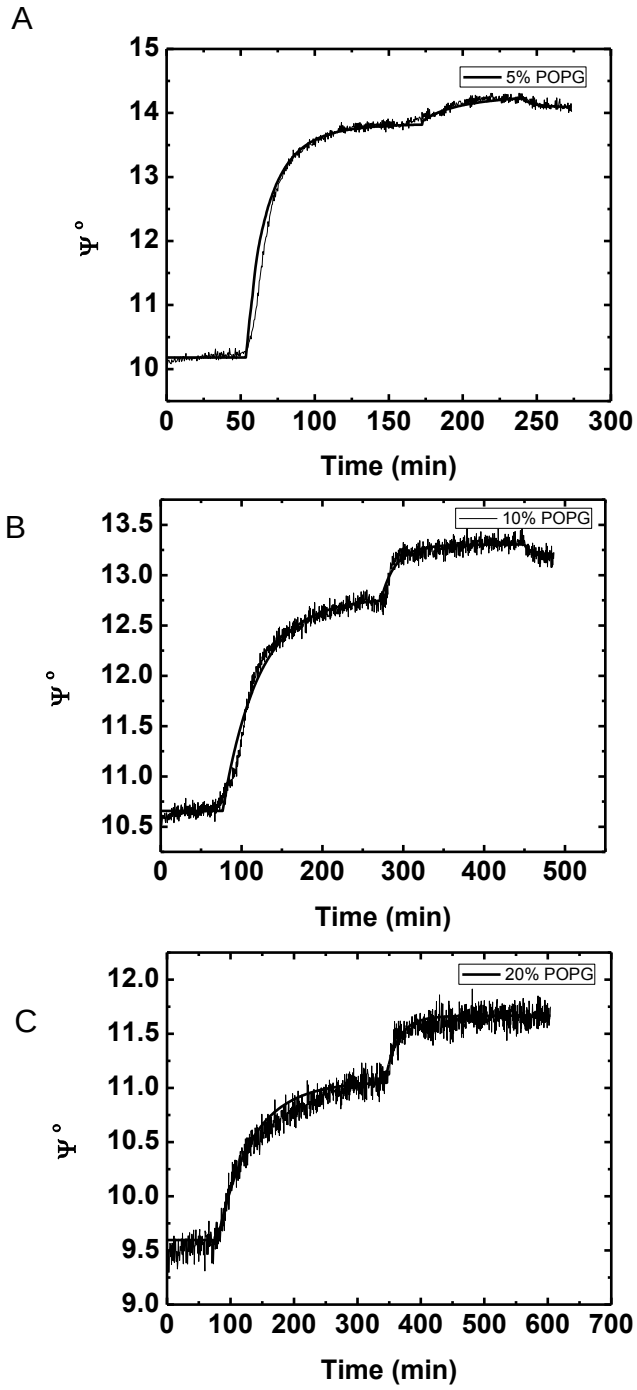

Figure 5-6. SPREE sensorgrams showing the binding of 50 uM GM2AP to octadecylmercaptan-phospholipid hybrid bilayers. The outer lipidlayer consisted of POPC/POPG lipids containing (A) 5%, (B) 10% and (C) 20% POPG. Lipid concentrations were 1 mg/L. The angle of incidence was 64° and measurements were taken at 24 °C

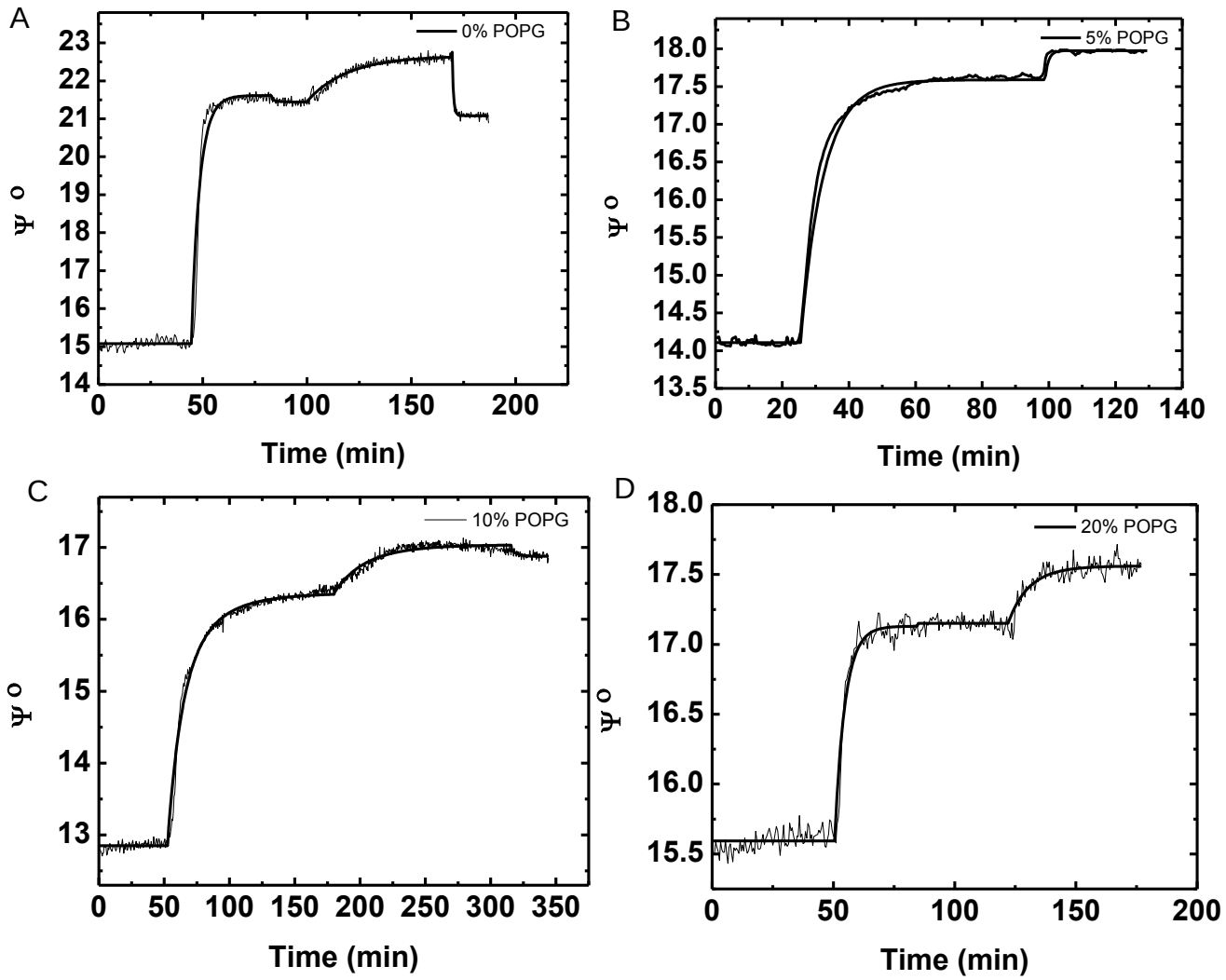

Figure 5-7. SPREE sensorgrams showing the binding of 50 uM GM2AP to zirconium octadecylphosphonate modified SLBs. The lipid bilayers consisted of POPC/POPG lipids containing (A) 0%, (B) 5%, (C) 10%, and (D) 20% POPG. Lipid concentrations were 1 mg/L. The angle of incidence was 64° and measurements were taken at 24 °C

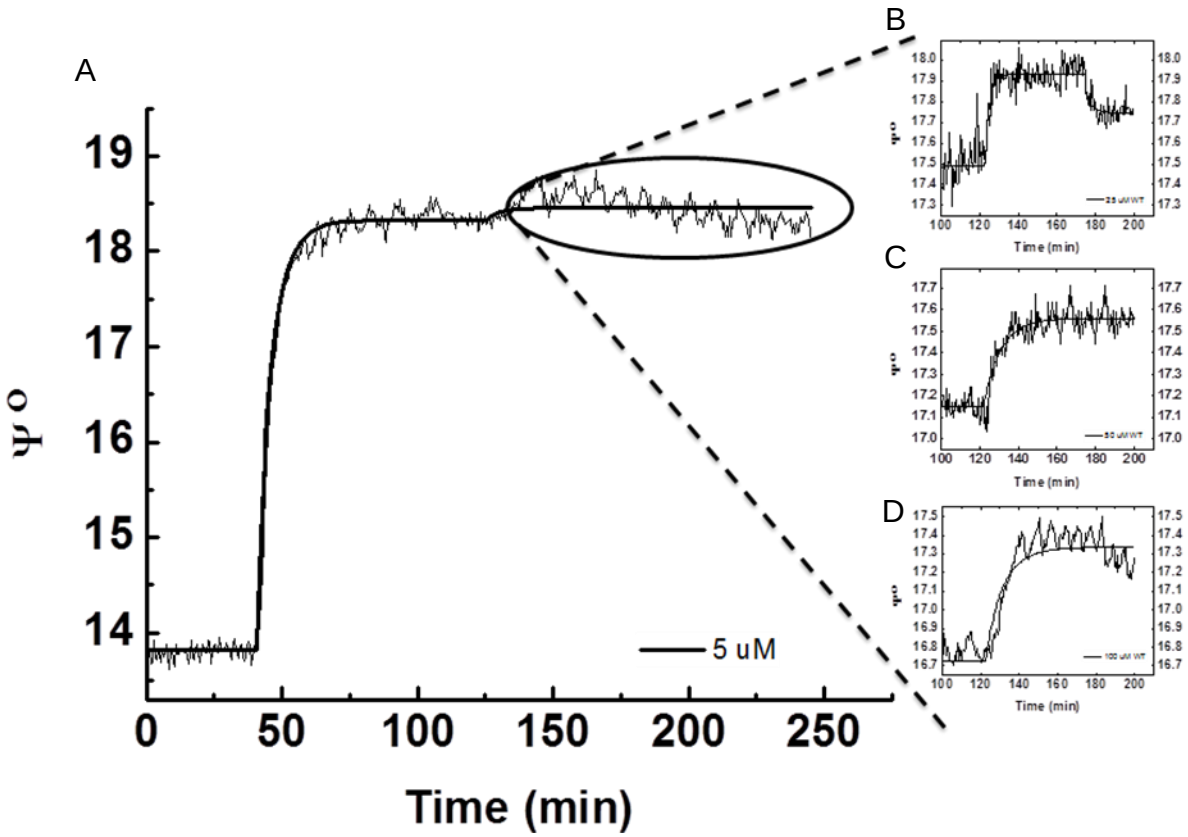

Figure 5-8. SPREE sensorgrams showing the binding of (A) 5 uM GM2AP to zirconium octadecylphosphonate modified SLBs. The lipid bilayers consisted of POPC/POPG lipids containing 20% POPG. The inset shows theprotein binding portion of (B) 25uM, (C) 50 uM, and (D) 100uM protein only. Lipid concentrations were 1 mg/L. The angle of incidence was 64° and measurements were taken at 24 °C

CHAPTER 6
CONCLUSIONS AND FURTHER DIRECTIONS

The site-directed mutagenesis and protein expression and purification methods W to A constructs of GM2AP were successfully performed. CD spectroscopy revealed that the amino acid substitutions did not alter proper protein folding. The variants were then used to characterize the intrinsic tryptophan fluorescence of the protein. Quenching results suggest that while the tryptophan residues were accessible to acrylamide and iodide, the degree of quenching varied. W63 seemed to be most accessible, followed by W131, and W5 was not as accessible due to its location in the hydrophobic region of GM2AP. These findings insinuate that since W63 and W131 are located in putative membrane binging regions of the protein, and are solvent exposed, intrinsic tryptophan fluorescence may be a useful technique for the further investigation of the precise molecular mechanism of GM2AP function without the need for attaching fluorescent probes to the protein.

GM2AP is essential for GM2 degradation in neuronal cells and also functions as a phospholipid transfer protein. As shown here, a dansyl based fluorescence assay to determine changes in lipid transfer, and a gel filtration assay to determine lipid extraction efficiency of a series of W to A GM2AP constructs was used to study the protein's molecular interactions with liposomes. Removal of tryptophan residues from the mobile loops of GM2AP resulted in slower lipid binding, but did not affect lipid extraction. Binding to lipid vesicles becomes more difficult because the hydrophobic characteristic of tryptophan residues located in the apolar and hydrophobic loops of GM2AP is favored for hydrophobic interactions at the lipid membrane interface. Our results corroborate previous findings that it is likely that GM2AP first binds to the

membrane via the hydrophobic loop, with then rotation to the orientation that has the opening to the lipid cleft, which includes the flexible loop containing W131 juxtaposed on the bilayer surface, allowing lipid to be extracted into the binding pocket of the protein. Additionally, while GM2AP also functions as a lipid transfer protein, an acidic environment (near pH 4.8) seems to be required for optimal protein function.

We were able to use planar solid supported lipid bilayers to monitor the interactions of GM2AP with lipid membranes. Because GM2AP functions as a phospholipid transfer protein with vesicles in solution, these systems provide a means by which membrane binding can be studied using SPREE. The POPC/ODM hybrid bilayer allowed for lipid extraction from the membrane, but upon addition of POPC, and anionic lipid the membrane, GM2AP bound to the membrane. Membrane binding was also observed with zirconium octadecylphosphonate modifies SLBs. While binding signals were similar for protein regardless of POPG concentration with both supports, an increase in signal was observed with increasing GM2AP concentration on the zirconium modified surfaces.

Other experiments should be performed, namely varying lipid compositions, and ionic strengths of the system, to confirm the suitability of stable supported lipid bilayers to studying membrane binding by GM2AP. Once confirmed, molecular interactions between GM2AP and lipid membranes can be investigated by mutating amino acid residues in the protein to probe regions of the protein involved in membrane binding.

LIST OF REFERENCES

(1) Giehl, A.; Lemm, T.; Bartelsen, O.; Sandhoff, K.; Blume, A. *European Journal of Biochemistry* **1999**, *261*, 650-658.

(2) Nagai, Y.; Iwamori, M. In *Biology of the sialic acids* Rosenberg, A., Ed.; Plenum Press: New York, 1995, p 197-241.

(3) Gravel, R. A.; Clarke, J. T. R.; Kaback, M. M.; Mahuran, D.; Sandhoff, K.; Suzuki, K. In *The Metabolic and molecular bases of inherited disease* 7th ed.; Scriver, C. R., Ed.; McGraw-Hill, Health Professions Division: New York, 1995, p 2839-2879.

(4) Hakomori, S. *Curr Opin Hematol* **2003**, *10*, 16-24.

(5) Kielczynski, W.; Harrison, L. C.; Leedman, P. J. *Proceedings of the National Academy of Sciences* **1991**, *88*, 1991-1995.

(6) Thompson, T. E.; Tillack, T. W. *Annu Rev Biophys Bio* **1985**, *14*, 361-386.

(7) Kolter, T.; Sandhoff, K. *Febs Letters* **2010**, *584*, 1700-1712.

(8) Tettamanti, G.; Bassi, R.; Viani, P.; Riboni, L. *Biochimie* **2003**, *85*, 423-437.

(9) Sandhoff, K.; Kolter, T. *Philos T Roy Soc B* **2003**, *358*, 847-861.

(10) Schulze, H.; Kolter, T.; Sandhoff, K. *Biochimica et Biophysica Acta (BBA) - Molecular Cell Research* **2009**, *1793*, 674-683.

(11) Sastry, P. S. *Prog Lipid Res* **1985**, *24*, 69-176.

(12) Wilkening, G.; Linke, T.; Uhlhorn-Dierks, G.; Sandhoff, K. *J Biol Chem* **2000**, *275*, 35814-9.

(13) Schuette, C. G.; Pierstorff, B.; Huettler, S.; Sandhoff, K. *Glycobiology* **2001**, *11*, 81R-90R.

(14) Fingerhut, R.; van der Horst, G. T.; Verheijen, F. W.; Conzelmann, E. *European Journal of Biochemistry* **1992**, *208*, 623-9.

(15) Zschoche, A.; Furst, W.; Schwarzmann, G.; Sanhoff, K. *European Journal of Biochemistry* **1994**, *222*, 83-90.

(16) Linke, T.; Wilkening, G.; Sadeghlar, F.; Mozcall, H.; Bernardo, K.; Schuchman, E.; Sandhoff, K. *J Biol Chem* **2001**, *276*, 5760-8.

(17) Meier, E. M.; Schwarzmann, G.; Furst, W.; Sandhoff, K. *Journal of Biological Chemistry* **1991**, *266*, 1879-1887.

(18) Kaback, M. M. *Prog Clin Biol Res* **1977**, *18*, 1-7.

(19) Suzuki, K. In *Biology of the Sialic Acids*; Rosenberg, A., Ed.; Plenum Press: New York, 1995, p 337-361.

(20) Myerowitz, R. *Hum Mutat* **1997**, *9*, 195-208.

(21) Barranger, J. A.; Cabrera-Salazar, M. A.; Charria-Ortiz, G.; Springer US: 2007, p 229-256.

(22) Tay, W. *Trans. Opthalmol. Soc. UK* **1881**, *1*, 3.

(23) Sachs, B. *J. Nerv. Ment. Dis.* **1887**, *14*, 13.

(24) Sandhoff, K.; Andreae, U.; Jatzkewitz, H. *Pathol Eur* **1968**, *3*, 278-85.

(25) Mahuran, D. J. *Bba-Lipid Lipid Met* **1998**, *1393*, 1-18.

(26) Sandhoff, K. *Febs Letters* **1969**, *4*, 351-354.

(27) Werth, N.; Schuette, C. G.; Wilkening, G.; Lemm, T.; Sandhoff, K. *J Biol Chem* **2001**, *276*, 12685-12690.

(28) Kytzia, H. J.; Sandhoff, K. *J Biol Chem* **1985**, *260*, 7568-72.

(29) Hepbildikler, S. T.; Sandhoff, R.; Kolzer, M.; Proia, R. L.; Sandhoff, K. *Journal of Biological Chemistry* **2002**, *277*, 2562-72.

(30) Yadao, F.; Hechtman, P.; Kaplan, F. *Biochim Biophys Acta* **1997**, *1340*, 45-52.

(31) Mehl, E.; Jatzkewitz, H. *Hoppe Seylers Z Physiol Chem* **1964**, *339*, 260-76.

(32) Furst, W.; Machleidt, W.; Sandhoff, K. *Biol Chem Hoppe Seyler* **1988**, *369*, 317-28.

(33) Hiraiwa, M.; O'Brien, J. S.; Kishimoto, Y.; Galdzicka, M.; Fluharty, A. L.; Ginns, E. I.; Martin, B. M. *Arch Biochem Biophys* **1993**, *304*, 110-6.

(34) Vielhaber, G.; Hurwitz, R.; Sandhoff, K. *J Biol Chem* **1996**, *271*, 32438-46.

(35) Li, S. C.; Wu, Y. Y.; Sugiyama, E.; Taki, T.; Kasama, T.; Casellato, R.; Sonnino, S.; Li, Y. T. *J Biol Chem* **1995**, *270*, 24246-51.

(36) Klima, H.; Klein, A.; van Echten, G.; Schwarzmann, G.; Suzuki, K.; Sandhoff, K. *Biochemical Journal* **1993**, *292 (Pt 2)*, 571-6.

(37) Klima, H.; Tanaka, A.; Schnabel, D.; Nakano, T.; Schroder, M.; Suzuki, K.; Sandhoff, K. *Febs Lett* **1991**, *289*, 260-4.

(38) Ahn, V. E.; Leyko, P.; Alattia, J. R.; Chen, L.; Prive, G. G. *Protein Science* **2006**, *15*, 1849-57.

(39) Ahn, V. E.; Faull, K. F.; Whitelegge, J. P.; Fluharty, A. L.; Prive, G. G. *Proc Natl Acad Sci U S A* **2003**, *100*, 38-43.

(40) Popovic, K.; Prive, G. G. *Acta Crystallogr D Biol Crystallogr* **2008**, *64*, 589-94.

(41) Kishimoto, Y.; Hiraiwa, M.; O'Brien, J. S. *Journal of Lipid Research* **1992**, *33*, 1255-67.

(42) Vaccaro, A. M.; Salvioli, R.; Barca, A.; Tatti, M.; Ciaffoni, F.; Maras, B.; Siciliano, R.; Zappacosta, F.; Amoresano, A.; Pucci, P. *J Biol Chem* **1995**, *270*, 9953-60.

(43) Vaccaro, A. M.; Ciaffoni, F.; Tatti, M.; Salvioli, R.; Barca, A.; Tognozzi, D.; Scerch, C. *J Biol Chem* **1995**, *270*, 30576-80.

(44) Linke, T.; Wilkening, G.; Lansmann, S.; Moczall, H.; Bartelsen, O.; Weisgerber, J.; Sandhoff, K. *Biol Chem* **2001**, *382*, 283-90.

(45) Bar, J.; Linke, T.; Ferlinz, K.; Neumann, U.; Schuchman, E. H.; Sandhoff, K. *Hum Mutat* **2001**, *17*, 199-209.

(46) Christomanou, H.; Aignesberger, A.; Linke, R. P. *Biol Chem Hoppe Seyler* **1986**, *367*, 879-90.

(47) Klein, A.; Henseler, M.; Klein, C.; Suzuki, K.; Harzer, K.; Sandhoff, K. *Biochem Biophys Res Commun* **1994**, *200*, 1440-8.

(48) Ciaffoni, F.; Salvioli, R.; Tatti, M.; Arancia, G.; Crateri, P.; Vaccaro, A. M. *Journal of Biological Chemistry* **2001**, *276*, 31583-9.

(49) Conzelmann, E.; Burg, J.; Stephan, G.; Sandhoff, K. *European Journal of Biochemistry* **1982**, *123*, 455-464.

(50) Smiljanic-Georgijev, N.; Rigat, B.; Xie, B.; Wang, W.; Mahuran, D. J. *Biochim Biophys Acta* **1997**, *1339*, 192-202.

(51) Li, S. C.; Hama, Y.; Li, Y. T. *Methods Enzymol* **2003**, *363*, 230-41.

(52) Ravasi, D.; Masserini, M.; Vecchio, G.; Li, Y. T.; Li, S. C. *Neurochem Res* **2002**, *27*, 785-792.

(53) Wright, C. S.; Li, S. C.; Rastinejad, F. *J Mol Biol* **2000**, *304*, 411-422.

(54) Albiach-Marti, M. R.; Robertson, C.; Gowda, S.; Tatineni, S.; Belliure, B.; Garnsey, S. M.; Folimonova, S. Y.; Moreno, P.; Dawson, W. O. *Molecular plant pathology* **2010**, *11*, 55-67.

(55) Xie, B.; Mcinnes, B.; Neote, K.; Lamhonwah, A. M.; Mahuran, D. *Biochem Bioph Res Co* **1991**, *177*, 1217-1223.

(56) Wendeler, M.; Hoernschemeyer, J.; Hoffmann, D.; Kolter, T.; Schwarzmann, G.; Sandhoff, K. *European Journal of Biochemistry* **2004**, *271*, 614-627.

(57) Wright, C. S.; Zhao, Q.; Rastinejad, F. *J Mol Biol* **2003**, *331*, 951-964.

(58) Wright, C. S.; Li, S. C.; Rastinejad, F. *J Mol Biol* **2000**, *304*, 411-22.

(59) Furst, W.; Sandhoff, K. *Biochim Biophys Acta* **1992**, *1126*, 1-16.

(60) Wright, C. S.; Mi, L. Z.; Lee, S.; Rastinejad, F. *Biochemistry-Us* **2005**, *44*, 13510-21.

(61) Wendeler, M.; Hoernschemeyer, J.; John, M.; Werth, N.; Schoeniger, M.; Lemm, T.; Hartmann, R.; Kessler, H.; Sandhoff, K. *Protein Expr Purif* **2004**, *34*, 147-57.

(62) Nakamura, S.; Akisue, T.; Jinnai, H.; Hitomi, T.; Sarkar, S.; Miwa, N.; Okada, T.; Yoshida, K.; Kuroda, S.; Kikkawa, U.; Nishizuka, Y. *Proc Natl Acad Sci U S A* **1998**, *95*, 12249-53.

(63) Jinnai, H.; Nakamura, S. *Kobe J Med Sci* **1999**, *45*, 181-90.

(64) Mundel, T. M. *Annals of Anatomy-Anatomischer Anzeiger* **2001**, *183*, 11-11.

(65) Mundel, T. M.; Heid, H. W.; Mahuran, D. J.; Kriz, W.; Mundel, P. *Journal of the American Society of Nephrology* **1999**, *10*, 435-443.

(66) Rigat, B.; Reynaud, D.; Smiljanic-Georgijev, N.; Mahuran, D. *Biochem Bioph Res Co* **1999**, *258*, 256-259.

(67) Lehninger, A. L.; Nelson, D. L.; Cox, M. M. *Lehninger principles of biochemistry*; 4th ed.; W.H. Freeman: New York, 2005.

(68) Gennis, R. B. *Biomembranes : molecular structure and function*; Springer-Verlag: New York, 1989.

(69) van Meer, G.; Voelker, D. R.; Feigenson, G. W. *Nat Rev Mol Cell Biol* **2008**, *9*, 112-24.

(70) Yeagle, P. *The membranes of cells*; 2nd ed.; Academic Press: San Diego, 1993.

(71) Edwards, K. A.; Baeumner, A. J. *Analytical and Bioanalytical Chemistry* **2006**, *386*, 1613-23.

(72) Foldvari, M.; Faulkner, G. T.; Mezei, C.; Mezei, M. *Cell Mater* **1992**, *2*, 67-85.

(73) Foldvari, M.; Gesztes, A.; Mezei, M. *J Microencapsul* **1990**, *7*, 479-489.

(74) Tamm, L. K.; McConnell, H. M. *Biophysical Journal* **1985**, *47*, 105-13.

(75) Castellana, E. T.; Cremer, P. S. *Surface Science Reports* **2006**, *61*, 429-444.

(76) Plant, A. L. *Langmuir* **1999**, *15*, 5128-5135.

(77) Fabre, R. M.; Talham, D. R. *Langmuir* **2009**, *25*, 12644-52.

(78) Brian, A. A.; McConnell, H. M. *Proc Natl Acad Sci U S A* **1984**, *81*, 6159-63.

(79) Plant, A. L. *Langmuir* **1993**, *9*, 2764-2767.

(80) Plant, A. L.; Gueguetchkeri, M.; Yap, W. *Biophys J* **1994**, *67*, 1126-33.

(81) Meuse, C. W.; Krueger, S.; Majkrzak, C. F.; Dura, J. A.; Fu, J.; Connor, J. T.; Plant, A. L. *Biophysical Journal* **1998**, *74*, 1388-98.

(82) Schwarzmann, G.; Wendeler, M.; Sandhoff, K. *Glycobiology* **2005**, *15*, 1302-1311.

(83) Ran, Y.; Fanucci, G. E. *Biophysical Journal* **2009**, *97*, 257-66.

(84) Kuwana, T.; Mullock, B. M.; Luzio, J. P. *Biochem J* **1995**, *308 (Pt 3)*, 937-46.

(85) Morimoto, S.; Kishimoto, Y.; Tomich, J.; Weiler, S.; Ohashi, T.; Barranger, J. A.; Kretz, K. A.; O'Brien, J. S. *J Biol Chem* **1990**, *265*, 1933-7.

(86) Voet, D.; Voet, J. G. *Biochemistry*; J. Wiley & Sons: Hoboken, NJ, 2004.

(87) Johnson, W. C., Jr. *Annu Rev Biophys Biophys Chem* **1988**, *17*, 145-66.

(88) Kelly, S. M.; Jess, T. J.; Price, N. C. *Biochim Biophys Acta* **2005**, *1751*, 119-39.

(89) Barrett, G. C.; Elmore, D. T. *Amino acids and peptides / G.C. Barrett and D.T. Elmore*; Cambridge University Press: Cambridge, U.K. ; New York, 1998.

(90) Tompkins, H. G.; McGahan, W. A. *Spectroscopic ellipsometry and reflectometry : a user's guide / by Harland G. Tompkins, William A. McGahan*; Wiley: New York, 1999.

(91) Greenfield, N. J. *Nat. Protocols* **2007**, *1*, 2876-2890.

(92) Wendeler, M.; Werth, N.; Maier, T.; Schwarzmann, G.; Kolter, T.; Schoeniger, M.; Hoffmann, D.; Lemm, T.; Saenger, W.; Sandhoff, K. *Febs Journal* **2006**, *273*, 982-991.

(93) Stryer, L. *Science* **1968**, *162*, 526-533.

(94) Lakowicz, J. R. *Principles of fluorescence spectroscopy / Joseph R. Lakowicz*; 3rd ed. ed.; Springer: New York, 2006.

(95) Schulman, S. G.; Sharma, A. *Introduction to fluorescence spectroscopy / <by> Stephen G. Schulman and Ashutosh Sharma*; John Wiley & Sons, Inc: New York, 1999.

(96) Demchenko, A. P. *Ultraviolet spectroscopy of proteins / Alexander P. Demchenko*; Rev. and enl. translation of the Russian ed. ed.; Springer-Verlag: Berlin ; New York, 1986.

(97) Waggoner, A. S.; Stryer, L. *Proc Natl Acad Sci U S A* **1970**, *67*, 579-89.

(98) Eftink, M. R. *Methods Biochem Anal* **1991**, *35*, 127-205.

(99) Eftink, M. R.; Ghiron, C. A. *Anal Biochem* **1981**, *114*, 199-227.

(100) Lehrer, S. *Biochemistry-Us* **1971**, *10*, 3254-3263.

(101) Eftink, M. R.; Ghiron, C. A. *Biochemistry-Us* **1976**, *15*, 672-680.

(102) Eftink, M.; Lakowicz, J., Ed.; Springer US: 2002; Vol. 2, p 53-126.

(103) Skoog, D. A.; Crouch, S. R.; Holler, F. J. *Principles of instrumental analysis*; 6th ed. / Douglas A. Skoog, F. James Holler, Stanley R. Crouch. ed.; Brooks/Cole: Belmont, CA, 2007.

(104) Chowdhury, M. H.; Aslan, K.; Malyn, S. N.; Lakowicz, J. R.; Geddes, C. D. *J Fluoresc* **2006**, *16*, 295-9.

(105) Westphal, P.; Bornmann, A. *Sensors and Actuators B-Chemical* **2002**, *84*, 278-282.

(106) Homola, J.; Yee, S. S.; Gauglitz, G. *Sensor Actuat B-Chem* **1999**, *54*, 3-15.

(107) Azzam, R. M. A.; Bashara, N. M. *Ellipsometry and polarized light*; North-Holland ; sole distributors for the USA and Canada, Elsevier Science Publishing Co., Inc.: Amsterdam ; New York, 1987.

(108) Arwin, H.; Poksinski, M.; Johansen, K. *Applied Optics* **2004**, *43*, 3028-3036.

(109) Poksinski, M.; Arwin, H. *Optics Letters* **2007**, *32*, 1308-1310.

(110) Tompkins, H. G. *A user's guide to ellipsometry / Harland G. Tompkins*; Academic Press: Boston, 1993.

(111) Born, M.; Wolf, E. j. a. *Principles of optics : electromagnetic theory of propagation, interference and diffraction of light / by Max Born and Emil Wolf, with contributions by A. B. Bhatia ... [et al.]*; 6th ed. ed.; Pergamon Press: Oxford ; New York, 1980.

(112) Salamon, Z.; Tollin, G. *Spectrosc-Int J* **2001**, *15*, 161-175.

(113) Salamon, Z.; Macleod, H. A.; Tollin, G. *Bba-Rev Biomembranes* **1997**, *1331*, 131-152.

(114) Cooper, M. *Analytical and Bioanalytical Chemistry* **2003**, *377*, 834-842.

(115) Iwata, T.; Maeda, S. *Applied Optics* **2007**, *46*, 1575-1582.

(116) Conzelmann, E.; Sandhoff, K. *Proc Natl Acad Sci U S A* **1978**, *75*, 3979-83.

(117) Burg, J.; Banerjee, A.; Sandhoff, K. *Biol Chem H-S* **1985**, *366*, 887-891.

(118) Zhou, D.; Cantu, C., 3rd; Sagiv, Y.; Schrantz, N.; Kulkarni, A. B.; Qi, X.; Mahuran, D. J.; Morales, C. R.; Grabowski, G. A.; Benlagha, K.; Savage, P.; Bendelac, A.; Teyton, L. *Science* **2004**, *303*, 523-7.

(119) Mundel, T. M. *Ann Anat* **2001**, *183*, 11.

(120) Mundel, T. M.; Heid, H. W.; Mahuran, D. J.; Kriz, W.; Mundel, P. *J Am Soc Nephrol* **1999**, *10*, 435-43.

(121) Conzelmann, E.; Burg, J.; Stephan, G.; Sandhoff, K. *Eur J Biochem* **1982**, *123*, 455-64.

(122) Wendeler, M.; Hoernschemeyer, J.; John, M.; Werth, N.; Schoeniger, M.; Lemm, T.; Hartmann, R.; Kessler, H.; Sandhoff, K. *Protein Expres Purif* **2004**, *34*, 147-157.

(123) Wendeler, M.; Lemm, T.; Weisgerber, J.; Hoernschemeyer, J.; Bartelsen, O.; Schevers, U.; Sandhoff, K. *Protein Expres Purif* **2003**, *27*, 259-266.

(124) Wu, Y. Y.; Lockyer, J. M.; Sugiyama, E.; Pavlova, N. V.; Li, Y. T.; Li, S. C. *J Biol Chem* **1994**, *269*, 16276-83.

(125) Ran, Y.; Fanucci, G. E. *Biophys J* **2009**, *97*, 257-266.

(126) Ladokhin, A. S.; Jayasinghe, S.; White, S. H. *Anal Biochem* **2000**, *285*, 235-245.

(127) Li, X. M.; Malakhova, M. L.; Lin, X.; Pike, H. M.; Chung, T. W.; Molotkovsky, J. G.; Brown, R. E. *Biochemistry-Us* **2004**, *43*, 10285-10294.

(128) Weiner, M. P.; Costa, G. L.; Schoettlin, W.; Cline, J.; Mathur, E.; Bauer, J. C. *Gene* **1994**, *151*, 119-23.

(129) Zheng, L.; Baumann, U.; Reymond, J. L. *Nucleic Acids Research* **2004**, *32*, e115.

(130) Burstein, E. A.; Vedenkina, N. S.; Ivkova, M. N. *Photochem Photobiol* **1973**, *18*, 263-79.

(131) Eftink, M. R.; Ghiron, C. A. *Biochemistry-Us* **1976**, *15*, 672-80.

(132) Wendeler, M.; Hoernschemeyer, J.; Hoffmann, D.; Kolter, T.; Schwarzmann, G.; Sandhoff, K. *Eur J Biochem* **2004**, *271*, 614-27.

(133) Wendeler, M.; Lemm, T.; Weisgerber, J.; Hoernschemeyer, J.; Bartelsen, O.; Schepers, U.; Sandhoff, K. *Protein Expr Purif* **2003**, *27*, 259-66.

(134) Ran, Y.; Fanucci, G. E. *Anal Biochem* **2008**, *382*, 132-4.

(135) Rao, C. S.; Chung, T.; Pike, H. M.; Brown, R. E. *Biophysical Journal* **2005**, *89*, 4017-28.

(136) Svennerholm, L. *Biochim Biophys Acta* **1957**, *24*, 604-11.

(137) Wright, C. S.; Zhao, Q.; Rastinejad, F. *J Mol Biol* **2003**, *331*, 951-64.

(138) Mathias, J. D.; Ran, Y.; Carter, J. D.; Fanucci, G. E. *Biophysical Journal* **2009**, *97*, 1436-1444.

(139) Wimley, W. C.; White, S. H. *Nat Struct Biol* **1996**, *3*, 842-8.

(140) Wendeler, M.; Reilaender, H.; Hoernschemeyer, J.; Schwarzmann, G.; Kolter, T.; Sandhoff, K. *Methods Enzymol* **2003**, *363*, 476-89.

(141) Hama, Y.; Li, Y. T.; Li, S. C. *Journal of Biological Chemistry* **1997**, *272*, 2828-33.

(142) Ballester, A.; Cervera, M.; Pena, L. *Plant cell reports* **2008**, *27*, 1005-15.

(143) Langmuir, I. *T Faraday Soc* **1920**, *15*, 0062-0074.

(144) Blodgett, K. B. *J Am Chem Soc* **1934**, *56*, 495-495.

(145) Kalb, E.; Frey, S.; Tamm, L. *Faseb Journal* **1992**, *6*, A290-A290.

(146) Qi, S. Y.; Groves, J. T.; Chakraborty, A. K. *P Natl Acad Sci USA* **2001**, *98*, 6548-6553.

(147) Tendian, S. W.; Lentz, B. R.; Thompson, N. L. *Biochemistry-Us* **1991**, *30*, 10991-10999.

(148) Yang, T. L.; Baryshnikova, O. K.; Mao, H. B.; Holden, M. A.; Cremer, P. S. *J Am Chem Soc* **2003**, *125*, 4779-4784.

(149) Ramsden, J. J.; Schneider, P. *Biochemistry-Us* **1993**, *32*, 523-529.

(150) Kalb, E.; Engel, J.; Tamm, L. K. *Biochemistry-Us* **1990**, *29*, 1607-1613.

(151) Luth, D.; Moore, G. A. *Plant Cell, Tissue and Organ Culture* **1999**, *57*, 219-222.

(152) Byrd, H.; Pike, J. K.; Talham, D. R. *Chem Mater* **1993**, *5*, 709-715.

(153) Mahuran, D. J. *Biochim Biophys Acta* **1998**, *1393*, 1-18.

(154) Pandey, A. P.; Haque, F.; Rochet, J.-C.; Hovis, J. S. *Biophysical Journal* **2009**, *96*, 540-551.

BIOGRAPHICAL SKETCH

Stacey-Ann Benjamin was born in Linstead, St Catherine on the island of Jamaica on St. Patrick's Day in 1984. She attended Trinity Prep in Linstead and Holy Childhood Catholic High School for girls in Kingston where she graduated in 2000. Stacey opted to return to high school for an additional two years at Hampton School for girls in St. Elizabeth where she took advanced level classes and sat the University of Cambridge A-level exams in chemistry, mathematics and general paper.

After graduating high school in 2002, Stacey-Ann left Jamaica for undergraduate studies at Wesleyan College in Macon, GA. She participated in two Summer Research programs in 2004 and 2005 at the Florida State University where she was introduced to, and developed an interest in chemistry research. During her senior year, Stacey-Ann did a co-op at J.M. Huber Corporation in Macon, GA where she assisted in the design of standard procedures for determining the surface area and pore size of kaoilin clay samples. In 2006, Stacey-Ann received a Bachelor of Arts degree in chemistry with a minor in Mathematics from Wesleyan College.

Stacey-Ann's scholastic journey continued at the University of Florida's graduate chemistry program in the fall of 2006 and soon after she joined the Fanucci research group. After a few years of being a teaching assistant for general chemistry courses, she developed a passion for teaching and decided that she wanted to commit her academic career primarily to undergraduate chemistry education. Stacey-Ann received a Masters of Science in teaching in May 2011 and a Ph.D. in chemistry in August 2012 from UF.